Functional Organization and Plasticity of Visual Cortex over the Lifespan of the Ferret

By

David Edward Whitney

BS, Engineering Physics, Colorado School of Mines 2006

BS, Chemistry, Colorado School of Mines 2007

Submitted to the faculty in the

Department of Biological Sciences at

Carnegie Mellon University

In partial fulfillment of the requirements for the degree of

Doctor of Philosophy

July 2013

ABSTRACT

An elaborate network of neurons along the visual pathway topographically maps fundamental stimulus features in visual space, such as stimulus location or orientation, into structured cortical representations within visual cortex. In carnivores and primates, these cortical representations are systematically distributed into functional maps of discrete columnar modules. We were interested in testing the hypothesis whether the functional responses of neural populations remain largely stable in cortical maps (Chapman et al., 1996; Godecke et al., 1997; Sengpiel et al., 1998) or undergo systematic functional changes, as is predicted by various computational studies modeling the self-organization of neuronal circuits (Wolf and Geisel, 1998; Shouval et al., 2000; Alexander et al., 2004; Wolf, 2005; Oster and Bressloff, 2006; Wright et al., 2006; Schnabel et al., 2008; Wright and Bourke, 2008).

First we investigated how the functional representation of visual cortex maps in ferrets matures during early postnatal development and into adulthood. We found that areal growth and shrinkage of the visual cortex corresponded with commensurate changes in cortical column spacing, which indicates a lack of functional reorganization in maps of the visual cortex; thus, the functional organization of cortical maps is normally stable throughout the lifespan of ferrets. Secondly, we sought to characterize the extent of neural plasticity in the ferret visual system using the classic monocular deprivation paradigm. We show a prolonged age-dependent decline in ocular dominance plasticity, lasting out to approximately a year, whereas previous reports indicated ocular dominance plasticity ended much earlier (Issa et al., 1999). We also show that chronic fluoxetine

treatment could not reinstate ocular dominance plasticity in adult ferrets, unlike it does in adult rats (Bastos et al., 1999; Maya Vetencourt et al., 2008; Maya Vetencourt et al., 2011). And lastly, we studied whether the functional organization of neural circuits constrains plasticity in the visual system. We perturbed the orientation tuning of visual cortex neurons by pairing a visual stimulation with direct intracortical activation of neurons in the visual cortex, and show that plasticity near pinwheel centers is reduced compared to neurons located in linear zones of the orientation map.

Dedicated to my grandfathers,
Bruce Whitney and Roy Banfield

ACKNOWLEDGEMENTS

The past six years have been immense period of growth for me as a person and as a young scientist learning the ropes of doing scientific research. When I arrived in Pittsburgh so many years, I could never have imagined all of the ups and downs of my PhD experience. However, like a wonderful roller coast, it's been an immensely fun ride. I have so many people to thank for their help over the last six years.

First off, I would like to thank my advisor Justin Crowley for his steadfast support of me over the years. I have learned so much from him, and I have always appreciated that he's been standing in my corning encouraging me to be a better scientist. Secondly I also want to acknowledge the generous support of Seong-gi Kim who took me into his lab two years ago, so that I could finish my PhD dissertation. I am immensely grateful to Seong-gi for not only allowing me into his lab, but letting me continue the research I had started in Justin's lab. Without the help and guidance of both Justin and Seong-gi, I wouldn't be where I am today.

Additionally, I want to acknowledge Nathan Urban, who is on my committee. He's been supportive of me over the years, and I appreciate his help in particular when I transitioned between the labs of Justin and Seong-gi. Fred Wolf, my IGERT advisor, has also been a steady source of wisdom, and I greatly treasure the one month I was able to spend in your lab (Gottingen, Germany). And the skiing in Austria was wonderful!

Next, I would like to thank all of my collaborators from the Crowley, Kim, and Wolf labs. I'd like to throw out a big shout out to Santosh, Corey, Alberto, Hiro, Chepe, and Wolfgang who were not only wonderful colleagues to work with through the years, but amazing friends! You guys are wonderful, and my life is the better for having met you all.

Finally I want to thank my family. My parents (Mark and Annette) and my twin brother (Richard) have always been there encouraging me, as have my grandparents. You not only encouraged and supported me as I pursued my PhD work, but also through the many long years of my K-12 and undergrad education. Thanks so much! I never would have made it this far without your continued support. Words cannot express how lucky I feel to have had such as wonderfully supportive family.

Table of Contents

TABLE OF FIGURES

1 INTRODUCTION

Humans, and other mammals with highly developed visual systems, rely heavily upon visual perception for awareness of their general surrounding environment. However, the processes by which animals translate visible light into a meaningful representation, requires reducing complicated visual stimuli in the visual scene into its most basic components. Mechanistically vision is a process by which photons first activate retinal photoreceptors in the eye, and that visual input is then transduced into structured neural responses that are propagated along the visual pathway: initially from the retina, to the lateral geniculate nucleus, and then finally arriving into the neocortex.

An elaborate network of neurons along the visual pathway topographically maps fundamental stimulus features in visual space into structured cortical representations within visual cortex (V1 and V2). In carnivores and primates, these cortical representations are systematically distributed into maps of discrete columnar modules. Functional maps of visual cortex are traditionally considered stable entities *unless* an experimental animal is subjected to altered visual experience during the developmental critical period (Hubel and Wiesel, 1970; Daw et al., 1992; Crair et al., 1997a; Issa et al., 1999; Sengpiel et al., 1999; White et al., 2001b; Tanaka et al., 2004; Li et al., 2006; Smith and Trachtenberg, 2007). However, recent data suggests that the organization of these functional maps may be more dynamic than previously thought and that the temporal boundaries of the critical period may be more flexible than previously believed (Das and Gilbert, 1995; Coppola and White, 2004; Hofer et al., 2006; Pizzorusso et al.,

2006; Keck et al., 2008; Lehmann and Lowel, 2008; Li et al., 2008b; Maffei and Turrigiano, 2008; Maya Vetencourt et al., 2008; Kaschube et al., 2009; Keil et al., 2010).

But why are functional maps useful to study at all? It's important to emphasize functional maps are convenient instantiations of brain architecture that can provide valuable knowledge into the function and connectivity of the local microcircuits they represent. Justin Crowley, one of my PhD advisors, and I were interested in testing the hypothesis whether the functional responses of neural populations remain largely stable (Chapman et al., 1996; Godecke et al., 1997; Sengpiel et al., 1998) or undergo systematic functional reorganization, as is predicted by various computational studies modeling the self-organization of neuronal circuits (Wolf and Geisel, 1998; Shouval et al., 2000; Alexander et al., 2004; Wolf, 2005; Oster and Bressloff, 2006; Wright et al., 2006; Schnabel et al., 2008; Wright and Bourke, 2008).

We then set out to design experiments to test this hypothesis. For all our studies, we chose to use the ferret as our animal model. The ferret is advantageous to study the development of the visual cortex, as it’s born with a developmentally immature visual system due to a shorter gestational period (as compared to cats). And like humans and cats, ferrets possess a highly developed visual system (Bonhoeffer and Grinvald, 1991; Hubener et al., 1997; Rao et al., 1997; Issa et al., 1999; Yacoub et al., 2007; Yacoub et al., 2008). Also in some cases, related studies have already been done in rat and cat visual cortex; thus, we thought it would be informative to contrast findings in a smaller

carnivore (ferrets) with that of a larger one (cats), as well as with an animal that has a less developed visual system (rat).

In our first set of experiments, we investigated how the organization, or functional representation, of visual cortex maps matures during early postnatal development and into adulthood. This time coincides with the developmental critical period of plasticity (Chapman and Stryker, 1993; Chapman et al., 1996; Issa et al., 1999; White et al., 2001b; Li et al., 2006), a period of rapid maturation in visual responses and significant growth of the visual cortex. We were specifically interested in whether growth of the areal boundaries of the visual cortex might induce functional reorganization, as it does in cats (Keil et al., 2010). Secondly, we then sought to characterize the extent of neural plasticity in the ferret visual system. For answering this question, we adopted the classic monocular deprivation model to study the age-dependent decline in critical period plasticity and then investigated whether neural plasticity could be reinstated in adult ferrets with the pharmacological drug fluoxetine. And lastly, we were interested whether the functional organization of neural circuits constrains plasticity in the visual system (ie are some regions of the visual cortex more plastic than others). To investigate this question, we perturbed the orientation tuning of visual cortex neurons by pairing a visual stimulation with direct intracortical activation of neurons in the visual cortex.

1.1 OVERVIEW OF DATA CHAPTERS

Before introducing some useful background, I will first provide a more detailed overview of the three data chapters, and additional rationale for conducting these studies:

1.1.1 Chapter 2 - Bidirectional, Age-Dependent Changes in Columnar Organization of Ferret Visual Cortex

Despite potential for considerable activity dependent modification from normal visual experience, longitudinal *in vivo* studies suggest neural circuits representing central visual space remains stable over the developmental critical period (Chapman et al., 1996; Godecke et al., 1997; Sengpiel et al., 1998). But questions remain as to how functional maps of the visual cortex, such as ocular dominance and orientation selectivity, respond during the developmental critical period to significant cortical growth in visual cortex (Purves and LaMantia, 1993; Duffy et al., 1998; Drenhaus et al., 2006; Keil et al., 2010). Two hypotheses have been proposed to account for these changes (Duffy et al., 1998; Oster and Bressloff, 2006; Keil et al., 2010). The first suggests the length of neuronal processes, such as axons and dendrites, scale linearly with neocortical growth (the balloon model), while the second indicates that synaptic connections must reorganize between neurons such that the length of axons and dendrites remains largely constant. As the two hypotheses dramatically differ from each other, they have important ramifications in our understanding how neural circuits organize and react to gross structural changes in brain size.

Most longitudinal imaging studies of cortical columns in cats and ferrets (Chapman et al., 1996; Godecke et al., 1997; Sengpiel et al., 1998) suggest the general layout of functional maps is stable and does not change substantially. In absence of other data, this stability might then be considered support for the “balloon” model being the most likely candidate

model. In support of the possibility, two studies in macaque monkey show that ocular dominance columns and blobs exhibit a 16-20% increase in size (Purves and LaMantia, 1993; Blasdel et al., 1995), which is comparable to the developmental growth of striate cortex (Purves and LaMantia, 1993). However, a key prediction of the balloon model hypothesis is that the cortical column spacing would increase in development. And the vast majority studies analyzing cat orientation and ocular dominance columns have failed to find significant increases in column spacing (Muller et al., 2000; Rathjen et al., 2003; Kaschube et al., 2009; Keil et al., 2010).

Thus, we were interested in determining whether cortical columns in ferrets, a closely related carnivore to cats, exhibited characteristics in support of either the balloon model or growth-related rearrangement. Surprisingly, in this chapter, optical imaging of intrinsic signal demonstrates that orientation, direction, and ocular dominance columns of the ferret visual cortex all undergo an initial expansion until ~PD60 (postnatal day), and then later shrinkage that is age-dependent. We also tracked the development of cortical columns longitudinally in a sub-set of animal experiments, and found little evidence for substantial columnar reorganization. Our work here suggests that unlike cat visual cortex, cortical columns in ferret visual cortex instead behave more consistently with the "balloon" model.

1.1.2 Chapter 3 - Impact of Monocular Deprivation and Systemic Fluoxetine Treatment in Adult Ferret Visual Cortex

Monocular deprivation has long been a favored tool by neuroscientists to probe activity dependent modification in neocortical circuits (Hubel and Wiesel, 1965, 1970; Gordon and Stryker, 1996). Monocular deprivation involves the unilateral closure of one eye through lid suture. The response properties of neurons in visual cortex are sensitive to alterations in sensory experience during an early critical period that begins after opening (Hubel and Wiesel, 1965, 1970; Daw et al., 1992; Gordon and Stryker, 1996; Issa et al., 1999). Cortical neurons can shift their ocular dominance during this sensitive period if one eye is deprived of vision through monocular deprivation. Ocular dominance shifts in the critical period involve decreases in the cortical response to the deprived eye, and a subsequent strengthening of the cortical response to the open eye (Frenkel and Bear, 2004; Mrsic-Flogel et al., 2007). Ocular dominance plasticity has traditionally been considered a developmental process restricted to younger animals, but recent reports indicate that ocular dominance plasticity lasts well into adulthood in rodents (Sawtell et al., 2003; Pham et al., 2004; Tagawa et al., 2005; Hofer et al., 2006; Lehmann and Lowel, 2008; Sato and Stryker, 2008).

A growing number of studies indicate that adult plasticity in the visual system can be enhanced through modulation of major neurotransmitter systems, such as nicotinic acetycholine signaling through a Lynx1 knockout (Morishita et al., 2010), serotonin signaling through fluoxetine treatment or direction infusion of serotonin (Maya Vetencourt et al., 2008; Maya Vetencourt et al., 2011; Bachatene et al., 2013), and

noradrenalinergic signaling through L-threo-3,4-dihydroxyphenylserine treatment (Mataga et al., 1992). These pioneering experiments demonstrate that ocular dominance plasticity in adult animals can be enhanced by combining monocular deprivation and manipulation of major neurotransmitter systems. Conversely, impairment of these same neuromodualtory systems have been shown to inhibit ocular dominance plasticity (Bear and Singer, 1986; Gu and Singer, 1995; Maya Vetencourt et al., 2011). We were particularly interested in chronic fluoxetine treatment, as fluoxetine is a potentially non-invasive therapeutic treatment for humans suffering amblyopia. But so far to our knowledge, chronic fluoxetine treatment has only been demonstrated in rats (Bastos et al., 1999; Maya Vetencourt et al., 2008; Maya Vetencourt et al., 2011), and it remains an open question whether re-instatement of adult ocular dominance plasticity could be achieved in another animal model. Indeed, anatomical studies of the neocortical layers of visual cortex show dramatically different innervation patterns of serotoninergic fibers across mammals (Lidov et al., 1980; Morrison et al., 1982; Foote and Morrison, 1984; Gu et al., 1990; Hornung et al., 1990; Voigt and de Lima, 1991). Thus, these differences suggest that modulation of serotonin signaling through chronic fluoxetine treatment might be specific-specific, and reinstatement of adult ocular dominance plasticity could depend on the animal model.

So in this chapter, we investigated long-term monocular deprivation in adult ferrets *in vivo*. The ferret visual system is a well-studied animal model of early visual system development (Chapman and Stryker, 1993; Chapman et al., 1996; Durack and Katz, 1996; Crowley and Katz, 1999; Issa et al., 1999; Ruthazer et al., 1999; White et al., 1999;

Li et al., 2006) and recently has become a popular model for ocular dominance plasticity (Issa et al., 1999; Liao et al., 2002; Medina et al., 2003; Liao et al., 2004; Krahe et al., 2005; Medina and Ramoa, 2005; Krahe and Medina, 2010; Paul et al., 2010; Mower et al., 2011; Yu et al., 2011; Paul and Medina, 2012). Additionally, ferrets possess a highly developed visual system like human and cats (Hubel and Wiesel, 1962; Horton and Hedley-Whyte, 1984), as the spatial organization of ocular responses are systematically clustered together into ocular dominance columns across the tangential plane of visual cortex (Ruthazer et al., 1999; White et al., 1999). Ocular dominance columns are advantageous to study, since imaging studies can track ocular dominance columns structures longitudinally (Sengpiel et al., 1998; Shtoyerman et al., 2000). For our study we longitudinally tracked ocular dominance plasticity using optical imaging of intrinsic signal. We observed a gradual, age-dependent decline in ocular dominance plasticity with significant ocular dominance shifts being induced in young adult ferrets (less than 6 months old). Additionally, chronic fluoxetine treatment in both young adult and adult ferrets did not re-instate ocular dominance plasticity. Instead we paradoxically detected a "reverse" ocular dominance shift in young adult ferrets, in which the deprived eye responses were stronger than the open eye responses. Thus, fluoxetine-mediated reinstatement of ocular dominance plasticity appears to be species-specific, and its action in other animal models, as well as humans needs to be assessed carefully.

1.1.3 Chapter 4 - Visual cortex plasticity depends on the local functional architecture

In Chapter 3, we looked at how alterations in visual experiences with monocular

deprivation can induce large scale changes in the ocular dominance map. In this chapter, we revisited neural plasticity, but this time focused on the orientation preference map. Like the ocular dominance map, the orientation preference map smoothly changes across the cortical surface, but is also systematically punctuated by heterogeneous regions, in which orientation preference converges at fracture lines or around singularities called pinwheel centers ((Bonhoeffer and Grinvald, 1991; Ohki et al., 2006). Thus, depending on a neuron's location in the orientation preference map, neurons may integrate intracortical synaptic input from a very narrow range of orientation preferences (iso-orientation domains) or from a much broader range (pinwheel centers and fracture lines). Thus, studying neural plasticity in the context of the orientation preference provides an opportunity to study how local intracortical interactions might play an important modulatory role.

Prior studies have indicated that the orientation preference of neurons in the cat visual cortex can be altered using plasticity-inducing paradigms (Fregnac et al., 1988; Dragoi et al., 2000; Dragoi et al., 2001; Schuett et al., 2001; Godde et al., 2002). Moreover two of these studies demonstrated that heterogeneity in the orientation preference of the local neural circuitry can constrain neural plasticity in the visual cortex: Dragoi et al. (2001) found that neurons in the visual cortex near pinwheel centers more strongly shift their orientation preference away from the orientation of an adapting stimulus. Schuett et al. (2001) demonstrated that pairing a brief visual stimulus with electrical microstimulation of the visual cortex was capable of inducing local shifts in orientation preference of neurons. However, Schuett et al. found that neurons near pinwheel centers exhibited *less*

plasticity than neurons in iso-orientation domains.

Taken together these two previous studies suggest that functional architecture is an important determinant in whether neurons can modify their functional responses. However, the above studies disagreed on the interaction between the plasticity produced and pinwheels centers, in addition to being limited in the spatial pattern by which the visual cortex could be stimulated. To address some of these challenges, Channelrhodopsin-2 (ChR2) provides the exciting possibilities of spatial patterned transfection and/or spatially patterned activation (Nagel et al., 2003; Boyden et al., 2005; Arenkiel et al., 2007). Here we show that the orientation preference map constrains the degree of neural plasticity. Specifically, we induced local shits in orientation preference tuning in ferret visual cortex by pairing visual stimulation with direct intracortical stimulation of layer 2/3 neurons. Intracortical stimulation was achieved using either: a.) optical stimulation of cell populations transfected with ChR2 or b.) electrical stimulation with a tungsten electrode. We demonstrate with intrinsic signal optical imaging and two-photon calcium imaging that pairing-induced changes in the orientation tuning of neurons is greatest when local cortical activation is far from regions with abrupt changes in orientation preference (pinwheels and fractures). Our results suggest pairing-induced plasticity is greatest whenever co-activated cell populations share similar functional properties and that local cortical connections play an important role in modulating the efficacy of non-associative learning in visual cortex.

.

1.2 BACKGROUND

1.2.1 Functional Maps of Visual Cortex

Electrophysiological recordings and imaging studies exploring the visual system have revealed multiple functional maps in the visual cortex. These maps are stimulus-selective population activity distributed spatially across visual cortex (Bonhoeffer and Grinvald, 1991; Shmuel and Grinvald, 1996; Issa et al., 2000). Functional maps are believed to arise from the spatial-temporal integration of receptive fields from each eye (Hubel and Wiesel, 1962; Priebe and Ferster, 2008). Receptive fields are distinct locations in visual space, in which the presence of a stimulus alters a neuron's activity. Visual cortex neurons act as spatiotemporal filters, as they are also particularly sensitive to the structural statistics of a visual stimulus. Thus, not only are neurons selective for visual stimuli in specific regions of the visual field, neurons respond selectively to visual stimuli within a narrow range of orientations, directions of motions, spatial frequencies, and temporal frequencies (Basole et al., 2003; White and Fitzpatrick, 2007; Issa et al., 2008).

The fundamental physiological map is the retinotopic map, a topographic representation of an animal's visual field across visual cortex neurons (Hubel and Wiesel, 1962; Blasdel and Salama, 1986). The retinotopic map reflects the precise and coordinated organization of cortical neurons' receptive fields (Figure 1a-b). Other functional maps are overlaid on the retinotopic map, as visual cortex neurons respond preferentially to other basic features of a visual stimulus. One of these maps is ocular dominance, which denotes cortical areas preferentially driven by eye-specific stimuli (Figure 1c). Other characteristic maps, such as orientation and direction preference (Figure 1d-e), reflect a

neuron's sensitivity to the spatiotemporal profile of a visual stimulus (Basole et al., 2003; Baker and Issa, 2005; Mante and Carandini, 2005).

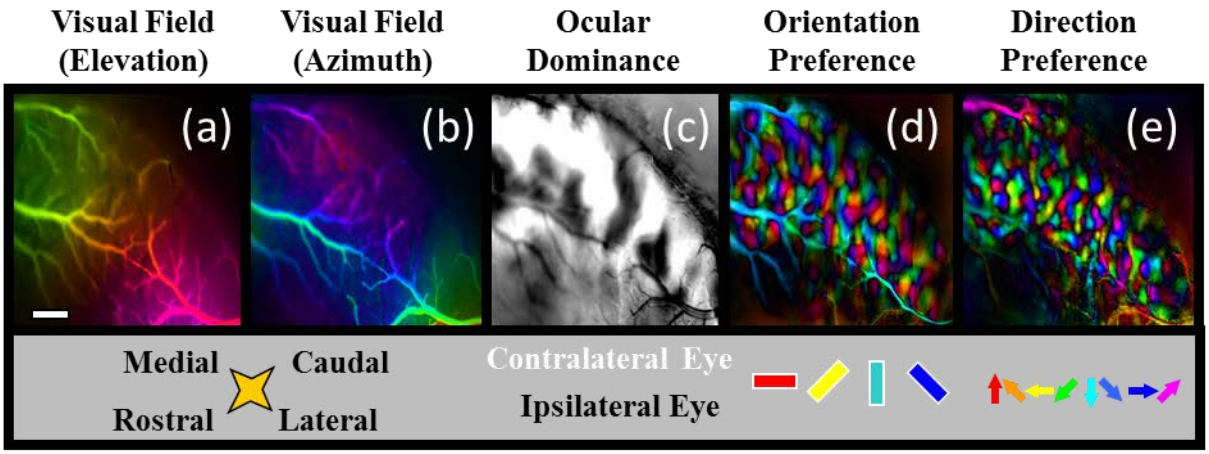

Figure 1-1: Example functional maps of the ferret visual cortex as assayed by optical imaging of intrinsic signal.
Saturation in all subsequent images denotes response magnitude. (a) Polar response of the retinotopic visual field map (mapped along elevation). Hue denotes the preferred location in the visual field. (b) Like (a), except a polar response of the retinotopic visual field map (mapped along azimuth). (c) Ocular dominance difference map (white pixels have a stronger contralateral eye response, while black pixels display a stronger ipsilateral eye response). (d) Polar response of the orientation preference map. Hue denotes the preferred orientation of a visual stimulus. (e) Polar response of the direction preference map. Hue denotes the preferred direction (or motion) of a visual stimulus. Scale bar is 1mm.

Functional maps superimpose upon each other and arrange in a mutually *dependent* manner. Feature edges of different maps tend to superimpose orthogonally upon each other, such as orientation singularities tending to be centered on ocular dominance peaks (Crair et al., 1997b, a; Hubener et al., 1997; Kim et al., 1999; Nakagama et al., 2006). This distinctive geometric organization in visual cortex maximizes coverage of stimulus properties across all of visual space and minimizes the amount of cortical wiring required (Swindale et al., 2000; Xu et al., 2007; Issa et al., 2008). While geometric relationships have been confirmed in macaques and cats (Bartfeld and Grinvald, 1992; Hubener et al., 1997), supporting data from ferrets has proven more ambiguous (Issa et al., 1999; White et al., 2001a; Yu et al., 2005). In chapter 4, we also confirm that there appears to be a weaker geometric relationship between the location of pinwheel centers and the centers of ocular dominance columns.

1.2.2 Columnar Organization in Functional Maps

In carnivores and primates, neurons sharing similar response properties systematically cluster together into discrete columnar modules across the tangential plane of visual cortex. These modules have a radial cross-section and span vertically through the cortical lamination (Hubel and Wiesel, 1962; LeVay et al., 1978; Blasdel and Salama, 1986). Cortical columns can be thought to represent cortical area that is responsive to a visual stimulus. The number, shape, and size of columns in visual cortex systematically vary depending on the animal species; however, there is significant inter-areal variation in column spacing. For example, ocular dominance columns in primates and humans have more of a stripe-like appearance, whereas ocular dominance columns in cats and ferrets

are patchier (Blasdel and Salama, 1986; Bonhoeffer and Grinvald, 1991; Issa et al., 1999; Adams et al., 2007). The average column spacing for ocular dominance and orientation columns is 900μm in ferrets and 1000μm in cats (Sengpiel et al., 1998; Issa et al., 1999; Kaschube et al., 2002; Rathjen et al., 2002; Kaschube et al., 2003; Kaschube et al., 2009; Keil et al., 2010). Though in ferrets, ocular dominance columns near the V1/V2 border tend to be much larger than 1mm (Ruthazer et al., 1999; White et al., 1999).

A distinctive feature of functional maps with columnar organization (eg ocular dominance, orientation preference, and direction preference) is the presence linear zones, regions of gradual change in local response properties along the tangential plane of cortical lamination (Bosking et al., 2002). Thus, while columns appear to represent an isotropic representation for a specific stimulus feature, the degree of cortical activation and neuronal tuning width varies within a column. Column centers represent regions most strongly activated by a stimulus and have narrow tuning widths, while neurons located progressively farther away from column centers are less strongly activated by the same stimulus due to offsets in their preferential tuning and broader tuning curves (Obermayer and Blasdel, 1993; Hubener et al., 1997; Schummers et al., 2002; Nauhaus et al., 2008). In effect, a gradient of cortical activation exists across cortical columns.

The local spatial structure of cortical columns makes them convenient instantiations of brain architecture to study. In chapter 2, we take advantage of the modular structure of cortical columns to study whether the layout of functional maps changes due to brain growth. Two different hypotheses have been proposed (Duffy et al., 1998; Oster and

Bressloff, 2006; Keil et al., 2010), and the column spacing between cortical columns is a central predictor to differentiate between the hypotheses.

1.2.3 Functional Architecture of Orientation and Direction Preference Maps

The response properties of neurons gradually shift across most regions in functional maps (ie linear zones). But both orientation and direction preference maps are also systematically punctuated by map locations where the orientation or direction preference of neurons changes rapidly. In these regions, orientation and direction columns with different preferences converge around orientation singularities, called pinwheel centers, or along line fractures (Blasdel and Salama, 1986; Bonhoeffer and Grinvald, 1991; Weliky et al., 1996; Rao et al., 1997; Ohki et al., 2006).

Electrophysiology has shown that sub-threshold membrane potential responses are more broadly tuned near pinwheel centers than in iso-orientation domains (i.e. the centers of orientation columns). This finding indicates neurons nearer to pinwheel centers receive more heterogeneous synaptic input (Maldonado et al., 1997; Schummers et al., 2002; Marino et al., 2005). However, there is less agreement in the literature whether the broadly tuned sub-threshold inputs at pinwheel centers also results in broadly tuned spiking responses (Ohki et al., 2006; Nauhaus et al., 2008; Schummers et al., 2008). Or whether the sub-threshold input is transformed into sharply tuned spiking responses (Maldonado et al., 1997; Schummers et al., 2002; Marino et al., 2005). As accurately targeting a neuron at a pinwheel center is non-trivial task, it's likely that the more recent reports suggesting broadly tuned spiking responses at pinwheel centers are more accurate.

This is because two-photon calcium imaging and electrode arrays were used over targeted electrode recordings. These techniques have the advantage over targeted electrode recordings, since a cell's location in the orientation preference can either: be directly observed using two-photon calcium imaging or indirectly inferred by maximizing the orientation preference of unit responses in an electrode array with the orientation map.

The arrangement and functional properties of pinwheel centers and line fractures are of great interest in this dissertation. In chapter 2, we took advantage of the periodic placement of pinwheel centers in the visual cortex. Computational studies have suggested that refinement of orientation preference maps results in the creation/annihilation of pinwheels (Wolf and Geisel, 1998; Wright et al., 2006; Kaschube et al., 2010); thus, any changes in the local pinwheel density per orientation column is likely to indicate functional reorganization. Additionally in data chapter 4, our key finding is that neural plasticity is weaker at pinwheel centers. One of our interpretations of these findings is that cell populations nearer to pinwheel centers likely have a higher spiking threshold (Schummers et al., 2007).

1.2.4 Functional Architecture of Ocular Dominance Maps

Ocular dominance maps of primary visual cortex (V1) can be described as having a monocular band representing the peripheral regions of the contralateral visual field (Wiesel et al., 1974; White et al., 1999; Schmidt et al., 2002). The monocular zone receives only input from the contralateral eye. The monocular zone then transitions into V1 regions corresponding to the central, contralateral visual field. In this zone ocular

dominance columns are intermingled together, as both contralateral and ipsilateral eye input project into this area (Wiesel et al., 1974; Ruthazer et al., 1999; White et al., 1999; Schmidt et al., 2002; Kaschube et al., 2003; Keil et al., 2010).

Normally the V1 binocular zone then transitions into the monocular V2 ipsilateral-eye segments that represent the central, ipsilateral visual field. This transition zone denotes a reversal of the retinotopic map and functionally defines the V1/V2 border (White et al., 1999). However, in ferrets there is an additional V1 monocular band inserted between the V1 binocular zone and the V2 ipsilateral eye band (Redies et al., 1990; Ruthazer et al., 1999; White et al., 1999). This is a V1 contralateral eye band representing the central, ipsilateral visual field (White et al., 1999). Thus, the structure of ocular dominance domains in a ferret's V1 can be roughly broken down into three regions (White et al., 1999). These regions are (see Figure 2) :

- Region I - A monocular zone of the contralateral eye representing the peripheral, contralateral visual field.
- Region II - A binocular zone of the central, contralateral visual field. Cortical columns in the binocular zone tend to be on the size of orientation columns and much smaller than their counterparts in Region 3.
- Region III - A monocular zone of the contralateral eye processing visual information from the central, ipsilateral visual field. This area intersects with the V2 monocular ipsilateral eye band. The intermingling of these two bands forms much larger and irregularly shaped ocular dominance columns.

Usually only the latter two zones (Regions II and III) are accessible to conventional optical methods *in vivo*, since these areas are exposed on the dorsal surface of the neocortex. Unfortunately much of the binocular zone (Region II) and the monocular zone for the peripheral, contralateral visual field (Region I) are located on the tentorial side of V1. Thus, these areas inaccessible to optical imaging, but can be imaged *in vivo* using fMRI (Moon et al., 2007). A discontinuous, mirror symmetric reversal of the retinotopic map is observed at the V1/V2 border (White et al., 1999). Notably at the V1/V2 border, the orientation selectivity map has been demonstrated to be unaltered despite the retinotopic map being discontinuous and the ocular dominance map undergoing significant structural change (White et al., 2001a).

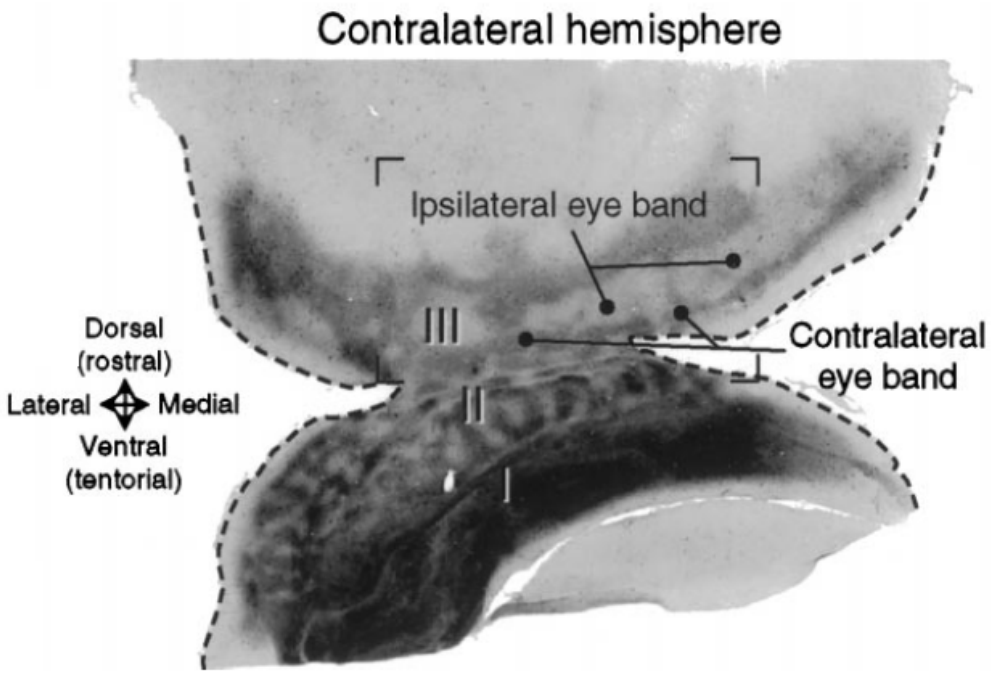

Figure 1-2: Ocular dominance columns revealed by a transneuronal tracer (WGA-HRP). The stained regions denote the contralateral eye, while the lighter regions are unlabeled. The three roman numerals in this figure correspond to the three main regions in ferret

ocular dominance maps (see section 1.2.4). This figures comes from White et al. (White et al., 1999).

1.2.5 The Critical Period and Establishment of Functional Maps

Maps emerge and mature rapidly during postnatal development (Chapman et al., 1996; Godecke et al., 1997; Crair et al., 1998; Issa et al., 1999; Li et al., 2006). Evidence suggests intrinsic cues and retinal waves drive preliminary map organization before eye opening (Crowley and Katz, 1999, 2000; Katz and Crowley, 2002; Dufour et al., 2003; Huberman et al., 2003; Mrsic-Flogel et al., 2005; Torborg et al., 2005). Cortical circuits then subsequently undergo considerable refinement from activity-dependent modification from patterned visual input, particularly during a postnatal critical period of developmental plasticity. The critical period is a limited time when cortical neurons remain highly susceptible to activity dependent modification (Hubel and Wiesel, 1963). The critical period lasts ~3-5 weeks after eye opening in cats and ferrets (Crair et al., 1998; Issa et al., 1999). Activity dependent modification is much weaker after the critical period has concluded (Hubel and Wiesel, 1963; Chapman and Stryker, 1993; Issa et al., 1999). The classic definition of the critical period is the susceptibility of cells to monocular deprivation (ie which simply means that cells responds better to the spared eye and weaken their responses to the monocularly deprived eye). In ferrets, the peak critical period is defined between postnatal day 35-58 (see Figure 3) , which is the time period where ocular dominance shifts are greatest (Issa et al., 1999)..

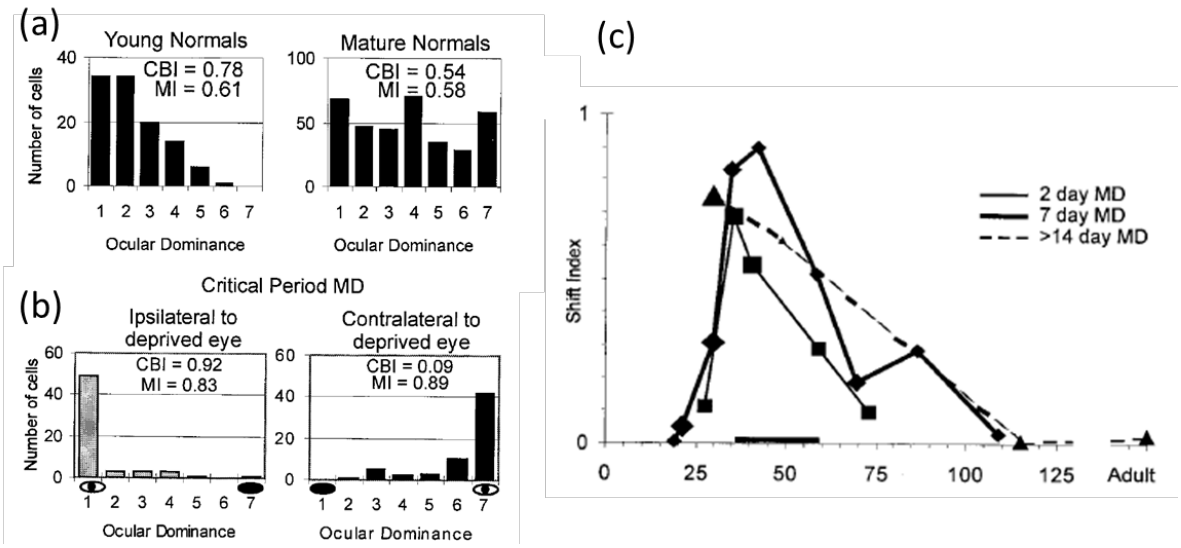

Figure 1-3: Ocular dominance plasticity in the ferret visual cortex, as assayed by electrophysiology.

(a) The ocular dominance of young ferrets (left panel) and adult ferrets (right panel). An ocular dominance bin value of 1 indicates a contralateral bias, while 7 indicates an ipsilateral bias, and 4 indicates binocular responses. Note how the initial contralateral bias in young ferrets is eliminated in adults (0.78 in young animals and 0.54 in adults). **(b)** The ocular dominance of cells after monocular deprivation in the critical period. Notice how cells in the ipsilteral and contralateral hemispheres predominantly only respond to the open eye. **(c)** A developmental plot comparing the strength of ocular dominance shifts. Qualitatively the shift index is a measure how much an animal's visual cortex neurons shift their preferred response towards the spared eye. Specifically, the measure is defined as the difference of contralateral bias index (CBI) of the ipsilateral hemisphere to the deprived eye versus the CBI of the contralateral hemisphere to the deprived eye. The CBI is weighted summation of the 7 ocular dominance bins shown in

(a) and (b). Notice how monocular deprivation experiments begun after PD115 are considered ineffective in this paper. Figures are taken from Issa et al.(Issa et al., 1999).

Immediately after eye opening, map contrast increases, an indirect measure to the strength of cortical activation to visual stimuli and individual neuronal tuning curves become narrower (Chapman and Stryker, 1993; Chapman et al., 1996; Godecke et al., 1997; Sengpiel et al., 1998). Furthermore, anisotropies that intrinsically arise in maps, such as the contralateral bias in ocular dominance maps and cardinal orientation bias in orientation preference maps, moderate to some extent in favor of isotropic representations (Crair et al., 1998; Coppola and White, 2004). Even so, longitudinal imaging studies in cats and ferrets indicate the overall functional organization of ocular dominance and orientation preference maps remains mostly stable over relatively short periods of 1-4 weeks (Chapman et al., 1996; Godecke et al., 1997; Sengpiel et al., 1998). An example of ferret orientation map development is shown in Figure 4 (Chapman et al., 1996). Thus, some researchers suggest an intended function of activity dependent modification during the critical period is to fine-tune maps intrinsically generated in neocortex with most structural changes being subtle (Chapman et al., 1996; Katz and Crowley, 2002; White and Fitzpatrick, 2007).

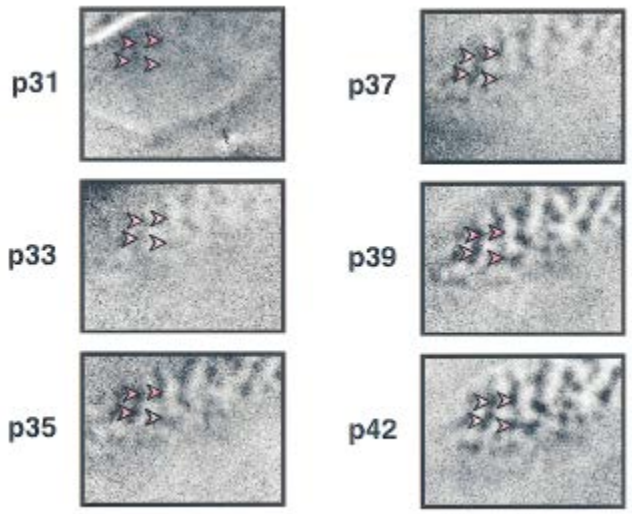

Figure 1-4: An example of the longitudinal imaging of orientation columns in a critical period ferret.

The above picture is tracking the development of the orientation response to a horizontal grating. Notice how at p31 the map contrast is low, and steadily increases over the next 11 days. Additionally, we can observe that the overall functional organization of the columns is stable throughout this period. Figures were taken from Chapman et al. (Chapman et al., 1996).

And despite longitudinal imaging studies suggesting functional maps might remain stable (at least over relatively short-time scales), there is cumulating evidence in cat visual cortex indicating that slow columnar reorganization does indeed occur in developing animals. For example, ocular dominance columns appear to reorganize in a “zig-zag” like manner to accommodate for brain growth (Keil et al., 2010). Likewise orientation columns in different functional areas (e.g. V1 and V2) are progressively matched in size if they correspond to the same region of the visual field, indicating coordinated

reorganization between mutually connected areas (Kaschube et al., 2009).It is worth emphasizing however that the aforementioned studies rely on a single autoradiographic labeled functional map for each animal. Hence, the presence of functional reorganization has not yet been corroborated by longitudinal imaging of the same functional map across different time points.

This discrepancy in the literature concerning the presence of the columnar reorganization was a primary motivator for my research conducted in chapter 2. Various studies suggest the mean size of columns in cats and ferrets do not change (Chapman et al., 1996; Muller et al., 2000; Rathjen et al., 2003; Kaschube et al., 2009; Keil et al., 2010). When taken in context that the areal extent of visual cortex also increases during development (Purves and LaMantia, 1993; Duffy et al., 1998; Drenhaus et al., 2006; Keil et al., 2010), this implies columnar reorganization must incur. Thus, initially we anticipated to verify the presence of functional reorganization in ferret visual cortex. However, this is actually not the case in ferret visual cortex. We instead report that cortical columns in ferrets expand and shrink in size, which is concomitant with the areal changes in visual cortex. In chapter 2, we describe these results in more detail. In fact, when I went back and re-analyzed the column spacing data from Chapman et al., I found that their data in fact supports my observations in Chapter 2.

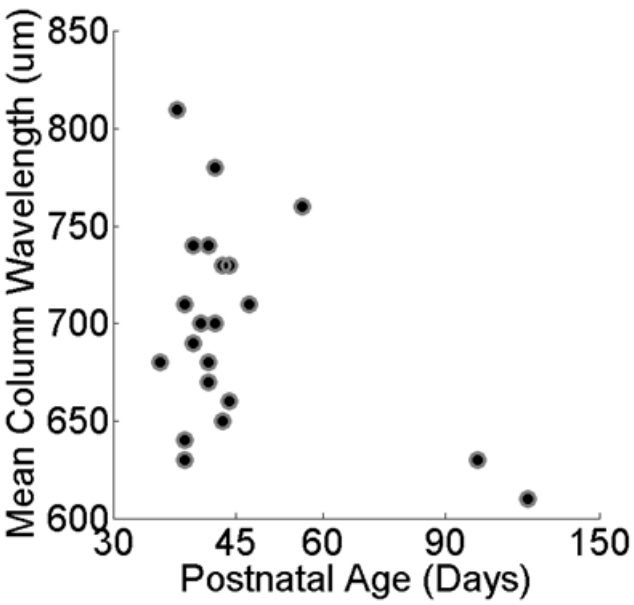

Figure 1-5: Developmental timecourse of column spacing measurements for orientation preference map.

This is the animal data from Chapman et al.. (Chapman et al., 1996). The actual wavelength measurements of column spacing were pulled from Table 1 in Muller et al. (Muller et al., 2000), and I replotted it here. The y-axis is wavelength, since the column spacing measurements were made using a Fourier transform on the orientation maps. Notice how there is a tendency for orientation columns to increase in size from PD30 to PD60. And then also note how the two adult time points have much smaller column wavelength than those at PD45-PD60.

1.2.6 Neural Plasticity Induced By Abnormal Visual Experience

Although functional maps of the visual cortex have been shown to be stable, aberrant sensory experience during the developmental critical period can result in overriding the initial map template. This can (1) profoundly degrade map structure, (2) instruct

organization of abnormal maps, and/or (3) alter how individual neurons represent and process features in the visual world (Chapman and Stryker, 1993; Crair et al., 1997a; Crair et al., 1998; White et al., 2001b; Coppola and White, 2004; Li et al., 2006). Manipulations of animal's visual experience during the critical period have proven remarkably useful for early investigations into activity dependent modification of cortical circuitry. Early studies in the visual system reveal that monocular deprivation, the occlusion of one eye, during a "critical period" can induce an ocular dominance shift. The shift retunes portions of cortical area to respond towards visual stimuli from the open eye, rather than predominantly processing vision from the occluded eye (Wiesel and Hubel, 1963; Hubel and Wiesel, 1965, 1970; LeVay et al., 1978). In contrast, dark rearing studies (ie where animals are initially raised in darkness, rather than in a normal light/dark cycle) display delayed development of functional maps and critical period plasticity (White et al., 2001b; Morales et al., 2002; Coppola and White, 2004; Li et al., 2006), while binocular deprivation results in the degradation of existing functional responses (Crair et al., 1998; White et al., 2001b). Thus, normal visual experience during the critical period is a requirement in maintaining functional responses in the visual cortex.

Orientation and direction selectivity also appear to be susceptible to activity dependent modification during the critical period. For example, stripe rearing causes an animal to favor a specific orientation, which increases the amount of cortical area that responds to that dominant orientation. The cortical enlargement is competitive like ocular dominance plasticity and occurs by readjusting response properties of local cortical circuits to

respond to the dominant orientation rather than the more weakly presented orthogonal orientation (Blakemore and Cooper, 1970; Sengpiel et al., 1999; Coppola and White, 2004; Tanaka et al., 2004). In contrast, direction selectivity develops fundamentally differently than ocular dominance or orientation selectivity. Investigations have shown that the direction selectivity of cortical neurons is not significant before eye opening and actually *requires* patterned visual activity immediately after eye opening to develop (Humphrey and Saul, 1998; Li et al., 2006; Li et al., 2008b).

Several recent reports also indicate that adult plasticity is still possible in rodents using monocular deprivation in conjunction with altering an animal's environment or visual experience (He et al., 2006; Sale et al., 2007), reduction of intracortical inhibition (Sale et al., 2007; Maya Vetencourt et al., 2008; Harauzov et al., 2010), transplant of immature inhibitory interneurons (Southwell et al., 2010), degradation of perineuronal nets with chondroitinase ABC (Pizzorusso et al., 2002), and disruption of the OTX2 homeoprotein that reduces the in vivo expression of paravalbumin cells and perineuronal nets (Sugiyama et al., 2008; Spatazza et al., 2013). A common theme from all these studies is that the reactivation of adult ocular dominance plasticity appears to involve finely modulating the ratio of cortical inhibition to excitation within a specific ratio to be permissive for ocular dominance plasticity (Hensch, 2005). Thus, this appears to require an enhancement of inhibition to begin the critical period in young animals, while a net reduction of cortical inhibition is required to reinstate ocular dominance plasticity in adults (Fagiolini and Hensch, 2000; Morales et al., 2002; Hensch, 2005; He et al., 2006;

Maya Vetencourt et al., 2008; Morishita and Hensch, 2008; Harauzov et al., 2010; Huang et al., 2010).

Additionally, a growing number of studies indicate that adult plasticity in the visual system can be enhanced through modulation of major neurotransmitter systems, such as nicotinic acetycholine signaling through a Lynx1 knockout (Morishita et al., 2010), serotonin signaling through fluoxetine treatment or direction infusion of serotonin (Maya Vetencourt et al., 2008; Maya Vetencourt et al., 2011; Bachatene et al., 2013), and noradrenalinergic signaling through L-threo-3,4-dihydroxyphenylserine treatment (Mataga et al., 1992). These pioneering experiments demonstrate that ocular dominance plasticity in adult animals can be enhanced by combining monocular deprivation and manipulation of major neurotransmitter systems. Conversely, impairment of these same neuromodualtory systems have been shown to inhibit ocular dominance plasticity (Bear and Singer, 1986; Gu and Singer, 1995; Maya Vetencourt et al., 2011).

In chapter 3, we were particularly interested in chronic fluoxetine treatment, as fluoxetine is a potentially non-invasive therapeutic treatment for humans suffering amblyopia. But so far to our knowledge, chronic fluoxetine treatment has only been demonstrated in rats (Maya Vetencourt et al., 2008), and it remains an open question whether re-instatement of adult ocular dominance plasticity could be achieved in another animal model. Indeed, anatomical studies of the neocortical layers of visual cortex show dramatically different innervation patterns of serotoninergic fibers across mammals (Lidov et al., 1980; Morrison et al., 1982; Foote and Morrison, 1984; Gu et al., 1990; Hornung et al., 1990;

Voigt and de Lima, 1991). Thus, these differences suggest that modulation of serotonin signaling through chronic fluoxetine treatment might be specific-specific, and reinstatement of adult ocular dominance plasticity could depend on the animal model. Indeed in chapter 3, we found that ocular dominance plasticity was not restored in ferrets. This suggests that although modulation of the major neurotransmitter systems is a valid approach to reinstate adult ocular dominance plasticity, species differences are a major concern. This is especially problematic in successfully translating the aforementioned research into the development of a therapeutic strategy to treat amblyopia in humans.

1.2.7 Underlying Neuronal Organization Resulting In Map Structure

Seminal studies of the visual system suggest cortical neurons become tuned to the spatial location and spatiotemporal properties of stimuli through the structured organization of feedfoward projections, namely retinogeniculate and thalamocortical connections (Hubel and Wiesel, 1962; Chapman et al., 1991; Ferster et al., 1996). A controversial subject, however, is the precise role that intracortical connections play in the proper functioning of neuronal response selectivity. Two major hypothesizes suggested to account for the response properties of cortical neurons in primary visual cortex are: 1.) lateral intracortical interactions through long-range lateral connections (Ringach et al., 1997; Shapley et al., 2003; Wolf, 2005) *and/or* 2.) feedforward thalamic input with spiking threshold (Hubel and Wiesel, 1962; Chung and Ferster, 1998; Priebe and Ferster, 2008).

Evidence supporting the first hypothesis is that clustering of layer 2/3 lateral connections linking orientation columns with similar orientation selectivity in V1 correlates well with

the emergence of orientation selectivity in visual cortex (Gilbert and Wiesel, 1983; Callaway and Katz, 1990; Chapman et al., 1996; Durack and Katz, 1996; Bosking et al., 1997). Additionally, some studies indicate a cortical contribution to the orientation tuning of cortical neurons and that massive inactivation of inhibitory intracortical neurons broadens tuning (Sillito, 1975; Sato et al., 1995, 1996; Chung and Ferster, 1998). However, other studies support the later hypothesis and indicate that the cortical contribution, as far as lateral inhibition, may provide little in the way of actual orientation tuning; instead cortical interneurons are suggested to raise the spiking threshold (Priebe et al., 2004; Sohya et al., 2007; Priebe and Ferster, 2008). One study may reconcile these disparate observations (Nauhaus et al., 2009). The study makes a strong case that feedforward thalamic input appears to dominate cortical responses in the presence of high contrast stimuli, whereas lateral connections become more active with low-contrast visual stimuli (Field et al., 1993; Kapadia et al., 1995; Nauhaus et al., 2009).

In this dissertation, we were primarily interested in investigating intracortical connectivity in the context of neural plasticity. And the functional architecture of the orientation preference affords the opportunity to study indirectly lateral connections. As mentioned in an earlier section, the orientation preference map smoothly changes across the cortical surface, and is systematically punctuated by heterogeneous regions, in which orientation preference converges at fracture lines or around singularities called pinwheel centers ((Bonhoeffer and Grinvald, 1991; Ohki et al., 2006). Thus, neurons integrate intracortical synaptic input from a very narrow range of orientation preferences (iso-orientation domains) or from a much broader range (pinwheel centers and fracture lines).

And this functional organization has not only profound influences on the orientation tuning for neurons (Maldonado et al., 1997; Schummers et al., 2002; Marino et al., 2005; Ohki et al., 2006; Nauhaus et al., 2008; Schummers et al., 2008), but also the ability for neurons to adaptively alter their functional properties.

Indeed some studies have indicated that the orientation preference of neurons in the cat visual cortex can be altered using plasticity-inducing paradigms (Fregnac et al., 1988; Dragoi et al., 2000; Dragoi et al., 2001; Schuett et al., 2001; Godde et al., 2002). But in two of these studies, the local neural circuitry constrained plasticity in the visual cortex. Specifically one group found that found that neurons in the visual cortex near pinwheel centers more strongly shifted their orientation preference away from the orientation of an adapting stimulus (Dragoi et al., 2001). In contrast, Schuett et al. (2001) demonstrated that pairing a brief visual stimulus with electrical microstimulation of the visual cortex was capable of inducing local shifts in orientation preference of neurons. However, Schuett et al. found that neurons near pinwheel centers exhibited *less* plasticity than neurons in iso-orientation domains.

These studies point to the intracortical connectivity being an important determinant in whether neurons can adaptively alter their orientation preferences. However, because the above studies disagreed on the interaction between the plasticity produced and pinwheels centers, we were interested in exploring this topic further in chapter 4. Although discussed in more detail in chapter 4, we were able to induce plasticity by pairing visual stimulation with direct intracortical stimulation of layer 2/3 neurons (Fregnac et al., 1988;

Schuett et al., 2001). We demonstrated this with intrinsic signal optical imaging and two-photon calcium imaging and showed that pairing-induced changes in the orientation tuning of neurons is greatest when local cortical activation is far from regions with abrupt changes in orientation preference (pinwheels and fractures). Directionally this plasticity was attractive, as local neurons of the visual cortex shifted their orientation preference towards the paired orientation, which is consistent with previous reports in the second study we described (Schuett et al., 2001). However, if we intracortically stimulated near pinwheel centers, we began seeing repulsive shifts in orientation preference away from the paired orientation that more closely resembled those observed in the first study (Dragoi et al., 2001). Our results, taken in the context of the work by Dragoi et al. (2001) and Schuett et al., (2001), suggest then that pinwheel centers might not necessarily be less plastic. Rather it seems that activity dependent modification in regions of the visual cortex with broad-tuned intracortical connections (e.g. pinwheels) is different from regions with narrowly tuned intracortical connectivity (iso-orientation domains).

2 Bidirectional, Age-Dependent Changes in Columnar Organization of Ferret Visual Cortex

2.1 ABSTRACT

Neocortical areas undergo dynamic changes in size throughout the lifetime of mammals; however, relatively little is known about how the functional layout of cortical circuits and modular/columnar processing units react to cortical growth and shrinkage. Here we show that in the ferret, modest scale reorganization does occur as the brains grows. As revealed by optical imaging of intrinsic signal, we demonstrate that cortical columns in three functional maps of the visual cortex (orientation preference, direction preference, and ocular dominance) all undergo an initial expansion until around postnatal day 60, and then begin to subsequently shrink. Cortical columns expand in a largely isotropic manner, but shrinkage was anisotropic and most pronounced along the medial-lateral axis. In a subset of experiments, we imaged functional maps longitudinally in young adult ferrets, with imaging experiments separated by multiple weeks. The chronic imaging experiments corroborated the observation of anisotropic shrinkage of the visual cortex, and indicated that the overall layout of the functional map did not change. Overall these results suggest the intrinsic functional organization of ferret visual cortex is robust and, unlike cats, does not undergo substantial morphological reorganization from brain growth or shrinkage. Rather these changes are more consistent with a “balloon” inflation/deflation model paradigm, in which gross areal increases and decreases in visual cortex are accompanied by compensatory expansion and shrinkage of cortical columns

respectively. Additionally, our imaging data suggests cortical shrinkage in the ferret neocortex might reflect an ongoing ontogenetic process, rather than merely a transitory developmental “overshoot.”

2.2 INTRODUCTION

The mammalian brain changes dramatically in size during postnatal development (Giedd, 1999; Malkova et al., 2006; Barnette et al., 2009), even after neurogenesis has completed in the neocortex (Rakic, 1974; Luskin and Shatz, 1985; Jackson et al., 1989; Bhardwaj et al., 2006). As the areal extent of cortical areas also increases substantially (Purves and LaMantia, 1993; Duffy et al., 1998; Drenhaus et al., 2006), this process implies that synaptic connections between cortical neurons must react in some way to accommodate growth. Two hypotheses have been proposed to account for these changes (Duffy et al., 1998; Oster and Bressloff, 2006; Keil et al., 2010). The first suggests the length of neuronal processes, such as axons and dendrites, scale linearly with neocortical growth (the balloon model), while the second indicates that synaptic connections must reorganize between neurons such that the length of axons and dendrites remains largely constant. As the two hypotheses dramatically differ from each other, they have important ramifications in our understanding how neural circuits organize and react to gross structural changes in brain size. This would also perhaps provide some clue how neurons in the mammalian brain also react to brain shrinkage, such as can happen in cerebral atrophy.

Mammals with highly developed visual systems, such as carnivores and primates, have become the model system to investigate how cortical neurons react to brain growth. This is because neural circuits of the visual cortex form functional maps, in which cortical neurons sharing similar response properties are systematically clustered together into discrete functionally identified cortical columns across the tangential plane of visual cortex (Hubel and Wiesel, 1962; LeVay et al., 1978; Blasdel and Salama, 1986). While

the functional role of cortical columns in visual processing remains controversial because some mammals like rodents and squirrel monkeys do not exhibit columnar architecture (Horton and Adams, 2005; Ohki et al., 2005; Van Hooser et al., 2005), cortical columns are still a measureable and functionally defined instantiation of brain architecture that makes them convenient structures to assay. A pioneering study by Duffy *et al*. reported a largely isotropic expansion of the visual cortex in macaque monkeys, cats, and rats (Duffy et al., 1998). This group suggested that the functional layout of global features, such that the position and shape of cortical columns, should remain unchanged, and that only overall isotropic stretching would occur (i.e. supporting the balloon model).

However, a key prediction of the balloon model hypothesis is that the cortical column spacing would increase in development. While one study suggested that cat ocular dominance columns might modestly enlarge during postnatal development (Sengpiel et al., 1998), the vast majority studies analyzing cat orientation and ocular dominance columns have failed to find significant increases in column spacing (Muller et al., 2000; Rathjen et al., 2003; Kaschube et al., 2009; Keil et al., 2010). The possibility of inserting new cortical columns to account for the increased cortical area is unlikely, or at least a possibility with large energetic cost, because developmental neurogenesis has already concluded by parturition. Two recent computational studies have attempted to reconcile this discrepancy. These studies suggest that new cortical columns might instead originate either from the fracture of existing modules or through a systematic reorganization of neuronal selectivities (Oster and Bressloff, 2006; Keil et al., 2010). In support of both of these hypotheses, some of the largest changes in brain growth coincide with the critical

period (Daw et al., 1992). And it's been suggested that critical period plasticity may facilitate growth-related rearrangements in cortical columns.

Unfortunately there is still little direct evidence for or against growth-related rearrangement of the functional map. Most longitudinal imaging studies of cortical columns in cats and ferrets (Chapman et al., 1996; Godecke et al., 1997; Sengpiel et al., 1998) suggest that the general layout of functional maps is stable and does not appear to change substantially. In absence of other data, this stability might be then considered support for the "balloon" model being the most likely candidate model. Two studies in macaque monkey show that ocular dominance columns and blobs exhibit a 16-20% increase in size (Purves and LaMantia, 1993; Blasdel et al., 1995), which is comparable to the developmental growth of striate cortex (Purves and LaMantia, 1993). We were interested in determining whether cortical columns in ferrets, a closely related carnivore to cats, exhibited characteristics in support of either the balloon model or growth-related rearrangement. A previous longitudinal imaging study tracking orientation column development in ferret visual cortex failed to find significant changes in orientation column spacing (Chapman et al., 1996; Muller et al., 2000); thus, we initially did not anticipate observing functional reorganization in ferrets. However, when a lack of column spacing change is considered in the context of significant brain size change, reorganization of some sort is implied (Keil et al., 2010). Surprisingly, optical imaging of intrinsic signal revealed that orientation, direction, and ocular dominance columns of the ferret visual cortex all undergo an initial expansion until ~PD60 (postnatal day 60), and then later shrinkage that is age-dependent. We also tracked the development of cortical

columns longitudinally in a sub-set of animal experiments, and found little evidence for substantial columnar reorganization. Our study suggests that unlike cat visual cortex, cortical columns in ferret visual cortex instead behave more consistently with the "balloon" model.

2.3 RESULTS

2.3.1 Assessing columnar structure in ferret visual cortex

We employed two quantitative methods to assess structural changes in cortical columns, such as orientation columns (Figure 1a): wavelet transforms and Euclidean distance. The first method, wavelet transforms, is based directly on the published method for examining columnar structure in cats and ferrets (Kaschube et al., 2002; Kaschube et al., 2003; Kaschube et al., 2009; Kaschube et al., 2010; Keil et al., 2010; Keil et al., 2012). In the wavelet method, Morlet wavelets of differing sizes and orientations are fit to a difference map at each location through a 2-d convolution (Figure 1b). The local column spacing at each pixel is then estimated from the scale of the best-fit wavelet (Figure 1d, *left two images*). This method of fitting wavelets to cortical columns is well suited to extract the local column spacing and shape (Figure 1b), and is roughly analogous to taking a Fourier transform to estimate the local columnar wavelength. However, the wavelet method presumes the local columnar structure of functional maps is periodic. This assumption is generally appropriate as functional modules of the visual cortex, particularly those of orientation and direction preference, are known to exhibit periodic structure (Chapman et al., 1996; Weliky et al., 1996; Rao et al., 1997).

However, wavelets are less suitable for assessing column spacing in ferret ocular dominance maps as they are aperiodic (Ruthazer et al., 1999; White et al., 1999). To assess the column spacing between ferret ocular dominance columns, we instead developed a complimentary approach to the wavelet method, which instead relies on the Euclidean distance between columns to estimate the local column spacing (Figure 1c). In this new approach, lines of differing orientations are projected from each pixel in a functional map. To estimate the local column spacing, we first need to find the distance of the nearest next column of the same functional selectivity. To do this, we first project a set of line to intersect with the nearest next column of the same functional selectivity (Figure 1c, blue lines in top image). However, to get full column spacing measurement, we also need to include the edge of the current column (Figure 1c, red lines in top image); thus, we project a second set of lines in the opposite direction, which intersect with the edge of the current column. The Euclidean distances (relative to the source location) for both line sets are then summed together. Summation of these lines can be assumed as approximately estimating the local column spacing (Figure 1d, *right two images*), and is comparable to using wavelets (Figure 1d).

Primary quantification of a large dataset of ferret orientation difference maps generated with the blockwise imaging approach (n = 168) showed a strong correlation (Figure 1c; $r = 0.73$, $p < 0.0001$) between the mean size of cortical columns representing the cardinal orientations (0˚ and 90˚) and the oblique orientations (45˚ and 135˚). For simplicity, we then functionally defined the mean orientation preference column spacing as the pooled mean column spacing for the difference maps of the cardinal and oblique orientations.

Additionally, we emphasize that the large dataset of orientation maps were generated from pooled imaging experiments coming either from the labs of Justin Crowley or Leonard White. We tested a sub-set of age-matched data (n = 25 for each lab) to ensure that there weren't systematic differences between the labs. With a two-sample Student's t-test, we found that there was not a significant difference in the column spacing data if orientation maps were generated in one lab versus the other ($p>0.05$).

In the orientation map dataset, there was a qualitative agreement in the measurement of the mean column spacing using either wavelets or Euclidean distance (Figure 1d; $r = 0.73$, $p < 0.001$). The line of best fit to the datasets exhibited a slope of 0.51 and y-intercept of 445μm, where the x-axis data was Euclidean distance and y-axis data was wavelets. However, for the ocular dominance dataset (n = 90), there was substantial disagreement in the measurement of the mean columns spacing. The line of best fit to the datasets was best described with a slope of 0.41 and y-intercept of 1290μm. Generally for smaller Euclidean distance values, there was more likely disagreement with the wavelet measure. This discrepancy between the two methods reveals some key differences between the methods. The more cylindrical (or "stripe" like) a cortical column is, the more likely the Euclidean distance measure will over-report its size. Conversely, the wavelet measure can also both under- and over-estimate the cortical column size if cortical columns exhibit structural anisotropies and are not locally periodic (see how in the example in Figure 1b on the right side, the vertically oriented wavelet does not perfectly fit the local cortical column). As both methodologies have some strengths and

weaknesses, we feel it's appropriate to report both measurements, as consistent changes between the two measurements are likely a robust indicator of column spacing changes.

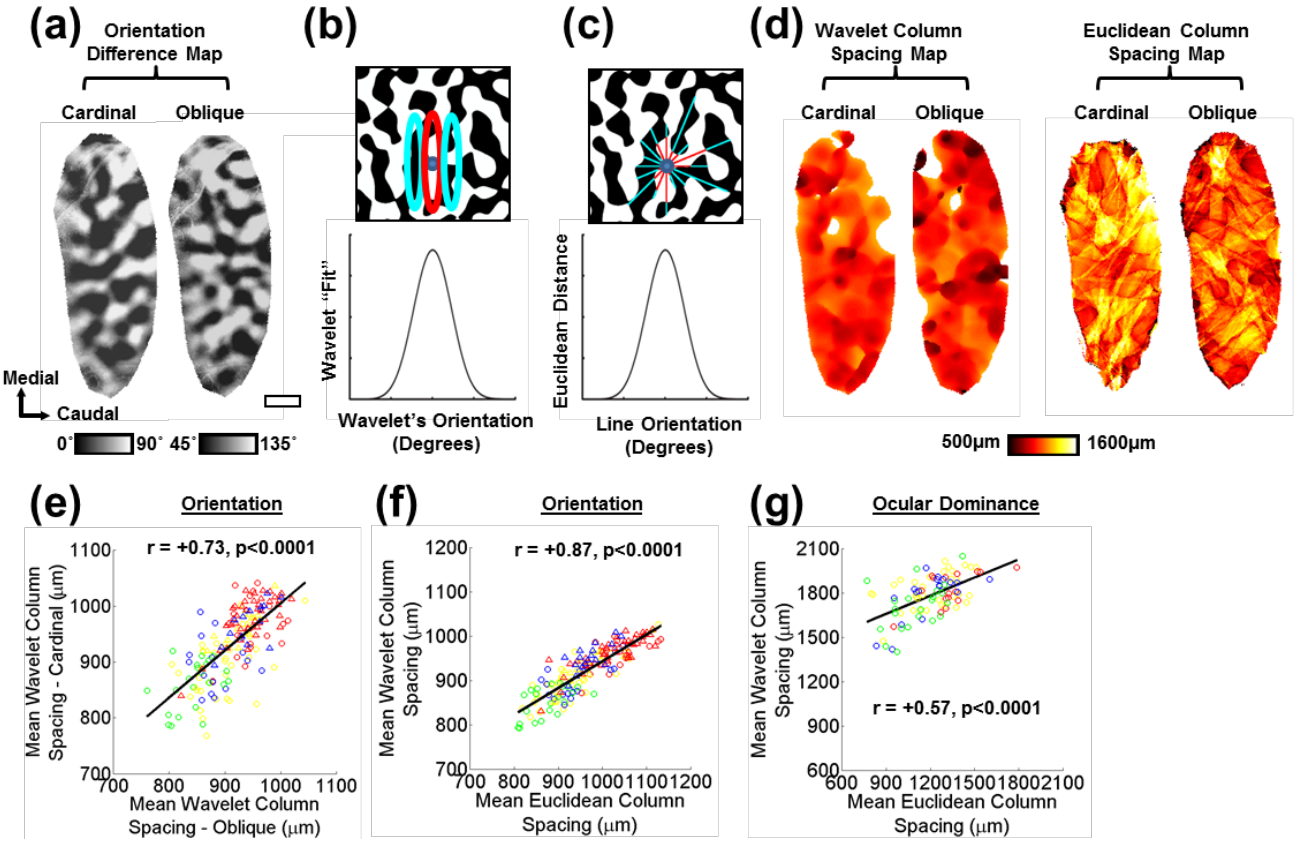

Figure 2-1: The local column spacing in visual cortex can be assessed quantitatively using two methods: wavelets and Euclidean distance.

(a) Example orientation difference images for a critical period ferret (difference map of cardinal orientations, *left*; difference map of oblique orientations). Saturation indicates orientation response bias (black – 0˚or 45˚Grating Bias, gray – no bias, and white – 90˚or 135˚Grating Bias). Scale bar is 1mm. **(b)** In the wavelet method, Morlet wavelets of different sizes and orientations are fit at each location of the functional map and the local column spacing is then estimated from the scale of the best-fit wavelet. **(c)** The local column spacing at each pixel is computed as the sum of two line sets in the Euclidean

distance method. In the first line set, lines of varying orientations project away from each map location and intersect the edge of the current column (red lines in top image), while in the second line set lines are projected in the opposite direction and instead intersect the nearest next column of the same orientation (blue lines in top image). In each line set, the mean Euclidean distance of the lines is used. **(d)** For (a), the corresponding wavelet column spacing maps (left two images; mean cardinal column spacing: 968μm; mean oblique column spacing: 928μm) and Euclidean Column spacing maps (right two images; mean cardinal column spacing: 1,107μm; mean oblique column spacing: 1008μm). **(e)** Comparison between the mean wavelet column spacing for the difference maps of cardinal and oblique orientations. **(f)** Comparison of the mean wavelet column spacing and the mean Euclidean column spacing for the same orientation difference maps (average of cardinal and oblique maps). **(g)** Comparison of the mean wavelet column spacing and the mean Euclidean column spacing for the same ocular dominance maps. For (e-g), each point denotes an imaged functional map. Circles denote 'Crowley' lab ferret, while triangles are 'White' lab ferret. The color indicates the age group (yellow: PD30-45, red: PD46-65, blue: PD66-365, green: PD366-730). Lines of best fit are shown, and the Pearson's Correlation Coefficient is computed for each comparison. The r-value and p-value are shown in each figure.

2.3.2 Age-dependent changes in the column spacing of the orientation preference map

The primary aim of this paper is to relate our measurements of column spacing in orientation preference maps (Figure 1a) to the ferret's postnatal age. Instead of observing a constant column spacing like cats (Keil et al., 2010), we unexpectedly observe a bidirectional relationship of column spacing with age, using either wavelets (Figure 2b) or Euclidean distance (Figure 2c). In an early development phase, orientation columns increase in size starting at eye opening and the onset of the critical period (PD30), and peak in size around PD50-60. However, the column spacing subsequently gets progressively smaller as cortical columns continuously shrink thereafter in a late developmental phase. We report the percent increase in column spacing between PD30-55 is a 11% or 22% change with wavelets and Euclidean distance respectively, while the percent decrease in column spacing between PD55-730 is 13% or 20% .We next split the map dataset into four age groups for the graphs in Figure 2, revealing significant differences between the sub-groups (early critical period: PD30-45, late critical period: PD46-65, young adult: PD66-365, adult: PD366-730).

Most notably there are differences between the early and late critical period, indicating early growth of cortical columns. Interestingly, however is that the adult group is significantly different from all other groups indicating the shrinkage of ferret cortical columns continues well after ferrets are considered adults at 1 year (i.e. ferrets reach adult size at 6 months, and sexual maturity before 1 year) (Fox, 1998). The expansion of cortical columns in the early phase could be described by either plotting the column

spacing data in Figure 2b and Figure 2c versus postnatal age (data now shown), or the logarithm of postnatal age. Shrinkage however is best described by a logarithmic relationship with postnatal age, indicating this process declines with age. It's also worth noting that the developmental critical period of ocular dominance plasticity begins around at eye-opening at PD35 and lasts for about four weeks (Issa et al., 1999). Thus, the increases in column spacing we report here coincide with the critical period, while the shrinkage of cortical columns occurs well after the critical period.

Although most regions of the orientation preference maps gradually shift in their orientation preference, the map is systematically punctuated by regions where the orientation preference changes rapidly around singularities called pinwheel centers (Bonhoeffer and Grinvald, 1991; Ohki et al., 2006). The density of a repeating map feature, such as pinwheels is a convenient assay to assess whether the underlying functional organization of the orientation preference map also changes with age. We find that the local pinwheel density per mm^2 also exhibits a bidirectional relationship with age: an initial decrease in pinwheel density per mm^2 until PD 50-60, and thereafter an increase (Figure 2d). This relationship is an inverted mirror image of the relationship of age and column spacing. The inversion is reasonable, since the local pinwheel density is expected to be inversely correlated with the local column spacing (Figure 2e). However, if we compute the local pinwheel density per local orientation column (Λ^2) (Wolf and Geisel, 1998), and eliminate the inverted relationship between column spacing and pinwheel density, the local pinwheel density per orientation column does not change (Figure 2f). This latter result suggests that the functional topography of the orientation

preference map remains preserved, despite structural changes in the size of orientation columns. We also report a mean pinwheel density of 3.07 per Λ^2 and this value is similar to the 3.16 mean pinwheel density per Λ^2 that has been described for tree shrews, ferrets, and galagos (Kaschube et al., 2010).

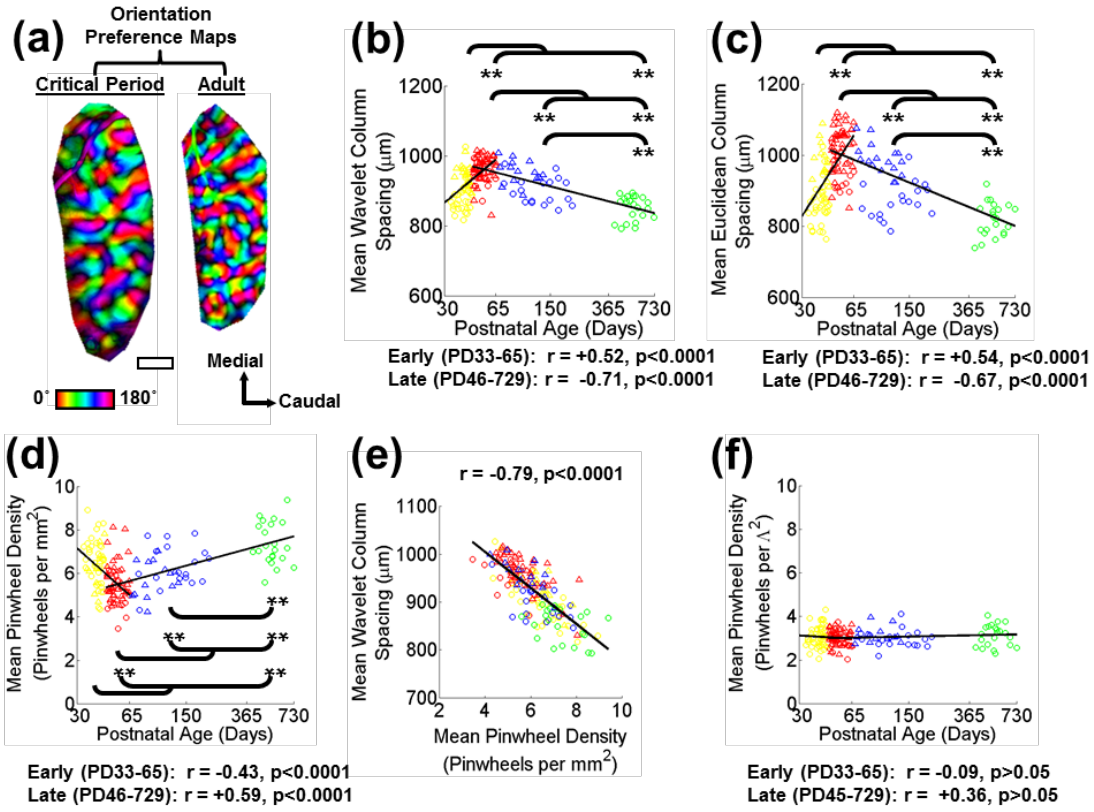

Figure 2-2: Age-dependent changes are observed in the mean column spacing of ferret orientation preference maps (n = 168).

(a) Example orientation preference maps are shown for a critical period ferret (PD42, same as in Figure 1a) and adult ferret (PD548). Hue denotes the preferred orientation according to the legend, while saturation indicates response magnitude. Scale bar is 1mm.

(b) Plot of the mean wavelet column spacing (average of cardinal and oblique difference maps) versus the log of the ferret's postnatal age. The mean wavelet column spacing

across animal experiments is 923μm. **(c)** Plot of the mean Euclidean column spacing (average of cardinal and oblique difference maps) versus the log of the ferret's postnatal age. The mean Euclidean column spacing across animal experiments is 936μm. **(d)** Plot of the mean pinwheel density per mm^2 versus the log of the ferret's postnatal age. **(e)** Plot of the mean wavelet column spacing (average of cardinal and oblique difference maps) versus the mean pinwheel density per mm^2. The mean pinwheel density per mm^2 across animal experiments is 6.17 pinwheels / mm^2. **(f)** Plot of the mean pinwheel density per orientation hypercolumn (Λ^2), ρ, versus the log of the ferret's postnatal age. The mean pinwheel density per Λ^2 across animal experiments is 3.07. For (b-f), each point denotes an imaged functional map. Circles denote 'Crowley' lab ferrets, while triangles are 'White' lab ferrets. The color indicates the age group (yellow: PD30-45 [n = 47], red: PD46-65 [n = 64], blue: PD66-365 [n = 35], green: PD366-730 [n= 22]). Lines of best fit are shown for both the early developmental (PD33-65) and the late phase (PD46-729), and the Pearson's Correlation Coefficient is computed for each comparison (except for (e) where there is only one group, rather than two groupings based on developmental phase). The r-value and p-value are shown in each figure. Age group comparisons were computed with Student's t-test and are shown in (b-d), with $p<0.01$ denoted as '**'. No significant differences were observed in (f).

2.3.3 Age-dependent change in the column spacing of other functional maps

As we observed dramatic changes in the size of orientation columns, we were next interested if other functional maps of ferret visual cortex exhibited similar behavior.

Although less striking than in the case of the orientation preference map, ocular dominance columns (Figure 3a) also show similar age-dependent changes for both wavelets (Figure 3b) and Euclidean distance (Figure 3c). The Euclidean distance measurements exhibit a bidirectional relationship with age, similar in behavior to the one we observe in the orientation preference map (Figure 2). The wavelets on the other hand are less sensitive to changes in column spacing in the ocular dominance map, most particularly in younger animals. This is consistent with wavelets being a less robust measure of column spacing in the more aperiodic ocular dominance columns.

Next we were interested in relating any age-dependent changes in the direction preference maps (Figure 3d). Direction preference maps were generated in a subset of imaging experiments (n = 38) using the temporally encoded approach (Kalatsky and Stryker, 2003). By the very nature of the visual stimuli used to generate the direction preference maps, we co-measure direction preference maps with orientation preference maps. We show both of these temporally encoded functional maps together in Figure 3e-f (both generated with the same visual stimulus), along with blockwise ocular dominance difference maps from the same animals. Although we did not find an early expansion of cortical columns between PD30-50 due to a small sample size, a decline in column spacing is seen across all three shown functional maps, using either wavelets or Euclidean distance. Overall, these imaging experiments demonstrate that the ocular dominance map, and perhaps the direction preference map, exhibit bidirectional, age-dependent changes in column spacing similar to those that we observed in the orientation preference map.

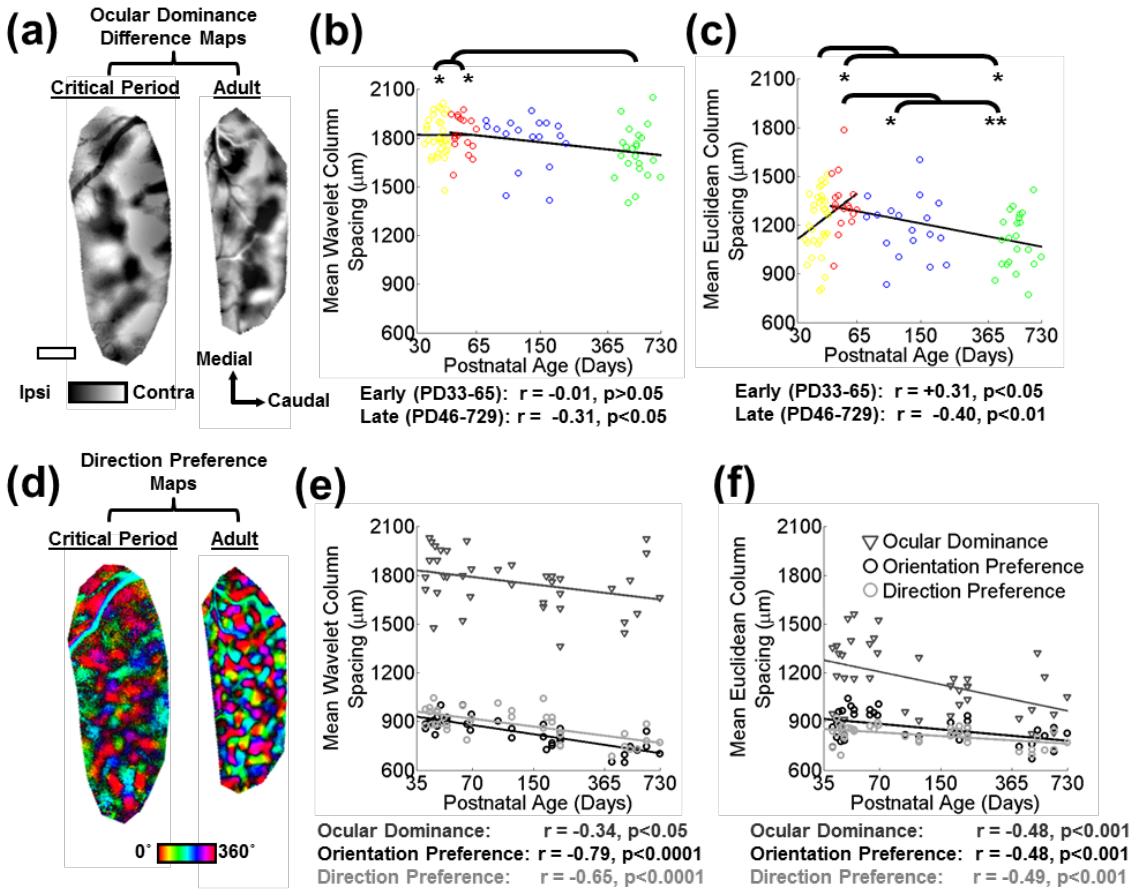

Figure 2-3: Age-dependent changes are observed in the mean column spacing of other functional maps, such as the ocular dominance maps and direction preference maps. **(a)** Example ocular dominance maps are shown for a critical period ferret (PD42) and adult ferret (PD548). These are the same animals as in Figure 2a. Saturation indicates ocular response bias (black – ipsilateral eye bias, gray – no bias, and white – contralateral eye bias). Scale bar is 1mm. **(b)** Plot of the mean wavelet column spacing for the ocular dominance map versus the log of the ferret's postnatal age (n = 90). The mean wavelet column spacing across animal experiments is 1,785μm. **(c)** Plot of the mean Euclidean column spacing for the ocular dominance map versus the log of the ferret's postnatal age (n = 90). The mean Euclidean column spacing across animal experiments is 1,204μm.

For (b-c), each circle denotes an imaged functional map. The color indicates the age group (yellow: PD30-45, red: PD46-65, blue: PD66-365, green: PD366-730). Lines of best fit are shown for both the early developmental (PD33-65) and the late phase (PD46-729), and the Pearson's Correlation Coefficient is computed for each comparison. The r-value and p-value are shown in each figure. Age group comparisons were computed with Student's t-test and are shown, with $p<0.05$ denoted as '*' and $p<0.01$ denoted as '**'. **(d)** Example direction preference maps are shown for a critical period ferret (PD42) and adult ferret (PD548). These are the same animals as in Figure 3a. Hue denotes the preferred direction according to the legend, while saturation indicates response magnitude. (**e)** Plot of the mean wavelet column spacing for the ocular dominance (dark gray triangles), orientation preference (black circles), and direction preference maps (gray circles) versus the log of the ferret's postnatal age ($n = 38$). For temporally encoded maps (ie orientation preference and direction preference maps), the mean column spacing is the average of real and imaginary components of the stimulus-specific response, z (see Methods). **(f)** Similar to (e), except the plot of the mean Euclidean column spacing for ocular dominance, orientation preference, and direction preference maps versus the log of the ferret's postnatal age. Each point in (e-f) denotes an imaged functional map. Lines of best fit are shown, and the Pearson's Correlation Coefficient is computed. The r-value and p-value are shown in each figure.

2.3.4 Age-Dependent Changes in Cortical Columns Related to Gross Areal Changes in Visual Cortex

So far we observed similar bidirectional, age-dependent changes in columnar spacing across three different functional maps. Since there was a preservation of the underlying functional topography in the orientation preference map, this led us to wonder if the changes in column spacing reflected map reorganization, or age-dependent changes in the areal extent of visual cortex. We computed the spatial gradient of the retinotopic visual field maps to test for areal changes in the visual cortex (elevation map, Figure 4a, and azimuth map, Figure 4b). The spatial gradient of the retinotopic maps is a measure of how much of the visual field is represented in a given region of the visual cortex. The rationale behind computing this spatial gradient was that if the visual cortex was simply changing in size, the amount of surface area devoted to the visual field per mm should also correspondingly change. Indeed, we find a pronounced increase in the spatial gradient of the elevation visual field map, but not for the azimuth visual field map. Since the animals we recorded visual field maps are the same subset of animals in Figure 3d-e, the increase of spatial gradient in the elevation field map entails that the shrinkage of cortical columns may at least partially be due to a pronounced shrinkage of the visual cortex along the medial/lateral axis (Figure 5a).

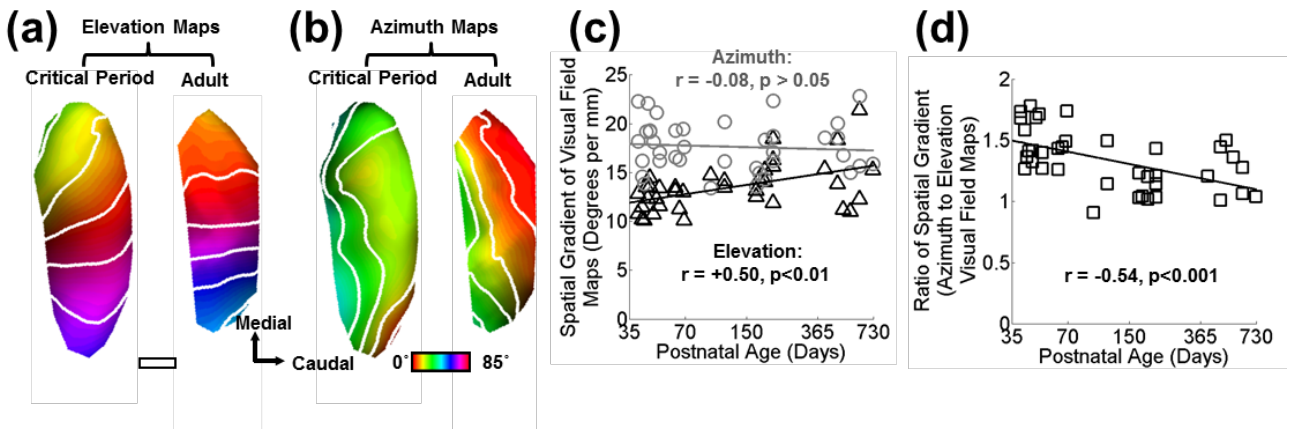

Figure 2-4: Shrinkage in cortical columns in the late phase (PD45+) is consistent with pronounced shrinkage of the visual cortex along the medial/lateral axis, as the elevation visual field map's spatial gradient increases (degrees of visual space per mm of cortex). **(a)** Example elevation visual field maps are shown for a critical period ferret (PD42) and adult ferret (PD548). These are the same animals as in Figure 2a. Hue denotes the preferred retinotopic location according to the legend, while saturation indicates response magnitude. Scale bar is 1mm. **(b)** Like (a), but instead the azimuth visual field map. **(c)** The spatial gradient of both visual field maps are plotted versus the log of the ferret's postnatal age (n = 38, same animals as Figure 3e-f). **(d)** The ratio of the spatial gradients in (b) are plotted versus the log of the ferret's postnatal age (Azimuth to Elevation Visual Field Maps). Each point in (c) denotes an imaged visual field map, while each point in (d) is the ratio of both visual field maps. Lines of best fit are shown, and the Pearson's Correlation Coefficient is computed. The r-value and p-value are shown in each figure.

If true, then we should also be able to detect anisotropic changes in the column spacing of the orientation preference map. For the same orientation maps shown in Figure 2, we next

measured the orientation column spacing by orienting the wavelets along either the rostral/caudal axis or the medial/lateral axis (instead of averaging across all orientations). We discovered that there is initial isotropic increase in columns from PD30-65, in which the column spacing increases equally along both the rostral/caudal and medial/lateral axes (Figure 5b). However, in the later phase of PD45-730 and consistent with the changes in the visual field maps, we find shrinkage of cortical columns is most pronounced along the medial-lateral axis (Figure 5b, right panel). The rate of the changes was faster during the early growth phase, while the subsequent shrinkage in the later phase was substantially slower along both axes (Figure 5c). While these changes do indicate a compression of cortical columns along the medial-lateral axis, this was not reflected in a systematic reorganization of orientation columns. We quantified this by estimating the mean bandedness of orientation columns, and compared it with the postnatal age of the animals (Figure 5d). Bandedness is bounded between 0 and 1. High values indicate that stripe-like columns dominate the orientation map, while lower values signify bent columns and isotropic patches are more prevalent. We failed to detect any age-dependent changes in the mean bandedness, although in some animals the bandedness tended to be higher in the two critical period animal groups (PD30-65).

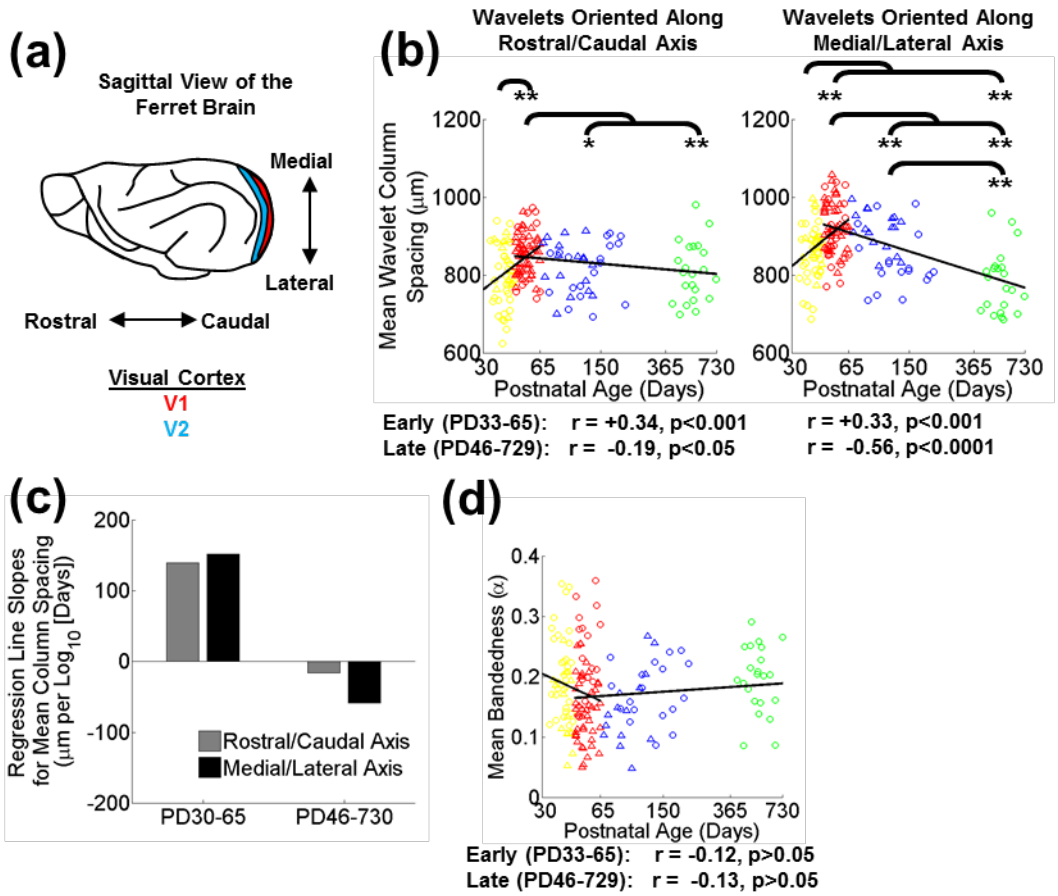

Figure 2-5**:** Age-dependent changes in column spacing are bidirectional: an initial, isotropic expansion versus an anisotropic shrinkage, most-pronounced along the medial/lateral axis.

(a) Sagittal view of the ferret brain with the approximate area of visual cortex shown (V1 – Red, V2 – Blue). The rostral/caudal and medial/lateral axes are respectively labeled. **(b)** Plot of the mean wavelet column spacing (average of cardinal and oblique difference maps) versus the log of the ferret's postnatal age. The wavelets are either fit along the rostral/caudal axis (left image) or the medial/lateral axis (right image). The mean wavelet column spacing (across animal experiments) along the rostral/caudal axis is 825μm, while its 875μm along the medial/lateral axis. For (b-c), each circle denotes an imaged functional map. Circles denote 'Crowley' lab ferret, while triangles are 'White' lab ferret.

The color indicates the age group (yellow: PD30-45, red: PD46-65, blue: PD66-365, green: PD366-730). Lines of best fit are shown for both the early developmental (PD33-65) and the late phase (PD46-729), and the Pearson's Correlation Coefficient is computed for each comparison. The r-value and p-value are shown in each figure. Age group comparisons were computed with Student's t-test and are shown, with $p<0.05$ denoted as '*' and $p<0.01$ denoted as '**'. **(c)** Regression line slopes for (b), which illustrate that the early phase exhibits isotropic expansion of cortical columns, but exhibits more pronounced anisotropic shrinkage in the late phase. **(d)** Plot of the mean bandedness (average of cardinal and oblique difference maps) versus the log of the ferret's postnatal age. The mean bandedness across animal experiments is 0.18.

2.3.5 Chronic, longitudinal imaging of ferret functional maps:

The acute imaging experiments presented in the previous figures are suggestive of age-dependent changes in column spacing that are consistent with the balloon model (ie as the visual cortex changes in size, cortical columns congruently change), but not direct proof. For example, our imaging data doesn't rule out subtle changes occurring in the functional maps indicative of map reorganization. To investigate conclusively whether there were changes in the layout of the functional maps, we conducted longitudinal imaging experiments to track cortical columns directly (n = 12). We chose to track the late phase (ie shrinkage in cortical columns), since this phase had not been well characterized in other longitudinal imaging experiments of ferrets (Chapman et al., 1996). Longitudinal imaging experiments in animals involving an initial imaging session, followed up by a

second imaging session sometime later (for this study at least one week difference, and sometimes up to eleven weeks later).

An example longitudinal imaging experiment is shown in Figure 6, in which a ferret was initially imaged at PD45 and then 7 weeks later at PD96. This case is representative of the longitudinal imaging experiments and helps visualize some of our previous findings. First, we can easily see that shrinkage of the visual cortex is most pronounced along the medial/lateral axis. And secondly, there is remarkable stability in the global features of the functional map if the initial imaging experiment is co-registered to the second imaging experiment through an affine transformation (using penetrating blood vessels on the brain's surface as landmarks). The image registration is used here to eliminate gross structural changes in the visual cortex, allowing us to assess whether there are more subtle changes in the longitudinal imaging data. For the most part, there only appears to be anisotropic shrinkage of the visual cortex without much accompanying map reorganization.

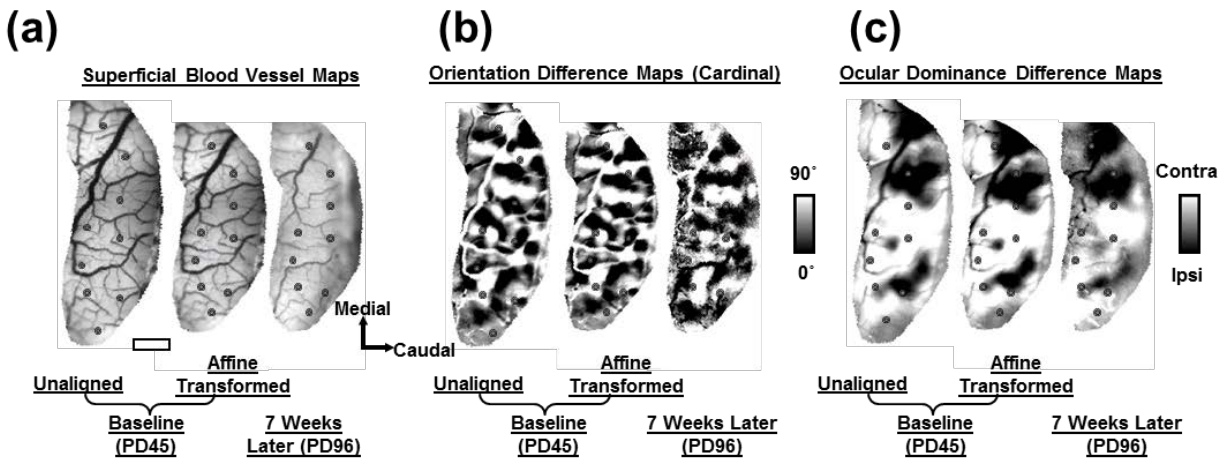

Figure 2-6: Example of chronic imaging of ferret visual cortex across two longitudinal, imaging experiments (separated by multiple weeks).

(a) Superficial blood vessel maps of a representative ferret brain. The first imaging experiment (ferret's age is PD45) is shown in the left image (original) and center image (co-registered with second imaging experiment through the Affine transform). The right image corresponds to the second imaging experiment (ferret's age is PD96), which is 51 days elapsed from first experiment. Fiducial landmarks on the blood vessel map are shown to aid with qualitative comparison of the images. Scale bar is 1mm. **(b)** Similar to (a), but instead an orientation difference map of the cardinal orientations. Saturation indicates orientation response bias (black – 0˚Grating (Horizontal) Bias, gray – no bias, and white – 90˚Grating (Vertical) Bias). **(c)** Similar to (a), but instead an ocular dominance difference map. Saturation indicates ocular response bias (black – ipsilateral eye bias, gray – no bias, and white – contralateral eye bias).

To quantify the changes in the chronic imaging experiments, we tested for the percent change in the mean column spacing (Figure 7 and Figure 8). In Figure 7, there is a clear

trend of shrinkage in columns spacing across longitudinal imaging experiments, in which the shrinkage is most pronounced in younger animals. Shrinkage of cortical columns is observable in the orientation map, using either wavelets (Figure 7a) or Euclidean distance (Figure 7b), as well as the ocular dominance map using Euclidean distance (Figure 7c). We did not detect any significant changes if the imaging experiments were initially co-registered through the affine method before analysis (Figure 8a). This negative result implies that the column spacing changes in ferrets do not likely reflect map reorganization. However, if the functional maps are not initially co-registered, we detected significant changes in the column spacing for experiments if the initial imaging experiment was conducted before PD120 (Figure 8c), as well as if the timelapse duration was greater than 6 weeks (Figure 8b). The first result is consistent with our previous findings that the shrinkage in column spacing is an age-dependent process. The second suggests though that the results from our longitudinal imaging data do merely arise from acute effects following the initial surgery in the first imaging experiment. Consistent with Figure 8c, we observe a positive correlation between age and the percent change in column spacing, regardless of whether wavelets (Figure 8d, left panel) or Euclidean distance (Figure 8d, right panel) are used.

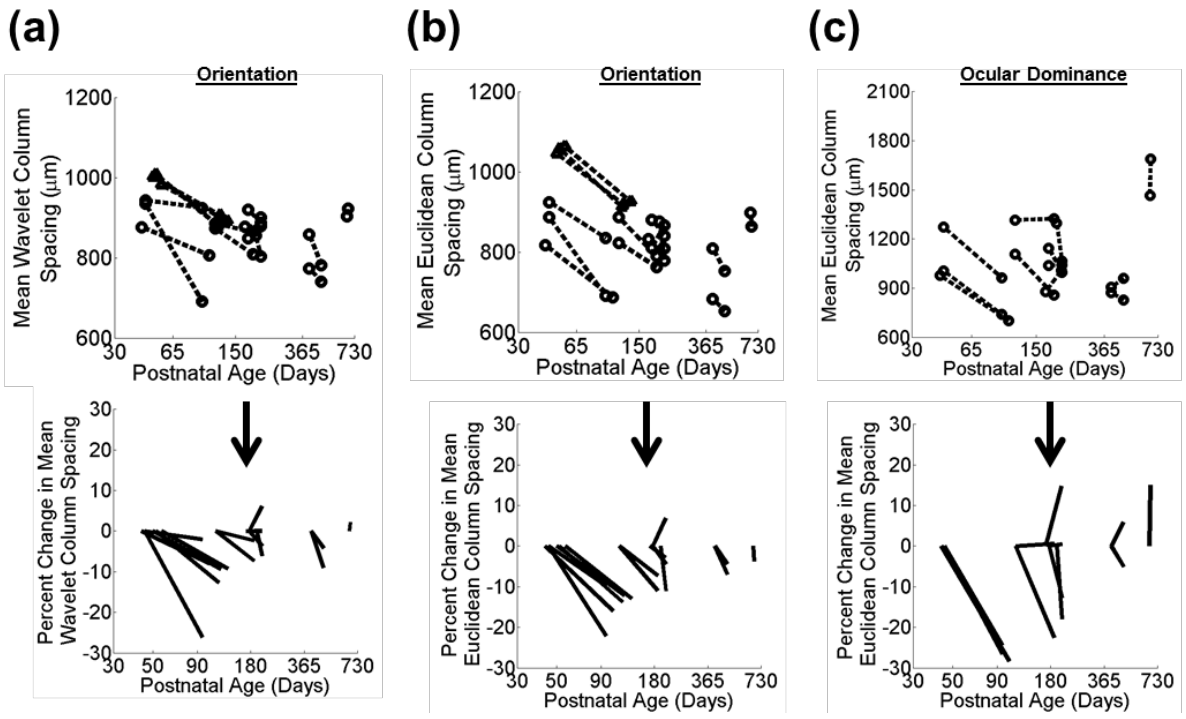

Figure 2-7: Chronic imaging of ferret visual cortex across two longitudinal, imaging experiments (separated by multiple weeks) also indicates shrinkage in cortical columns (n = 15 for Orientation Maps and n = 12 for Ocular Dominance Maps).

(a) Plot of the mean wavelet column spacing for the orientation map (average of cardinal and oblique difference maps across all imaged hemispheres) versus the log of the ferret's postnatal age (top panel). The first and second imaging experiments for each animal are connected by a dotted line. Circles denote 'Crowley' lab ferret, while triangles are 'White' lab ferret. To aid in qualitative inspection of the chronic imaging data, we also show with the percent change in mean column spacing plotted vs. the log of the ferret's postnatal age (bottom panel). The length of each line is the timelapse duration for each animal (in postnatal days), while the line slope indicates the rate of percent change in mean column spacing per unit time (ie Log of timelapse duration in days). **(b)** Similar to (a), except the mean Euclidean column spacing for the orientation map is plotted versus

the log of the ferret's postnatal age. **(c)** Similar to (a), except the mean Euclidean column spacing for the ocular dominance map is plotted versus the log of the ferret's postnatal age.

Interestingly if we measure the percent change in orientation column spacing by orienting the wavelets along the medial/lateral axis, we still find significant shrinkage ever after PD120 (Figure 8c). And unlike the other measures tested, there is not a significant correlation with age ($r = 0.49$, $p < 0.05$). Both results imply the possibility that anisotropic shrinkage of the visual cortex might reflect an ongoing, albeit decelerating with age, ontogenetic process that continues well into adulthood, rather than merely a transitory developmental overshoot.

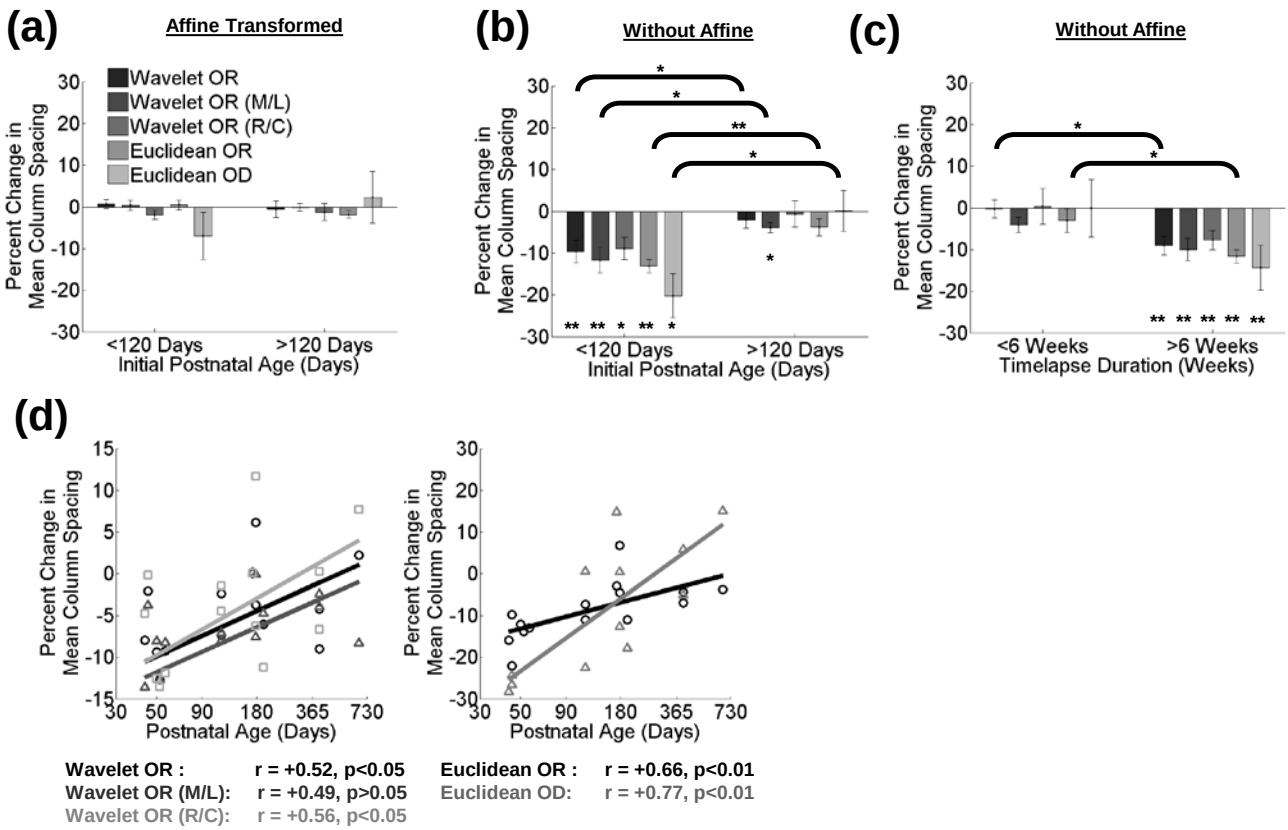

Figure 2-8: Quantification of chronic imaging experiments corroborates the previous findings of anisotropic shrinkage in cortical columns.

(a) Bar plot of the percent change in mean column spacing, using either wavelets or Euclidean Distance. The data in this bar plot involves co-registering the first imaging experiment to the second imaging experiment through the affine transformation (eliminating structural changes in the visual cortex). Each data method is split into two groups based on the initial postnatal age of the ferret (first imaging experiment): younger animal group (<120 Days, n = 8, except Euclidean OD where n = 5) and older animal group (>120 Days, n = 7). The five data methods in this panel are (shaded from black to light gray): Wavelet OR – Mean wavelet column spacing for orientation preference map, Wavelet OR (M/L) – Mean wavelet column spacing for orientation preference map, but

wavelets are oriented only along medial/lateral axis, Wavelet OR (R/C) – Mean wavelet column spacing for orientation preference map, but wavelets are oriented only along rostral/caudal axis, Euclidean OR - Mean Euclidean column spacing for orientation preference map, and Euclidean OD - Mean Euclidean column spacing for ocular dominance map. As expected, no changes were observed in any group or method. **(b)** Same as (a), except the data from the first imaging experiment is not co-registered with the second imaging experiment. Shrinkage is observed in the younger animal group, as well as the Wavelet OR (M/L) data method in the older animal group. **(c)** Same as (b), except the grouping is based on the length of the time-lapse duration between imaging experiments: <6 Weeks (n = 4), and >6 Weeks (n = 10, except Euclidean OD where n = 7). Shrinkage is observed in the >6 Weeks group (except Euclidean OD data method). 1-way ANOVA across all groups and data types was significant for (b-c). For (a-c), 1-way Student's t-test was used to assess whether a data method in a group exhibited significant changes, while a 2-way Student's t-test was used to assess whether there was a significant change in a data method based on the grouping criteria. Significant changes with $p<0.05$ are denoted as '*' and $p<0.01$ are denoted as '**'. **(d)** The percent change in mean column spacing is plotted versus the log of the initial postnatal age of the ferrets (first imaging experiment). In the left panel, wavelets are shown (Black Circles - Wavelet OR [n = 15], Dark Gray Triangles – Wavelet OR (M/L) [n = 15], Light Gray Squares – Wavelet OR (R/C) [n = 15]). In the right panel, Euclidean distance is shown (Black Circle – Euclidean OR [n = 15], Gray Triangles – Euclidean OD [n = 12]). Lines of best fit are shown, and the Pearson's Correlation Coefficient is computed. The r-value and p-value are shown in each figure.

2.4 DISCUSSION

Most mammalian species display a classic sigmoidal growth curve, in which the mammalian neocortex initially grows rapidly in early development, eventually peaking at adult levels. However some mammals, such as the ferret but also the ranch mink, the marmoset, and the tree shrew, exhibit a so-called developmental "overshoot" in the size of neocortex (Zilles, 1978; Apfelbach and Kruska, 1979; Fritschy and Garey, 1986; Kruska, 1993; Drenhaus et al., 2006; Barnette et al., 2009). In these animals, the early growth phase is followed by a subsequent shrinkage of the neocortex to its adult levels, ~20-30% smaller. The loss of brain matter is characterized to be heavily biased towards gray matter (Kruska, 1993). Curiously, while this phenomenon is normally ascribed to other animals, MRI scans show humans display a strikingly similar bidirectional time course in terms of overall brain matter growth and loss (Courchesne et al., 2000; Sowell et al., 2003; Sherwood et al., 2011). A major, obvious difference is that in humans this process takes places over decades, rather than months. Although it's interesting to speculate if both processes in fact may reflect the same ontogenetic process, as the ferret lifespan is approximately ~11x less than humans (i.e. average human lifespan in the United States is ~78 years, rather than 7 in ferrets) (Hoyert and Xu, 2012).

2.4.1 Potential mechanisms behind structural changes in the visual cortex

The expansion and shrinkage of the visual cortex appears to strikingly parallel GABA levels in the ferret and human visual cortex. One group has shown that the proportion of

immuno-reactive labeled GABA neurons compared to overall number of Nissl-stained cells in the ferret visual cortex (ie the ratio of GABA to all other cells) fluctuates with a similar timecourse to the column spacing measurements we report here (Gao et al., 1999). Specifically they found that the proportion of immuno-reactive GABA cells increased from 5% at PD20 to 12.5% at PD60, and then the ratio reduced to 7% in young adult ferrets (>PD 120). Likewise the expression of GAD-65 expression (a GABA synthesizing enzyme) in human visual cortex increases until humans are 12-21 years of age, and then it begins to declines with age (Pinto et al., 2010). Consistent with the possibility that GABA levels might be correlated to brain size, the onset of age-dependent brain shrinkage in humans appears to begin roughly around 20 years of age (Courchesne et al., 2000; Sherwood et al., 2011).

A pioneering study conducted by two authors provides tantalizing clues suggesting that GABA might actually be a mediator of age-dependent expansion and shrinkage of cortical columns, rather than being merely correlated (Hensch and Stryker, 2004). In this study, Hensch et al. chronically infused the benzodiazepine diazepam (a GABA agonist) into the developing cat visual cortex. They found that the local column spacing in ocular dominance maps increased at the infusion site. Conversely, the local column spacing decreased when they applied the inverse-GABA agonist DMCM (methyl-6,7-dimethoxy-4-ethyl-β-carboline). These results when taken together with our study and Gao et al. (Gao et al., 1999) imply that increasing levels of GABA result in a larger local column spacing, while lower levels of GABA result in smaller column spacings. An important caveat to these results is that alteration of cortical inhibitions may not necessitate a

function reorganization of cortical columns. The longitudinal imaging data in this paper and Chapman et al. (Chapman et al., 1996) demonstrates that the functional layout of ferret orientation columns does not change substantially, despite changing levels of GABA in ferret visual cortex (Gao et al., 1999). Rather it seems conceivable that the perturbation of GABA circuits could instead be altering the gross structure of the visual cortex itself.

2.4.2 Comparisons to Previous Longitudinal Study in Ferrets:

A previous longitudinal imaging study of developing ferret visual cortex showed that the functional layout of the orientation map was stable after the emergence of orientation preference maps at eye opening, at least up until PD55 (Chapman et al., 1996). The reported stability in the functional layout of the orientation preference map is consistent with the results we report here. Indeed changes in the column spacing between orientation columns because of areal changes in visual cortex (even if they are anisotropic), do not appear to necessitate functional reorganization, as a previous study in macaque monkey suggested might happen in the case of anisotropic growth (Blasdel et al., 1995).

Follow-up analyses of the same longitudinal imaging data also suggested orientation column spacing did not significantly change in ferrets (Muller et al., 2000). While this finding may seem to be at odds with our study, the most likely explanation is methodological. The study used a map's Fourier spectrum to estimate the local column spacing. Unfortunately, a Fourier spectrum is less sensitive than wavelets in detecting the

local column spacing in functional maps (Kaschube et al., 2010). And this is because while orientation columns are periodic, local variations in the column spacing can broaden the frequency spectrum; thereby, making it more difficult to determine a map's mean column spacing. And although the longitudinal data did not display a significant age-dependence between ferrets of the ages PD35-55 (Pearson's Correlation Coefficient: $r = 0.22$, $p > 0.05$), there was a general trend consistent with ours in showing expansion of cortical columns. Data values we used for the above correlation coefficient were taken from Table 1 (Muller et al., 2000).

2.4.3 Relationship of Ferret Development to that of Cats and Primates

A major motivation behind this study was to assess the similarity of development in functional maps between primates, cats and ferrets (i.e. are there general rules for mammalian cortical development). Cats and ferrets, both being carnivores, share similar developmental milestones, except that ferrets appear to be delayed by 21 postnatal days due to a cat's longer gestational period (reviews can be found in Jackson and Hickey, 1985; Issa et al., 1999)). However, unlike ferret cortical columns, the column spacing in cat ocular dominance columns is reportedly preserved (Rathjen et al., 2002; Keil et al., 2010). The number of ocular dominance columns in cat visual cortex also increases, and is accompanied by a drop in the bandedness of ocular dominance columns (Keil et al., 2010). Combined these three factors strongly imply that growth-induced reorganization occurs in the cat ocular dominance map. A recent computational study demonstrates ocular dominance columns can exhibit "zig-zag" type reorganization (Keil et al., 2010) with an Elastic Network model, a popular model to study the activity-dependent

formation of cortical columns (Durbin and Mitchison, 1990; Wolf and Geisel, 1998; Goodhill and Cimponeriu, 2000). In “zig-zag” reorganization, new ocular dominance columns are created within the ocular dominance map from existing stripe-like columns becoming more bended and patchy.

In contrast, we find little evidence for such dynamic reorganization in the ferret, a closely-related carnivore. Fortunately an interesting prediction was made in the aforementioned computational study. They showed that zig-zag type reorganization only occurs in a model system where both the areal boundaries expand, yet the length of the lateral connections remains constant (Keil et al., 2010). When the group allowed the length of lateral connections to grow at the same rate as the areal expansion, the model more closely resembled the balloon model. And an important prediction of lateral connections growing at a non-zero rate is that the column spacing would increase, just as we observe in the ferret. However, the model also predicts that if the lateral connections are unable to keep up perfectly with the areal expansion of the visual cortex, some zig-zag type reorganization is expected to occur. We reported in Figure 5d that the mean bandedness did not exhibit an age-dependence. According to the model, this would then imply that the growth rate of lateral connections in ferret does not perfectly track the rate of areal expansion (ie the mean bandedness should generally increase in a perfect balloon model system); thus, although we were not able to detect significant reorganization of ferret functional maps, the models suggest the possibility of subtle reorganization.

Accordingly, the prevalence of growth-induced reorganization in functional maps may then depend on whether the areal extent of growth is faster than the lateral connections grow. In an animal such as the cat, where the column spacing is large (1.16mm for ocular dominance and 1.01mm for orientation) and the lateral connections are predicted to be relatively constant (Kaschube et al., 2003; Keil et al., 2012), the column spacing would be preserved and substantial map reorganization should occur. In contrast, an animal with smaller cortical columns, such as the ferret, the growth of lateral connections might be more significant, and increases in column spacing would be more significant than map reorganization.

This scheme might also explain why changes in macaque monkeys are more consistent with the balloon model (Blasdel et al., 1995). Blasdel and colleagues showed that orientation and ocular dominance columns in macaque monkeys are similar in scale to ferret orientation columns. Moreover, paralleling the ferret, they demonstrated that ocular dominance columns exhibit an age-dependent, anisotropic expansion along the medial/lateral axis, as well as a subsequent age-dependent shrinkage. Specifically they reported that ocular dominance column spacing increased from 724μm at PD25 peaking at 875μm at PD98, and then declining to the adult macaque column spacing of 815μm. Although their orientation column data was more mixed, their negative result is most likely explained by less sensitivity in using a map's Fourier spectrum to estimate column spacing (like Muller et al., 2000). In contrast, the macaque ocular dominance map is better suited for Fourier analysis, since macaque ocular dominance columns have a strong tendency to form long stripes that run orthogonal to the medial/lateral axis.

If the growth dynamics observed in cat, ferret, and macaque form a generalizable rule, how might we predict what happens in human visual cortex? Studies have reported that human ocular dominance columns have a spacing on the scale of ~2mm (Horton and Hedley-Whyte, 1984; Yacoub et al., 2007; Yacoub et al., 2008), while orientation columns are ~1.5mm (Yacoub et al., 2008). Since the column spacing is much larger than even cat visual cortex, this might suggest human visual cortex could undergo significant growth-induced reorganization. Though areal increases in visual cortex might be slow enough and the lateral connections grow substantially, the human visual cortex might behave more like the ferret and macaque monkey.

2.5 METHODS

2.5.1 Basic Experimental Procedures

Optical imaging experiments were performed in ferrets with ages ranging from PD 35 to PD 730 (n = 162). Animal experiments were pooled from the Crowley (n = 80) and White (n = 82) groups. Experimental procedures were approved and carried out in accordance with protocols approved by either the local IACUC of Carnegie Mellon University or Duke University.

2.5.2 Imaging Experiments

We maintained animal anesthesia with isoflurane (1-3% for surgery, in either a 1:2 or 1:1 mixture of O2 and N_2O). All ferrets were tracheotomized and artificially ventilated. We

monitored the animal's vital signs at all times during imaging experiments: a rectal probe for animal temperature (37.5-38°C), EKG for heart-rate (270-300bpm), and a capnometer for expired CO_2 (3-4%). Ferrets were initially placed in a stereotaxic device to stabilize the head. Next we performed a midline scalp incision and a craniotomy over the visual cortex (also consisting of a duratomy). The imaging window was stabilized by filling the exposed craniotomy with 2% agarose, and then fastening a small glass window with dental acrylic on top of the agarose.

In the first longitudinal imaging experiment, we placed artificial dura (made of transparent, soft thermoplastic polyurethane) between the cortex and the resected dura. The skull was fastened back into place with tissue acrylic cement and the scalp was closed with surgical suture. We provided antibiotics for 5 days to prevent post-surgical infection. All steps in the first longitudinal imaging experiment followed standard aseptic practices. At the termination of all acute imaging experiments or all second longitudinal imaging experiments, ferrets were euthanized with an overdose of sodium pentobarbital.

Intrinsic signal images were acquired using software and hardware from Optical Imaging Inc. (Imager 2001 or 3001). We recorded the surface blood vasculature map under illumination with green light (595nm) and measured intrinsic signal changes with red light (604, 620nm, or 700nm) with a tandem lens macroscope attached to CCD camera. Acquired images consisted of either 1020x1020 pixels with a 157pixels/mm resolution (Crowley) or 655x480 pixels with a 75 pixels/mm resolution (White). Temporally encoded maps were continuously acquired at 6Hz.

2.5.3 Visual Stimulation:

Visual stimuli were presented on a 24” monitor using a visual stimulus generator (*Cambridge Systems*). Visual stimulation involved the presentation of 100% contrast, square-wave gratings (0.1-0.5 cycles per degree). We presented gratings at four different orientations in blockwise intrinsic signal experiments (0°, 45°, 90°, and 135°). For the generation of ocular dominance maps, eye-specific responses were measured by covering one eye with mechanical shutters. The temporally encoded stimulus used to generate orientation and direction preference maps was rotated clockwise or counter-clockwise (60s cycle) and drifted at a rate of 2.5 cycles/s. For mapping visual field maps, the temporally encoded stimulus consisted of a single white bar (0.125 cycles per degree) drifting respectively upward/downward (mapping elevation) or left/right (mapping azimuth) across a black screen (8s cycle).

2.5.4 Image Processing

We computed difference orientation maps by subtracting the average optical responses to a visual stimulus ($\Delta R/R$) from its orthogonal pair (ie cardinal difference maps: responses from a 0º grating are subtracted from a 90º grating; oblique difference maps: responses from a 45º grating are subtracted from a 135º grating). Similarly, we estimated ocular dominance difference maps by subtracting the average contralateral eye response from the average ipsilateral eye response. Monocular eye responses were estimated from the average optical response to the presentation of 4 gratings (0º, 45º, 90º, and 135º gratings).

The vector addition approach was used to compute orientation preference maps by summing up the cardinal and oblique difference orientation maps, using the following formula:

$$z = R_{0-90} + i * R_{45-135}$$

$$\theta_{pref} = z/(R_{0-90} + R_{45-135})$$

, where z is the orientation response (complex-field), $\theta_{pref}$is the pixel's orientation preference, R_{0-90} is the cardinal difference map, R_{45-135} is the oblique difference map. Imaging ROIs were manually selected to include only regions that responded to the visual stimulus. In the longitudinal imaging data, we either a.) co-registered all functional maps in the first imaging experiment to the second imaging experiment via a 2-d affine transform (using penetrating blood-vessels as fiducial landmarks), or b.) carefully ensured that the imaging ROIs in both imaging experiments corresponded to the same region of visual cortex.

In some animals, maps of orientation preference, direction preference, and visual field maps (azimuth and elevation) were produced from a temporally encoded stimulus (Kalatsky and Stryker, 2003). We used the discrete Fourier transform at the stimulation frequency (1/30s for orientation, 1/60s for direction, and 1/8s for visual field maps) to extract the stimulus-specific response (z) from the raw reflectance measurements. This step was performed for each trial and then the trial data was averaged. The hemodynamic phase-delay was estimated and then subtracted from each orientation preference map. The hemodynamic delay, $\theta_{delay}$was computed as:

$$\theta_{delay} = \arg[(\sin\theta_{Forward} + i\cos\theta_{Reverse}) \times (\sin\theta_{Forward} + i\cos\theta_{Reverse})]/2$$

where $\theta_{Forward}$ is a pixel's preferred orientation for clockwise stimulation (for orientation/direction preference) or a drifting bar moving left/up (for azimuth/elevation), $\theta_{Reverse}$ is a pixel's preferred orientation for counterclockwise stimulation (for orientation/direction preference) or a drifting bar moving right/down (for azimuth/elevation), and arg is the argument (complex-analysis).

We applied a 2-d bandpass spatial filter to eliminate signal strength variations, measurement noise, and hemodynamic artifacts in all difference maps (orientation preference, direction preference, and ocular dominance). The following bandpass filter was applied to each image (Fermi-filter):

$$Filter(\lambda_{cutoff}, \lambda) = \frac{1}{1 + e^{-\frac{\lambda_{cutoff}}{T}(\frac{1}{\lambda_c} - \frac{1}{\lambda})}}$$

$$\mathcal{F}^{-1}(\mathcal{F}(Image) \times Filter(\lambda_{lp}, \lambda)) \times (1 - Filter(\lambda_{hp}, \lambda)))$$

, where $\mathcal{F}$ is the Fourier Transform, λ is the spatial wavelengths present in the image, λ_{cutoff} is the filter cutoff (low-pass cutoff (λ_{lp}): 0.3mm, except in cases where the goal was to compute pinwheel density (see estimation for pinwheel density); high-pass cutoff (λ_{hp}): 1.4mm for orientation and direction preference, and 2.5mm for ocular dominance), and T is the "temperature" parameter of the fermi-filter (T = 0.05). The chosen bandpass cutoffs for the orientation preference maps are the same filter parameters used in another paper investigating pinwheel density in ferrets (Kaschube et al., 2010).

2.5.5 Data Analysis

Fittings wavelets to a functional map, has been extensively used to estimate the column spacing in cat orientation and ocular dominance maps (Kaschube et al., 2002; Kaschube et al., 2003; Kaschube et al., 2009; Kaschube et al., 2010; Keil et al., 2010). We used this method to estimate a 2D map of local column spacing in the ferret orientation, direction, and ocular dominance maps. For each differential map, we estimated an array of wavelet coefficients, $\hat{I}(\boldsymbol{x}, \theta, l)$:

$$\hat{I}(\boldsymbol{x}, \theta, l) = \int_{ROI} \left(Image(\boldsymbol{y})\, l^{-1}\ \psi_{\boldsymbol{x},\theta,l}\left(\Omega^{-1}(\theta)\frac{\boldsymbol{y}-\boldsymbol{x}}{l}, l\right)\right) d^2y$$

$$\psi(\boldsymbol{r}, l) = \exp\left(i\mathbf{k}_{\varphi}(l)\boldsymbol{r} - \frac{1}{2}\left(r_1^2 + \frac{r_2^2}{\sigma^2}\right)\right)$$

$$\Omega(\theta) = \begin{pmatrix} cos\theta & -sin\theta \\ sin\theta & cos\theta \end{pmatrix}$$

, where $\psi_{\boldsymbol{x},\theta,l}$ is the complex Morlet wavelet, Ω(θ) is the 2D rotation matrix, (x, θ, l) are the position, orientation, and scale of the wavelet, and k_{φ} and σ are the characteristic wavenumber and anisotropy of the wavelet.

We used relatively small, isotropic wavelets in this paper ($\mathbf{k}_{\boldsymbol{\varphi}}$= (2,0) and σ=1). Each wavelet's orientation (θ) was rotated between 16 uniformly spaced orientations with a range of [0 π], except when the wavelet was simply oriented along either the medial/lateral or rostral/caudal axis of a functional map. The wavelet's scale (l) was varied between a range of [0.4 1.3]mm for orientation/direction preference maps and [0.4 2.4]mm for ocular dominance maps, each with a step size of 0.05mm. The wavelet

column spacing, $\Lambda(\mathbf{x})$, at each position of the difference map was computed with the following formulas:

$$l(x) = \arg\max_l \left(\sum_{j=1}^{n} \hat{l}(\boldsymbol{x}, \theta_j, l) \right)$$

$$\Lambda(\boldsymbol{x}) = l(x) \left(\frac{2\pi}{k_\varphi} \right)$$

, where **x** is the location in the difference map, n is the number of wavelet orientations (n = 1 or 16), and $l(x)$ corresponds to the scale of the wavelet that maximized the angle averaged array of wavelet coefficients (using cubic splines interpolation). The mean wavelet column spacing ($\overline{\Lambda}$) is defined as the local wavelet column spacing averaged across the entire imaging ROI: $\overline{\Lambda} = \Lambda(\mathrm{ROI})$.

We also introduce an alternative method for estimating a 2D map of local column spacing using Euclidean distance. This method has the desirable quality that it does not require periodicity in a functional map. We computed the angle-averaged Euclidean column spacing, $\Lambda(\mathbf{x})$, at each position of the difference map with the following formulas:

$$d(\boldsymbol{x}, \boldsymbol{r}) = \sqrt{(x_1 - r_1)^2 + (x_2 - r_2)^2}$$

$$\Lambda(\boldsymbol{x}, \theta) = d\left(\boldsymbol{x}, \boldsymbol{r}_{\boldsymbol{Edge\ Of\ Column}}(\boldsymbol{x}, \theta)\right) + d(\boldsymbol{x}, \boldsymbol{r}_{\boldsymbol{Edge\ Of\ Nearest\ Next\ Column}}(\boldsymbol{x}, \theta + \pi)$$

$$\Lambda(\boldsymbol{x}) = \frac{\sum_{j=1}^{16} \Lambda(\boldsymbol{x}, \theta_j)}{16}$$

, where $\boldsymbol{x}$ is the position in the difference map, $\boldsymbol{r}_{\boldsymbol{Edge\ Of\ Column}}(\boldsymbol{x}, \theta)$ is the position of the current cortical column's edge (as defined by a vector projecting away from $\boldsymbol{x}$ with angular coordinate θ), $\boldsymbol{r}_{\boldsymbol{Edge\ Of\ Nearest\ Next\ Column}}(\boldsymbol{x}, \theta)$ is the position of the nearest next

column's edge of the same functional selectivity (as defined by a vector projecting away from $\boldsymbol{x}$ with angular coordinate θ), $d(\boldsymbol{x}, \boldsymbol{r})$ is the Euclidean distance between $\boldsymbol{x}$ and $\boldsymbol{r}$, and $\Lambda(\boldsymbol{x}, \theta)$ is the Euclidean column spacing estimate at $\boldsymbol{x}$ with angular coordinate θ (16 equally spaced directions ranging from [0 2π]). The mean Euclidean column spacing ($\overline{\Lambda}$) is defined as the local Euclidean column spacing averaged across the entire imaging ROI: $\overline{\Lambda} = \Lambda(\text{ROI})$.

Pinwheel density was computed using the same, previously introduced method by Kaschube et al. (Kaschube et al., 2010). First we applied a bandpass filter to each orientation preference map, ($z(\boldsymbol{x}, \lambda_{lp})$, and pinwheel-centers were identified as the zero-crossing of a spatially filtered orientation preference map (where λ_{lp} is the low-pass cutoff wavelength for the bandpass filter). The filter-dependent local frequency of pinwheel occurrence, $\hat{p}(\boldsymbol{x}, \lambda_{lp})$, was calculated by superimposing normalized Gaussians centered on the identified pinwheel locations (σ = $\overline{\Lambda}$, where $\overline{\Lambda}$ is the mean wavelet column spacing for the orientation preference map). The filter-dependent, local pinwheel density per Λ^2 was assumed as $p(\boldsymbol{x}, \lambda) = \hat{p}\left(\boldsymbol{x}, \lambda_{lp}\right) \Lambda(\mathbf{x})^2$, where $\Lambda(\mathbf{x})$ is the wavelet column spacing and $\boldsymbol{\lambda}(\boldsymbol{x}) = \lambda_{lp}/\Lambda(\mathbf{x})$. For estimating the pinwheel density per mm^2 (such as in Figure 2d), we estimated the pinwheel density with a low-pass cutoff wavelength of 0.3mm, and operationally defined $\overline{\Lambda}$ = 1mm and $\Lambda(\mathbf{x})$ =1mm for all **x.**

However to obtain a filter-independent estimation of the local pinwheel density per Λ^2, we varied the low-pass cutoff wavelengths over 90 equally spaced values ranging from (λ_{lp} =[0.1, 0.99]mm). We computed a filter-independent, local pinwheel density per Λ^2 at

each location, by fitting the following piecewise linear function to $p(\boldsymbol{x}, \lambda)$ in the interval $0.2 < \lambda < 1$ (using SVD):

$$\mathrm{h}(\lambda) = \mathrm{c}_0 + \mathrm{c}_1[-\lambda + \lambda_0]_+ + \mathrm{c}_2[\lambda - (\lambda_0 + \Delta\lambda)]_+$$

, where $[]_+$ denotes rectification, c_0 represents the filter-independent estimation of the pinwheel density in the interval $[\lambda_0, \lambda_0 + \Delta\lambda]$, $\mathrm{c}_1$and $\mathrm{c}_2$represent the filter-dependent portions of the pinwheel density. The fitting was fit with the following constraints: $\lambda_0 \geq 0.2, \Delta\lambda \geq 0.4$, and $0.2 + \lambda_0 + \Delta\lambda \leq 1$. The filter-independent, local pinwheel density per Λ^2, $p(\boldsymbol{x})$,was defined as the fitted value c_0. The mean pinwheel density per Λ^2, $\bar{p}$, is defined as the filter-independent, local pinwheel density per Λ^2 averaged across the entire imaging ROI: $\overline{p(\boldsymbol{x})} = p(\mathrm{ROI})$.

The spatial gradient of the visual field maps, $z(\boldsymbol{x})$, was computed from: $\partial(\arg(z(\boldsymbol{x}))/\partial\boldsymbol{x})$. We spatially smoothed arg(z) before estimating the spatial gradient and used mean filter (real domain) with a kernel size equal to mean wavelet column spacing ($\bar{\Lambda}$).

3 Impact of Monocular Deprivation and Systemic Fluoxetine Treatment in Adult Ferret Visual Cortex

3.1 ABSTRACT

We used relatively long-term monocular deprivation of the contralateral eye (14-days) to investigate ocular dominance plasticity in adult ferrets *in vivo*. We found that ocular dominance plasticity, as assayed by longitudinal optical imaging, still exhibits significant age-dependent decline after the previously reported end of ocular dominance plasticity for ferrets (approximately around postnatal day 65). This extended window of declining ocular dominance plasticity completes around 1 year, when ferrets are sexually mature ($r= -0.83$, $p<0.01$). Young adult ferrets then appear to exhibit "post-critical period" ocular dominance plasticity consistent with recent reports in mouse studies. In some areas of visual cortex, we also observed rapid recovery of orientation-selective responses to the deprived eye under anesthesia in critical period animals (within 1 hour). In young adult ferrets, we also found rapid recovery in all regions of the ocular dominance map. These results suggest the adult ocular dominance plasticity in young adult ferrets is mostly a synaptic reweighting without axonal pruning. Additionally, we investigated whether chronic fluoxetine treatment resulted in a re-opening of ocular dominance plasticity in ferrets, as was shown recently in rat visual cortex. We did not observe reopening of ocular dominance plasticity in adult ferrets; however, young adult ferrets exhibited a "reverse" ocular dominance shift similar to that seen with manipulation of GABA signaling, in which the relative response of the open eye was weaker than the deprived

eye. Thus, fluoxetine-mediated reopening of ocular dominance plasticity in adult animals may be species-specific.

3.2 INTRODUCTION

Monocular deprivation has long been a favored tool by neuroscientists to probe activity dependent modification in neocortical circuits (Wiesel and Hubel, 1963; Hubel and Wiesel, 1965, 1970; Gordon and Stryker, 1996). Monocular deprivation involves the unilateral closure of one eye through lid suture. The response properties of neurons in visual cortex are sensitive to alterations in sensory experience during an early critical period that begins after opening (Hubel and Wiesel, 1965, 1970; Daw et al., 1992; Gordon and Stryker, 1996; Issa et al., 1999). Cortical neurons can shift their ocular dominance during this sensitive period if one eye is deprived of vision through monocular deprivation. Ocular dominance shifts in the critical period involve decreases in the cortical response to the deprived eye, and a subsequent strengthening of the cortical response to the open eye (Frenkel and Bear, 2004; Mrsic-Flogel et al., 2007). Ocular dominance plasticity has traditionally been considered a developmental process restricted to younger animals, but recent reports indicate that ocular dominance plasticity lasts well into adulthood in rodents (Sawtell et al., 2003; Pham et al., 2004; Tagawa et al., 2005; Hofer et al., 2006; Lehmann and Lowel, 2008; Sato and Stryker, 2008).

A growing number of studies indicate that adult plasticity in the visual system can be enhanced through modulation of major neurotransmitter systems, such as nicotinic acetycholine signaling through a Lynx1 knockout (Morishita et al., 2010), serotonin signaling through fluoxetine treatment or direction infusion of serotonin (Bastos et al., 1999; Maya Vetencourt et al., 2008; Maya Vetencourt et al., 2011; Bachatene et al., 2013), and noradrenalinergic signaling through L-threo-3,4-dihydroxyphenylserine

treatment (Mataga et al., 1992). These pioneering experiments demonstrate that ocular dominance plasticity in adult animals can be enhanced by combining monocular deprivation and manipulation of major neurotransmitter systems. Conversely, impairment of these same neuromodualtory systems have been shown to inhibit ocular dominance plasticity (Bear and Singer, 1986; Gu and Singer, 1995; Maya Vetencourt et al., 2011). We were particularly interested in chronic fluoxetine treatment, as fluoxetine is a potentially non-invasive therapeutic treatment for humans suffering from amblyopia. But so far to our knowledge, chronic fluoxetine treatment has only been explored as a plasticity modulator in rats (Bastos et al., 1999; Maya Vetencourt et al., 2008; Maya Vetencourt et al., 2011), and it remains an open question whether re-instatement of adult ocular dominance plasticity could be achieved in another animal model. Indeed, anatomical studies of the neocortical layers of visual cortex show dramatically different innervation patterns of serotoninergic fibers across mammalian clades (Lidov et al., 1980; Morrison et al., 1982; Foote and Morrison, 1984; Gu et al., 1990; Hornung et al., 1990; Voigt and de Lima, 1991). Thus, these differences suggest that modulation of serotonin signaling through chronic fluoxetine treatment might be specific-specific, and reinstatement of adult ocular dominance plasticity could depend on the animal model.

In this study, we investigated relatively long-term monocular deprivation in adult ferrets *in vivo*. The ferret visual system is a well-studied animal model of early visual system development (Chapman and Stryker, 1993; Chapman et al., 1996; Durack and Katz, 1996; Crowley and Katz, 1999; Issa et al., 1999; Ruthazer et al., 1999; White et al., 1999; Li et al., 2006) and recently has become a popular model for ocular dominance plasticity

(Issa et al., 1999; Liao et al., 2002; Medina et al., 2003; Liao et al., 2004; Krahe et al., 2005; Medina and Ramoa, 2005; Krahe and Medina, 2010; Paul et al., 2010; Mower et al., 2011; Yu et al., 2011; Paul and Medina, 2012). Additionally, ferrets possess a highly developed visual system like primates and other carnivores (Hubel and Wiesel, 1962; Horton and Hedley-Whyte, 1984), as the spatial organization of ocular responses are systematically clustered together into ocular dominance columns across the tangential plane of visual cortex (Ruthazer et al., 1999; White et al., 1999). Ocular dominance columns are advantageous to study, since imaging studies can track ocular dominance columns structures longitudinally (Sengpiel et al., 1998; Shtoyerman et al., 2000). For our study we longitudinally tracked ocular dominance plasticity using optical imaging of intrinsic signal. We observed a gradual, age-dependent decline in ocular dominance plasticity with significant ocular dominance shifts being induced in young adult ferrets (less than 6 months old). Additionally, chronically treatment of fluoxetine in both young adult and adult ferrets did not re-instate ocular dominance plasticity. Instead we paradoxically detected a "reverse" ocular dominance shift in young adult ferrets, in which the deprived eye responses were stronger than the open eye responses. Thus, fluoxetine-mediated reinstatement of ocular dominance plasticity appears to be species-specific, and its action in other animal models, as well as humans needs to be assessed carefully.

3.3 RESULTS

3.3.1 Overview of Experiments and Analysis

We used monocular deprivation (MD) of the contralateral eye (14-days) to investigate ocular dominance plasticity in young and adult ferrets. In ferret visual cortex, a previous

study has shown that the peak critical period of ocular dominance plasticity for monocular deprivation is between postnatal day (PD) 30-35 (eye-opening in ferrets) to PD60-65 (Issa et al., 1999). The classic definition for the critical period of ocular dominance plasticity is the period of susceptibility to the effects of monocular deprivation. Thus in this paper, we functionally classified any animals between the ages of PD30-65 as being critical period animals (Figure 1a). Animals between the ages of PD66 and 6 months were considered young adult ferrets. Likewise 6+month old ferrets were considered adults. In all our *in vivo* experiments, we longitudinally imaged the same ocular dominance maps before and after monocular deprivation using optical imaging of intrinsic signal (Figure 1b). At the conclusion of the first imaging experiment, the contralateral eye was sutured shut, while the second imaging experiment began as soon as the deprived eye was re-opened. In ferrets we chronically treated with fluoxetine, fluoxetine treatment began 4-5 weeks before the first imaging experiment.

Optical imaging of intrinsic signal has been used for decades to visualize the functional architecture of visual cortex in carnivores and primates (Bonhoeffer and Grinvald, 1991; Chapman et al., 1996; Godecke et al., 1997; Sengpiel et al., 1998; Shtoyerman et al., 2000). The standard approach to intrinsic signal optical imaging is to present the same visual stimulus set repeatedly and average the response to individual stimuli. Unfortunately, this process can result in unacceptably noisy functional maps and artifacts that can be potentially misleading indicators of plasticity, especially in longitudinal imaging experiments. Thus, for our imaging analysis, we computed probability difference maps using receiver operating characteristic (ROC) analysis (Figure 3c). This method has

been demonstrated to reduce vascular artifact and improve signal-to-noise in functional maps of the visual cortex in bush babies (Purushothaman et al., 2009).

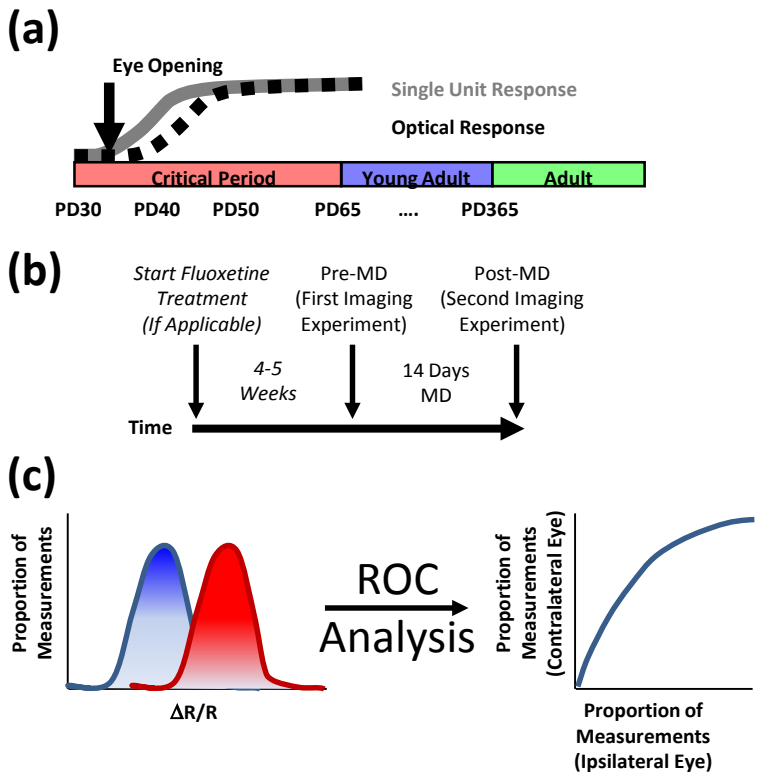

Figure 3-1: Experimental overview of monocular deprivation experiments.

(a) Schematic of the developmental critical period in ferrets. The critical period for ocular dominance plasticity starts at eye-opening at ~PD30 and ends around PD65 (Issa et al., 1999). This early critical period coincides with the rapid maturation of orientation and direction responses to their adult levels (Chapman et al., 1993; Chapman et al., 1996; Li et al., 2006). **(b)** Schematic of the monocular deprivation experiments. Chronic fluoxetine treatment is started 4-5 weeks before the first imaging experiment (when applicable), and is continued until termination of the second imaging experiment. At the conclusion of the first imaging experiment (Pre-MD), one of the ferret's eyes is sutured shut for 14 days

(unless otherwise noted). The second imaging experiment begins when the deprived eye is re-opened. **(c)** In each imaging experiment, measurements of intrinsic signal responses ($\Delta R/R$) were repeated 16-32 times for the monocular presentation of each visual stimulus to either eye (0˚, 45˚, 90˚, and 135˚ gratings). Ocular responses were grouped together for each pixel to form a distribution for the contralateral and ipsilateral eyes (shown red and blue respectively in the above example). From these two distributions, a pixel's contralateral response is estimated non-parametrically as the probability of the area under a ROC curve. This differentiates the true positive response (i.e. the contralateral eye) from the false positive response (i.e. the ipsilateral eye).

3.3.2 Gradual, Age-Dependent Decline in Ocular Dominance Plasticity in Adult Ferrets

First, we investigated the extent of adult ocular ocular dominance plasticity in normal ferrets (n = 9, 3 in each age group: critical period, young adult, and adult). To our knowledge, longitudinal imaging of long-term monocular deprivation has not been attempted before. Most monocular deprivation studies are done in acute experiments, and we thought it would be valuable to directly observe changes in the ocular dominance map. These experiments would also serve as a useful baseline to compare against ferrets chronically treated with fluoxetine.

In this paper, the strength of monocular deprivation was assessed by computing each map's contralateral bias index. The contralateral bias index indicates the proportion of pixels that more strongly respond to the contralateral eye than the ipsilateral eye. A value

of 1 indicates complete contralateral response in a map, while 0 indicates complete ipsilateral response. Previous studies indicate that both the cat and ferret visual cortex initially exhibit a contralateral bias that is gradually eliminated by visual inexperience, the contralateral bias is slowly eliminated by visual experience (Crair et al., 1998; Issa et al., 1999). These findings are consistent with our data, as we observe a significant age-dependent in the contralateral bias index (Figure 2).

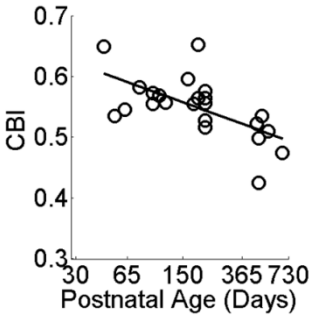

Figure 3-2: Age-dependent decline in the contralateral bias index.
Each datapoint indicates the CBI of an imaged ocular dominance map (n = 23). The line of best fit is shown (CBI = -m*log10(age)+b, where m=0.092 and b=0.76), and the Pearson's Correlation Coefficient is computed ($r = -0.62$, $p < 0.01$).

Next we show some example longitudinal imaging experiments of long-term monocular deprivation for critical period (Figure 3a), young adult (Figure 3b), and adult ferrets (Figure 3c), as well as a ferret that was just imaged longitudinally for 14 days (without MD, Figure 3d). For an initial point of comparison, we compared protracted monocular deprivation in three animals (14day MD) with a short-term monocular deprivation experiment (5d MD). The results were quantitatively similar (Figure 3e), as the contralateral bias index in all four animals decreased by a similar amount (ΔCBI = -0.25

in the 5d MD experiment and ΔCBI = -0.24±0.015 for the 14d MD). These results are similar to another ferret study that reported that >2day MD is needed to create a saturating shift in ocular dominance (Issa et al., 1999), unlike cats which require 2 days (Hubel and Wiesel, 1970; Crair et al., 1997a). We also observed an extended age-dependent decline in monocular deprivation (Figure 3f). Significant ocular dominance shifts could still be induced in young adult ferrets (n = 3, ages between PD114-178, ΔCBI = -0.078±0.013), which is longer than the reported end of ocular dominance plasticity in ferrets at ~PD115 (Issa et al., 1999). However, significant ocular dominance shifts could not be achieved in much older adult ferrets (n =3, ages between PD442-524, ΔCBI = -0.01±0.0015).

There was a non-significant decline in the ΔCBI of normal ferrets that were longitudinally imaged across many weeks (n = 13, no MD, and timelapse durations ranging from 7-75days). This reduction in contralateral bias is consistent with our findings in Figure 2. As this could confound our MD results, we checked whether this was problematic by computing the ΔCBI for each animal, and then normalized the result by the length of the timelapse duration (Figure 3g). We found that with the normalized ΔCBI, critical period and young adult MD experiments were significantly different than their normal counterparts. Also, the strong age-dependent decline in ΔCBI we observed in MD animals is not present in normal animals. We estimated this by computing the Pearson's Correlation Coefficient of the normalized ΔCBI with the logarithm of animal's initiate age (MD animals: $r= -0.83$, $p<0.01$; Normal animals: $r = +0.41$, $p>0.05$). Additionally, the slope for the line of best to the CBI data in Figure 2 is m = 0.002 ,

where CBI = m*age +b. This means for a 14 day timelapse experiment, the expected CBI is small (ΔCBI = -0.0028). Thus, the normal decline in CBI by age is slow and unlikely to be a confounding factor in our monocular deprivation experiments.

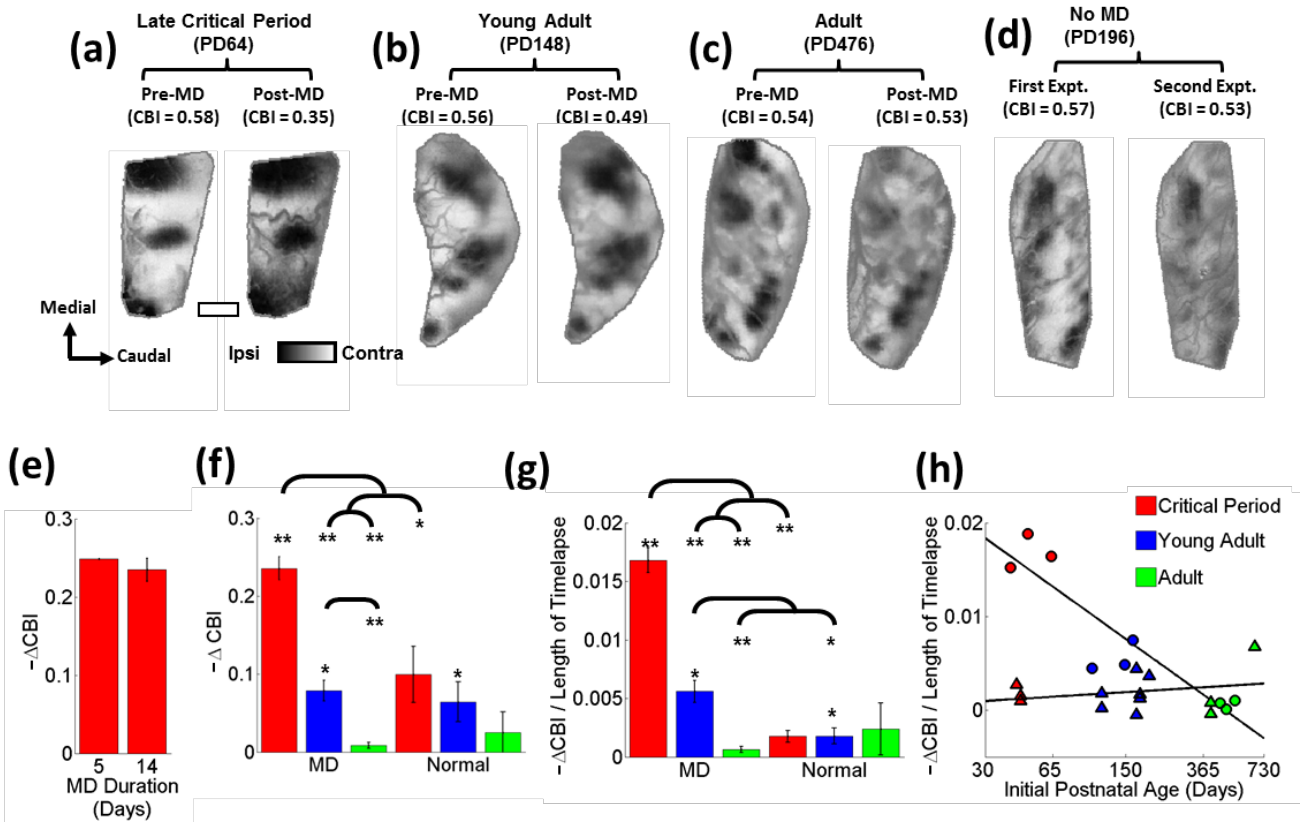

Figure 3-3: Age-dependent decline in ferret ocular dominance plasticity.

(a-d) Example longitudinal imaging of ocular dominance maps before and after monocular deprivation (14 day MD). The initial age of the ferret and contralateral bias index (CBI) are shown. Saturation indicates ocular response bias (black – ipsilateral eye bias, gray – no bias, and white – contralateral eye bias). Scale bar is 1mm. **(a)** Late critical period MD imaging experiment (14 Day MD). See Figure 3a for an animal experiment earlier in the critical period. **(b)** Young Adult MD imaging experiment. **(c)** Adult MD imaging experiment (14 day timelapse). **(d)** Adult imaging experiment, but no

MD. **(e)** Change in the mean contralateral bias index (-ΔCBI) for 5 day MD (n = 1 map) and 14 day MD (n = 3 maps). **(f)** -ΔCBI for 14 day MD experiments and normal animals (no MD, but timelapse varied between 7-75 days). 6 groups are shown: Critical Period MD (red, n = 3 maps), Young Adult MD (blue, n = 3 maps), Adult MD (green, n = 3 maps), Normal CP (red, n = 3 maps), Normal Young Adult (blue, n = 7 maps), and Normal Adult (green, n = 3 maps). 1-way ANOVA across all groups was significant ($p<<0.01$). A 1-way Student's t-test was used to evaluate whether a group's -ΔCBI was significant. A 2-way Student's t-test was then used to assess whether there was a significant change between groups. Significant changes with $p<0.05$ are denoted as '*' and $p<0.01$ are denoted as '**'. **(g)** Same as (f), except -ΔCBI is normalized by the length of the timelapse between imaging experiments in days (14 days for MD experiments, and between 7-75days for normal animals). 1-way ANOVA across all groups was significant ($p<<0.01$) **(h)** Semi-log plot of the initial age of each ferret and -ΔCBI / length of timelapse. Each data point is an imaged map (circles are MD animals and triangles are normal animals). Lines of best fit are shown for both MD and normal animal groups. The Pearson's Correlation coefficient is computed for either group (MD: $r= -0.83$, $p<0.01$; Normal: $r = +0.41$, $p>0.05$).

3.3.3 Rapid Recovery from Monocular Deprivation

One of the benefits of intrinsic signal optical imaging is that functional maps can be visualized relatively rapidly. We took advantage of this feature to track the recovery of monocular deprivation in both critical period and young adult ferrets (Figure 4). Other research in ferret visual cortex has shown that short-term monocular deprivation

experiments of 7 days result in a rapid recovery of the deprived eye (Krahe et al., 2005; Yu et al., 2011); however, it's unknown if longer lapses between monocular deprivation show similar rates of recovery. In Figure 4a-c, we show an example of recovery in a critical period animal (PD49) from 14 days of monocular deprivation. We show the ocular dominance maps in Figure 4a, the deprived eye orientation preference polar map in Figure 4b, and the spared eye orientation preference polar map in Figure 3c. We initially observed a strong reduction in the responses of the deprived eye; however, within about an hour there was some recovery of deprived-eye orientation selected responses in some regions of the visual cortex. We found that this MD recovery in critical period animals (n = 2) was significant in both the binocular zone, as well as in monocular regions initially biased towards the deprived eye (Figure 4d). Thus, MD recovery does not appear to depend on a pixel's initial ocular dominance (Figure 4d). Additionally, the time course of recovery in critical period ferrets (Figure 4e) is not substantially different from young adults (Figure 4f), except the effect in young adult ferrets was less pronounced in magnitude and the recovery more global.

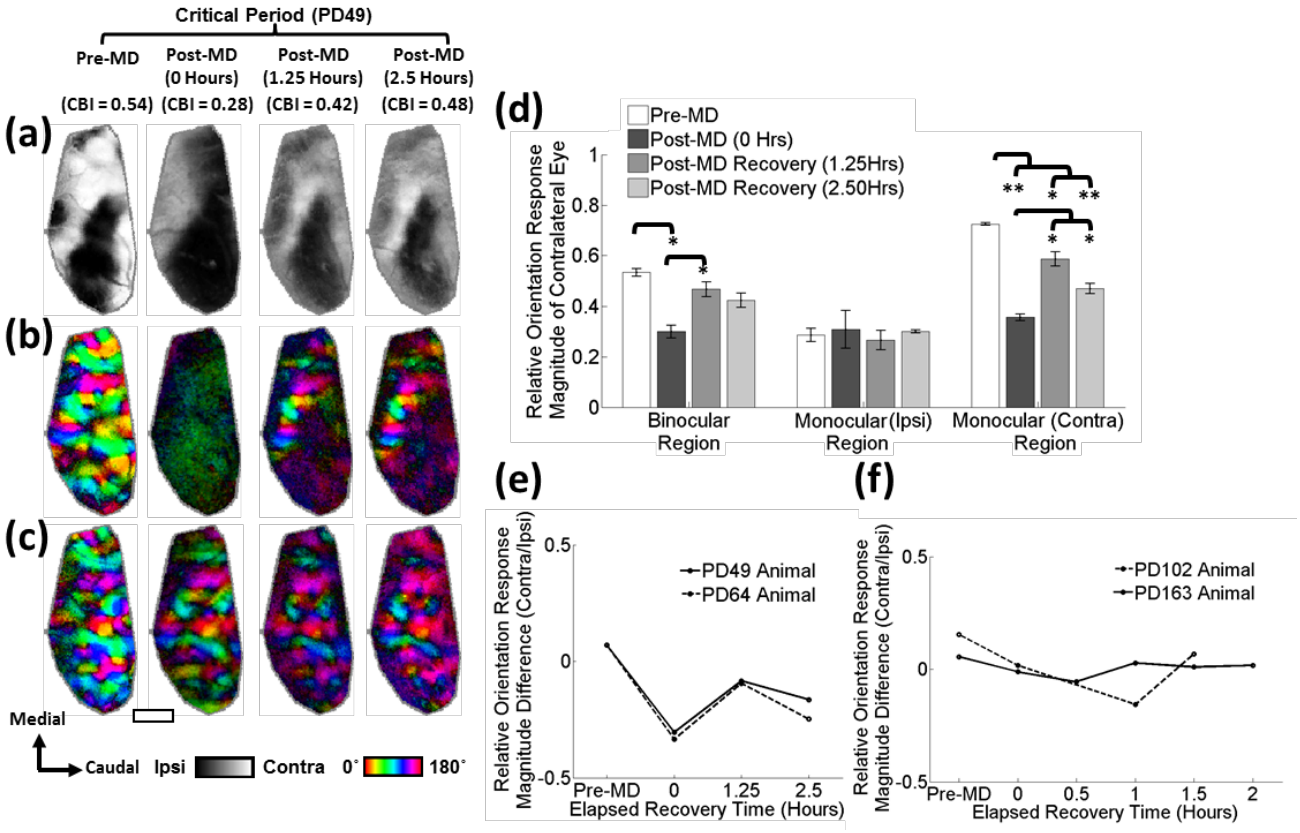

Figure 3-4: Regions of the deprived-eye recover rapidly after long-terms monocular deprivation.

An example longitudinal imaging experiment is shown in (a-c), where the contralateral eye was sutured shut for 14 days (PD49). **(a)** The ocular dominance map is shown before MD (left image), and then after MD (right three images). For the post-MD imaging experiment, responses are shown after opening up the deprived eye: 0 hours (left image), 1.25 hours (center image), and 2.5 hours (right image) elapsed. Saturation indicates ocular response bias (black – ipsilateral eye bias, gray – no bias, and white – contralateral eye bias). Scale bar is 1mm. **(b)** Same as (a), except the contralateral (deprived) eye orientation preference polar map is shown. Hue denotes the preferred orientation according to the legend, while saturation indicates response magnitude. **(c)** Same as (b), except the ipsilateral (spared) eye orientation preference polar map is shown. **(d)** Relative

orientation response magnitude of contralateral-eye response (~0.3 indicates response fully favoring the spared eye, while 0.7 indicates responses favoring the deprived eye). The response magnitude for each animal is the mean response of the imaging ROI. The ratios are shown for four conditions: Pre-MD (white), Post-MD with 0 hours elapsed after opening the deprived eye (dark grey), and Post-MD recovery with either 1.25 hours elapsed (grey) or 2.5 hours elapsed (light grey) after opening the deprived eye, as well as for three maps regions: binocular region, the spared-eye region (monocular ipsilateral eye), and deprived-eye region (monocular contralateral eye). 1-way ANOVA across the three conditions and spared eye regions was significant ($p<<0.01$). A student's t-Test was used to compared across the three conditions and map regions. Significant changes with $p<0.05$ are denoted as '*' . **(e)** Overall time course of the relative response magnitude difference between the contralateral and ipsilateral eyes is shown for two critical period animals (Solid Line – PD49 Animal; Dotted Line – PD64 Animal). **(f)** Same as (e), except two young adult animals are shown (Solid Line – PD102 Animal; Dotted Line – PD163 Animal).

3.3.4 3.2.4 Fluoxetine-Treatment Does Not Restore Adult Ocular Dominance Plasticity

Next we chronically treated young adult and adult ferrets with fluoxetine for 4-5 weeks (oral dosage: 8-12mg/kg per day, n = 7) before beginning 14d monocular deprivation experiments. Our goal was to observe whether chronic fluoxetine treatment could restore ocular dominance plasticity in "post-critical" period animals. We did not observe enhanced ocular dominance plasticity in these ferrets. An example young adult ferret

(Figure 5a) and adult ferret (Figure 5b) are shown. Young adult animals (n = 2) paradoxically displayed a reverse ocular dominance shift (ΔCBI = +0.08±0.001), in which the open eye's response was weaker than closed eye. In contrast, adult ferrets showed no significant changes (n = 5, ΔCBI = +0.007±0.01). Fluoxetine dosage did not appear to be a significant factor in adult ferrets (Figure 5c, 12mg/kg or 6-8mg/kg). A comparison of the fluoxetine MD treated animals with normal animals (with and without MD) revealed that the fluoxetine animals showed similar shifts to their aged-match counterparts, but that the sign of the shift was reversed (i.e. indicating a reverse ocular dominance shift).

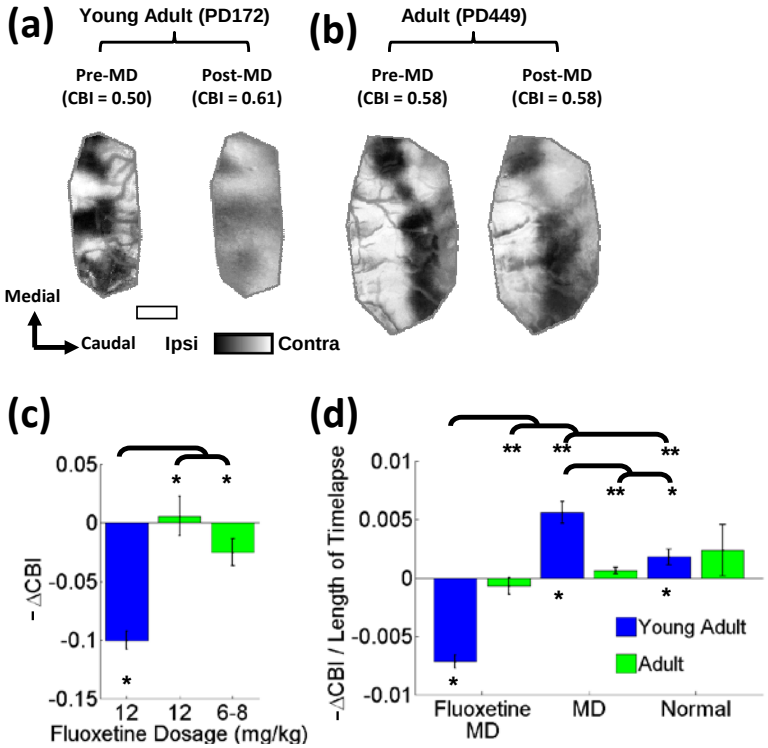

Figure 3-5: Impact of chronic fluoxetine treatment on ocular dominance plasticity in adult ferrets.

(a-b) Example longitudinal imaging of ocular dominance maps before and after monocular deprivation (MD). The initial age of the ferret and contralateral bias index (CBI) are shown. Saturation indicates ocular response bias (black – ipsilateral eye bias, gray – no bias, and white – contralateral eye bias). Scale bar is 1mm. **(a)** Young Adult MD imaging experiment (14 Day MD). **(b)** Adult MD imaging experiment (14 Day MD). **(c)** Change in the contralateral bias index (ΔCBI) for fluoxetine treated animal groups (14 day MD): young adult MD (n=2 maps, treated with 12mg/kg per day) and adult MD (n = 3 maps, treated with 12mg/kg per day; n = 2 maps, treated with 6-8mg/kg per day). 1-way ANOVA across all groups was significant ($p<0.01$). A 1-way Student's t-test was used to evaluate whether a group's ΔCBI was significant. A 2-way Student's t-test was then used to assess whether there was a significant change between groups. Significant changes with $p<0.05$ are denoted as '*' and $p<0.01$ are denoted as '**'. **(d)** ΔCBI normalized by the length of the timelapse between imaging experiments (14 days for all MD experiments, and between 7-75days for normal animals). 6 groups are shown: Young Adult MD - Fluoxetine-treated (blue, n = 2 maps, treated with 12mg/kg per day), Adult MD - Fluoxetine-treated (green, n = 5 maps, treated with 6-12mg/kg per day), Young Adult MD (blue, n = 3 maps), and Adult MD (green, n = 3 maps). Young Adult (blue, n = 7 maps), and Normal Adult (green, n = 3 maps). 1-way ANOVA across all groups was significant ($p<<0.01$).

3.4 DISCUSSION

3.4.1 Efficacy of monocular deprivation in young adult ferrets

In this paper, we combined longitudinal imaging with relatively long-monocular deprivation experiments in ferret visual cortex. We found that the critical period for ocular dominance plasticity appears to exhibit a much longer decline than previously reported (Issa et al., 1999), in which the visual cortex of young adult ferrets could still display ocular dominance shifts. Our results are likely more sensitive than previous experiments, since we directly imaged the same ocular dominance maps longitudinally. Past measurements instead relied on a shift index (Issa et al., 1999), which is computed as the difference of the CBI for the same animal's contralateral and ipsilateral visual cortices. A shift index largely assumes a similar CBI measurement across an animal's hemispheres. Unfortunately, the irregularity in the pattern of ferret ocular dominance columns on the dorsal surface often means the CBI measurement of the contralateral and ipsilateral hemisphere are not the same; thus, the shift index is more vulnerable to intrinsic inter-hemispheric CBI differences.

Our study of adult ocular dominance plasticity in ferret visual cortex is also consistent with reports in mouse visual cortex. 7-14 day monocular deprivation studies in mice also demonstrate the presence of "adult" ocular dominance plasticity that lasts much longer than the critical period (Sawtell et al., 2003; Pham et al., 2004; Tagawa et al., 2005; Lehmann and Lowel, 2008; Sato and Stryker, 2008). But this age-declining ocular dominance plasticity in young adults is eventually absent in adult mice older than 200 days (Lehmann and Lowel, 2008). Similarly we show that adult ferrets (older than one

year) do not display significant ocular dominance shifts. Thus, our study in conjunction with mice implies that there is an extended period of adult ocular dominance plasticity in mammals, and that this phenomenon may not be a peculiar feature of rodent visual cortex.

3.4.2 Features of Adult Ocular Dominance Plasticity

An open question is whether substantial anatomical rearrangement of geniculocortical axons accompanies adult ocular dominance plasticity, akin to cortical plasticity observed after retinal lesions or monocular deprivation in the critical period (Kaas et al., 1990; Antonini and Stryker, 1993; Darian-Smith and Gilbert, 1994; Das and Gilbert, 1995; Antonini and Stryker, 1996; Trachtenberg and Stryker, 2001). Or is adult ocular dominance plasticity mediated merely through compensatory homeostatic mechanisms that maintain an overall tonic level of neural activity (Mrsic-Flogel et al., 2007; Sato and Stryker, 2008; Yu et al., 2011)? In this second paradigm, synaptic weakening of existing synapses to the deprived eye concurrently occurs with synaptic strengthening to afferents of the open eye. This process can occur in the absence of eye-specific thalamo-cortical reorganization. The progressive stability of ocular dominance maps with age after monocular deprivation (as can be seen in Figures 2 and 3) suggest less axonal pruning of thalamo-cortical projections in adults. The rapid recovery of deprived eye responses in both critical period and adult ferrets also points to homeostatic mechanisms being involved. Homeostatic mechanisms are consistent with the report that recovery of the deprived eye in ferret visual cortex is independent of protein synthesis (Krahe et al., 2005). Thus, it appears likely that compensatory homeostatic mechanisms are playing a

much greater role in adult ocular dominance plasticity, unlike in the critical period where both homeostatic mechanisms and geniculocortical reorganization dominate.

3.4.3 Failure of Fluoxetine-Treatment to Reinstate Ocular Dominance Plasticity in Adults

A previous report demonstrated that ocular dominance plasticity in adult rats could be reinstated with chronic fluoxetine treatment (Maffei and Turrigiano, 2008). However, in this present study, we were unable to reinstate ocular dominance plasticity in adult ferrets using chronic fluoxetine treatment. A potential explanation for these results is that the mechanism of fluoxetine's actions in rat visual cortex is not conserved across the species. Fluoxetine, a selective-serotonin reuptake inhibitor, may only promote neural plasticity in a species-specific manner, because anatomical studies show different innervation patterns of serotoninergic fibers across mammals (Lidov et al., 1980; Morrison et al., 1982; Foote and Morrison, 1984; Gu et al., 1990; Hornung et al., 1990; Voigt and de Lima, 1991).

Serotonin signaling is also known to influence GABA signaling in the visual cortex (Reader, 1978; Gu and Singer, 1995; Roerig and Katz, 1997; Edagawa et al., 2000; Jakab and Goldman-Rakic, 2000; Edagawa et al., 2001; Xiang and Prince, 2003). However due to the different innervations patterns across mammals, the net action of fluoxetine may either shift the intracortical inhibition/excitation balance in a circuit-dependent manner. Indeed, one the underlying mechanism for the physiological ocular dominance plasticity appears to involve finely modulating the ratio of cortical inhibition to excitation within a specific ratio to be permissive for ocular dominance plasticity (Hensch, 2005). Thus, this

appears to require an enhancement of inhibition to begin the critical period in young animals, while a net reduction of cortical inhibition is required to reinstate ocular dominance plasticity in adults (Fagiolini and Hensch, 2000; Morales et al., 2002; Hensch, 2005; He et al., 2006; Maya Vetencourt et al., 2008; Morishita and Hensch, 2008; Harauzov et al., 2010; Huang et al., 2010).

Interestingly our data is still in support of this model. The young adult ferrets chronically treated with fluoxetine displayed a paradoxical "reverse" ocular dominance shift. While seemingly a bizarre phenomenon, this may serve as important clue for the action of fluoxetine in ferrets. Similar reverse ocular dominance shifts have been reported by other groups in cat visual cortex. These groups have shown that when monocular deprivation is combined with the pharmacologically infusion of either muscimol, a GABAA agonist (Reiter and Stryker, 1988), or neurotrophic factors, such as BDNF or NGF (Gu et al., 1994; Galuske et al., 1996; Galuske et al., 2000), deprived-eye responses become stronger than the spared eye. These findings are striking, as local infusions of either BDNF or diazepam, a $GABA_A$ agonist, are also known to expand ocular dominance columns in kittens (Hata et al., 2000; Hensch and Stryker, 2004). Thus, neurotrophic signaling and the tonic level of inhibition appear to be strongly coupled together. Indeed, it's been shown that BDNF signaling in mouse visual cortex promotes the maturation of cortical inhibition during the critical period (Huang et al., 1999; Yamada et al., 2002).

Curiously chronic treatment with fluoxetine, or the infusion of serotonin and BDNF promotes adult ocular dominance plasticity in adult rat visual cortex (Bastos et al., 1999;

Maya Vetencourt et al., 2008; Maya Vetencourt et al., 2011). Hence, serotonin-signaling and BDNF appear to promote a reduction of GABA tone in adult rats, which is hypothesized to play an important role in the reactivation of ocular dominance plasticity in adult mammals (Sale et al., 2007; Maya Vetencourt et al., 2008; Harauzov et al., 2010; Maya Vetencourt et al., 2011). But it's possible then that in young carnivores, such as cats and ferrets, promotion of neurotrophic factors enhances cortical inhibition, while in adult rats, neurotrophic factors lowers inhibition. Thus, the mechanisms of BDNF signaling may not be conserved across species. If true, this might provide an explanation why chronic fluoxetine treatment induces a reverse ocular dominance shift in young adult ferrets and not in fully mature ferrets. Similar to fluoxetine treatment, BDNF infusion in adult cat visual cortex also fails to promote any ocular dominance plasticity (Galuske et al., 2000), while in the critical period local BDNF infusion results in the "reverse" ocular dominance shift we described earlier. Thus, it's tempting to speculate whether the underlying mechanisms of chronic fluoxetine treatment in ferrets might be related to those involved in the local infusion of BDNF in cat visual cortex.

3.5 METHODS

3.5.1 Basic Experimental Procedures

Longitudinal optical imaging experiments were performed in ferrets with ages ranging from PD40 to PD677 (n = 23). Experimental procedures were approved and carried out in accordance with protocols approved by the local IACUC of Carnegie Mellon University. A subset of ferrets (n = 7) were treated with fluoxetine for 6-7 weeks (4-5 weeks prior to

MD, plus 14 days of MD). Chronic treatment involved the oral administration of fluoxetine with a dosage of either 6-12mg/kg per day.

3.5.2 Imaging Experiments

We maintained animal anesthesia with isoflurane (1-3% for surgery, in either a 1:2 or 1:1 mixture of O2 and N_2O). All ferrets were tracheotomized and artificially ventilated. We monitored the animal's vital signs at all times during imaging experiments: a rectal probe for animal temperature (37.5-38°C), EKG for heart-rate (270-300bpm), and a capnometer for expired CO_2 (3-4%). Ferrets were initially placed in a stereotaxic device to stabilize the head. Next we performed a midline scalp incision and a craniotomy over the visual cortex (also consisting of a duratomy). The imaging window was stabilized by filling the exposed craniotomy with 2% agarose, and then fastening a small glass window with dental acrylic on top of the agarose.

In the first longitudinal imaging experiment, we placed artificial dura (made of transparent, soft thermoplastic polyurethane) between the cortex and the resected dura. The skull was fastened back into place with tissue acrylic cement and the scalp was closed with surgical suture. In monocular deprivation experiments, the contralateral eye was shut using surgical suture. We provided antibiotics for 5 days to prevent post-surgical infection. All steps in the first longitudinal imaging experiment followed standard aseptic practices. At the termination of the second longitudinal imaging experiments, ferrets were euthanized with an overdose of sodium pentobarbital.

Intrinsic signal images were acquired using software and hardware from Optical Imaging Inc. (Imager 3001). We recorded the surface blood vasculature map under illumination with green light (595nm) and measured intrinsic signal changes with red light (700nm) with a tandem lens macroscope attached to CCD camera. Acquired images consisted of 1020x1020 pixels with a 157pixels/mm resolution.

3.5.3 Visual Stimulation

Visual stimuli were presented on a 24" monitor using a visual stimulus generator (*Cambridge Systems*). Visual stimulation involved presenting a 8s visual stimulus of 100% contrast, square-wave gratings (0.1-0.5 cycles per degree). We presented gratings at four different orientations in blockwise intrinsic signal experiments (0°, 45°, 90°, and 135°). For the generation of ocular dominance maps, eye-specific responses were measured by covering one eye with mechanical shutters.

3.5.4 Image Analysis

Raw data is recorded as consecutive datasets of single condition activity maps. Measurements of intrinsic signal responses (ΔR/R) were repeated 16-32 times with the monocular presentation of each visual stimulus to either eye (0˚, 45˚, 90˚, and 135˚ gratings). We performed a "first-frame" subtraction to each single-condition trial map using the first 2s pre-stimulus period as a baseline, and subtracting it from the average of the 8s trial (with visual stimulation). Next we applied a 2-d gentle bandpass spatial filter to eliminate signal strength variations and measurement noise, in all single-condition

maps (orientation preference, direction preference, and ocular dominance). The following bandpass filter was applied to each image (Fermi-filter):

$$Filter(\lambda_{cutoff}, \lambda) = \frac{1}{1 + e^{-\frac{\lambda_{cutoff}}{T}(\frac{1}{\lambda_c} - \frac{1}{\lambda})}}$$

$$\mathcal{F}^{-1}(\mathcal{F}(Image) \times Filter(\lambda_{lp}, \lambda)) \times (1 - Filter(\lambda_{hp}, \lambda)))$$

, where $\mathcal{F}$ is the Fourier Transform, λ is the spatial wavelengths present in the image, λ_{cutoff} is the filter cutoff (low-pass cutoff (λ_{lp}): 0.05mm; high-pass cutoff (λ_{hp}): 4.5mm for orientation and direction preference, and 2.5mm for ocular dominance), and T is the "temperature" parameter of the fermi-filter (T = 0.05).

Probability difference maps were computed using the same approach as has been described elsewhere (Purushothaman et al., 2009). Briefly for each pixel, ocular responses to all four orientation gratings were grouped together. This formed a distribution of contralateral and ipsilateral eyes. We combined these distributions into a normalized histogram, and estimated a pixel's contralateral response non-parametrically as the probability of the area under a ROC curve (using the trapezoidal rule). This differentiates the true positive response (i.e. the contralateral eye) from the false positive response (i.e. the ipsilateral eye). This probability map, differentiating the contralateral eye responses from the ipsilateral eye responses, is taken as the ocular dominance map. Values of +1 indicate a perfectly discriminated contralateral response, -1 indicates a perfectly discriminated ipsilateral response, and 0 indicates the responses are binocular (and cannot be discriminated from each other). We also computed probability difference maps for orientation maps, but in this case we compared the ocular responses of the brain

to a single-condition visual stimulus against its orthogonal pair (ie differentiating orientation responses of a 0º grating from a 90º grating (cardinal orientations) or a 45º grating from a 135º grating (oblique orientations)).

The vector addition approach was used to compute orientation preference maps by summing up the cardinal and oblique probability difference orientation maps, using the following formula:

$$z = R_{0-90} + i * R_{45-135}$$

$$\theta_{pref} = z/(R_{0-90} + R_{45-135})$$

, where z is the orientation response (complex-field), θ_{pref} is the pixel's orientation preference, R_{0-90} is the cardinal probability difference map, R_{45-135} is the oblique probability difference map. Imaging ROIs were manually selected to include only regions that responded to the visual stimulus. In the longitudinal imaging data, we co-registered all functional maps in the first imaging experiment to the second imaging experiment via a 2-d affine transform (using penetrating blood-vessels as fiducial landmarks).

3.5.5 Data Analysis

We computed the contralateral bias index (CBI) for estimating the strength of contralateral responses in an ocular dominance map (Reiter et al., 1986; Issa et al., 1999). The ocular dominance map is split into 7 bins based on the strength of a pixel's ocular dominance:

$$CBI = [(N_1 - N_7)^2 + (2/3) \cdot (N_2 - N_6)^2 + (1/3) \cdot (N_3 - N_5)^2 + N_{Total}]/2 \cdot N_{Total}$$

, where N_{Total} is the total number of pixels in an imaging ROI, and N_X is the number of pixel's in an ocular dominance bin (eg X = 1 favors contralateral eye response, X=4 indicates binocular responses, and X=7 favors ipsilateral eye responses). A major benefit of the contralateral bias index index is that it's less error-prone. A categorical error of placing a pixel in ocular dominance bin that is immediately above or below its true ocular dominance bins, results in the same contralateral bias index. In some cases, we also estimated a pixel's orientation selectivity (OSI), which is the absolute value of the complex-field orientation response: OSI = abs(z).

4 Ferret visual cortex plasticity depends on the local functional architecture

4.1 ABSTRACT

Under different experimental conditions, the functional architecture of visual cortex has been described as either stable and robust, or plastic and responsive to visual stimulation. Here we show that while neurons can undergo changes in their response properties, the orientation preference map they form constrains their degree of neural plasticity. Specifically, we induced local shits in orientation preference tuning in ferret visual cortex by pairing visual stimulation with direct intracortical stimulation of layer 2/3 neurons. We demonstrate with intrinsic signal optical imaging and two-photon calcium imaging that pairing-induced changes in the orientation tuning of neurons is greatest when local cortical activation is far from regions with abrupt changes in orientation preference (pinwheels and fractures). Our results suggest pairing-induced plasticity is greatest whenever co-activated cell populations share similar functional properties and that local cortical connections play an important role in modulating the efficacy of non-associative learning in visual cortex.

4.2 INTRODUCTION

The capacity for neo-cortical circuits in the mammalian brain to alter their functional responses adaptively based on changes in sensory experience is believed to play an important role in the early establishment and maturation of the visual cortex, as well as perceptual learning in adulthood (White et al., 2001b; Li and Gilbert, 2002; Li et al., 2008a; Li et al., 2008b; Wang et al., 2010). This is in contrast to the traditional view that orientation tuning is a stable property of visual cortex and visual cortex neurons are simply static filters reflecting feedfoward thalamo-cortical visual input (Hubel and Wiesel, 1962). Accumulating evidence over the last couple decades has suggested that the responses of visual cortex neurons remain dynamic, such that neurons can alter their spiking responses based on spatial-temporal contextual information beyond a cell's classical receptive field (Toth et al., 1996; Levitt and Lund, 1997; Polat et al., 1998; Somers et al., 1998; Hashemi-Nezhad and Lyon, 2011), combinatorial variations in the spatial-temporal properties of the visual stimulus itself (Basole et al., 2003), as well as prior sensory experience (Das and Gilbert, 1995; Sengpiel et al., 1998; Dragoi et al., 2000; White et al., 2001b; Hofer et al., 2006; Wang et al., 2010; Berkes et al., 2011; Yu et al., 2011). Another significant factor that has begun to receive some attention over the last decade is the influence of local functional architecture (Dragoi et al., 2000; Dragoi et al., 2001; Schummers et al., 2002; Schummers et al., 2007; Hashemi-Nezhad and Lyon, 2011); however, the influence that local functional architecture can have on the plasticity of cortical neurons still remains poorly understood.

The visual cortex also serves an ideal candidate to study local functional interactions

between neural circuits and how they constrain neural plasticity in the neocortex. This is in large part due to the robust diversity in the functional organization of the primary visual cortex, namely the presence of homogeneous and heterogeneous zones of orientation preference. Neurons in the visual cortex of mammals with highly developed visual systems, such as carnivores and primates, are functionally organized into distinct domains or cortical columns (Hubel and Wiesel, 1962). Many of these homogenous domains exhibit similar functional selectivity for the orientation of a visual stimulus and form a local 2-D functional map of orientation preference across the surface of the primary visual cortex. The orientation preference map smoothly changes across the cortical surface, but is also systematically punctuated by heterogeneous regions, in which orientation preference converges at fracture lines or around singularities called pinwheel centers ((Bonhoeffer and Grinvald, 1991; Ohki et al., 2006). Thus, depending on a neuron's location in the orientation preference map, neurons may integrate intracortical synaptic input from a very narrow range of orientation preferences (iso-orientation domains) or from a much broader range (pinwheel centers and fracture lines).

Prior studies have indicated that the orientation preference of neurons in the cat visual cortex can be altered using plasticity-inducing paradigms (Fregnac et al., 1988; Dragoi et al., 2000; Dragoi et al., 2001; Schuett et al., 2001; Godde et al., 2002). Moreover two of these studies demonstrated that heterogeneity in the orientation preference of the local neural circuitry can constrain neural plasticity in the visual cortex: Dragoi et al. (2001) found that neurons in the visual cortex near pinwheel centers more strongly shift their orientation preference away from the orientation of an adapting stimulus. Schuett et al.

(2001) demonstrated that pairing a brief visual stimulus with electrical microstimulation of the visual cortex was capable of inducing local shifts in orientation preference of neurons. However, Schuett et al. found that neurons near pinwheel centers exhibited *less* plasticity than neurons in iso-orientation domains.

Taken together these two previous studies suggest that functional architecture is an important determinant in whether neurons can modify their functional responses. However, the above studies disagreed on the interaction between the plasticity produced and pinwheels centers, in addition to being limited in the spatial pattern by which the visual cortex could be stimulated. To address some of these challenges, Channelrhodopsin-2 (ChR2) provides the exciting possibilities of spatial patterned transfection and/or spatially patterned activation (Nagel et al., 2003; Boyden et al., 2005; Arenkiel et al., 2007). Here we have extended previous results by pairing brief visual stimulation with direct activation of neural tissue in ferret visual cortex with either ChR2 optical stimulation or electrical stimulation. Direct optical activation was achieved by selectively transfecting layer 2/3 neurons in the visual cortex with a viral vector containing ChR2, which enabled transfected neural populations to be subsequently activated by blue light. The functional activity of the primary visual cortex was assayed using: optical imaging of intrinsic signal to measure activity-related changes in tissue reflectance at the resolution of the orientation preference map (spanning multiple millimeters of visual cortex) and two-photon calcium imaging to measure visually-evoked fluorescence changes in single layer 2/3 neurons. Our specific aims in this study were to investigate:

- the spatial extent and magnitude of pairing-induced modification in ferrets, a closely related carnivore to cats.
- whether pairing-induced modification of orientation preference in ferrets depends on either a cell's position in the orientation preference map (i.e. near or far from pinwheel centers) or its initial orientation preference.
- whether co-activation of multiple stimulation sites, within interaction range of each other, non-linearly influences pairing-induced modification.

4.3RESULTS

4.3.1 Pairing Protocol

We adopted a similar pairing-protocol to the one used by Schuett et al. to perturb the orientation preference tuning of cells in the ferret visual cortex (Schuett et al., 2001). We paired a brief, 20-ms visual stimulus followed by direct cortical stimulation of neural tissue in layer 2/3 of the visual cortex (Figure 1). Cells were directly activated using either: photostimulation of transfected cell populations with Channelrhodopsin-2 (Figure 1d, left) or monopolar electrical stimulation with a tungsten electrode (Figure 1d, right). For photostimulation experiments, neurons were transfected with Channelrhodopsin-2/YFP approximately two-to-three weeks prior to any imaging experiments to allow sufficient time for cells to express Channelrhodopsin-2. Effectiveness of direct cortical stimulation was confirmed by optical imaging of intrinsic signals without visual stimulus (Figure 1e).

Cortical stimulation was delayed relative to the onset latency of cortical responses to a visual stimulus. This step ensured that the direct activation of neural tissue in visual cortex coincided with responses to the presentation of the paired orientation. Single-unit recordings in the visual cortex of one ferret showed the latency of neural responses to a 20-ms visual stimulus was 34.95ms (n = 11 cells). Our measured latency to a visual stimulus is consistent with a recent study in ferret visual cortex, which reported a latency to onset of 33.5ms (Tolhurst et al., 2009). For our experiments, we chose a delay of 30-65ms relative to the onset of the visual stimulus (Figure 1b).

To ensure that the visual stimulation paradigm did not simply evoke non-specific changes in the visual cortex, we also interleaved the presentation of the paired stimulus with the orientation orthogonal to the paired angle (Figure 1c). However, the presentation of the orthogonal stimulus was not paired with direct cortical stimulation. The presentation of each visual stimulus was repeated at a rate of 7Hz for 3s, which was then followed by a 3s blank period. During pairing experiments, the entire block trial of 12s was repeated continuously for 2-4 hours. In this way, one stimulus orientation was favored by pairing with cortical stimulation, while the orthogonal orientation was not.

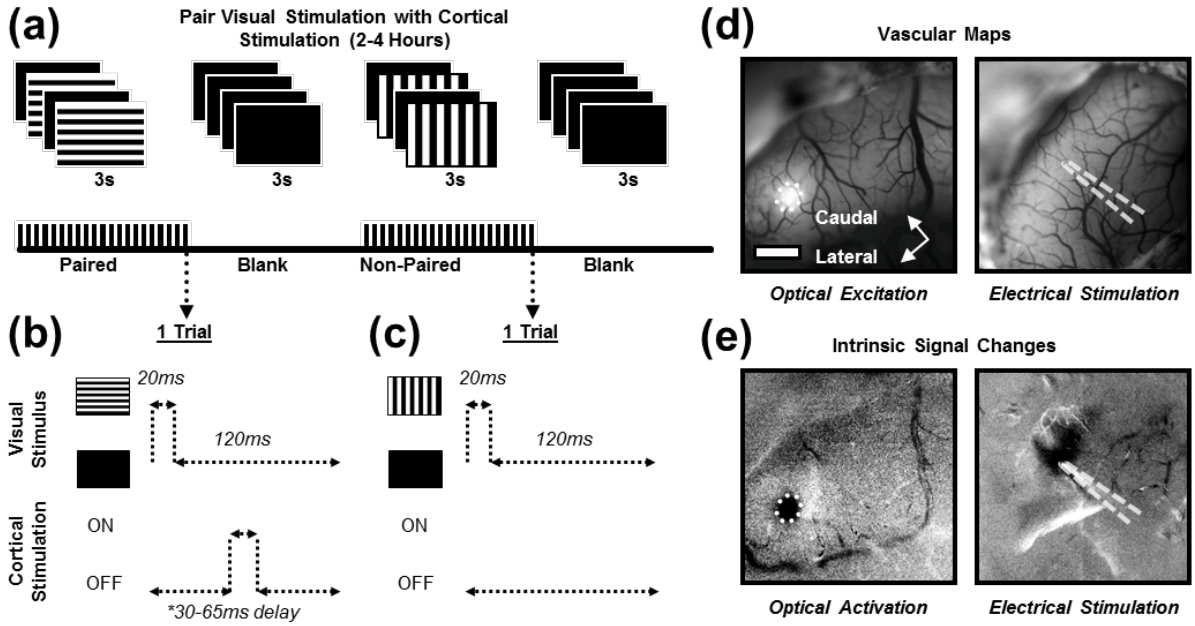

Figure 4-1: Experimental schematic of the pairing-protocol.

(a) For 2-4 hours, two orthogonally orientated gratings are flashed on a screen for 20-ms at a rate of ~7Hz for 3s. Each 3s period is interleaved between 3s blank periods, in which no visual stimulus is presented. (b) One of the two presented orientations is followed by direct activation of local neurons in the visual cortex using cortical stimulation after a 30-65ms delay. This delay ensures that cortical neurons receive cortical stimulation after the onset of visually evoked activity. (c) For the non-paired orientation, no cortical stimulation is applied. (d) Cortical stimulation of layer 2/3 neurons is achieved either by optically activating cells transfected with ChR2/YFP using 473-nm light (see the YFP fluorescence in the dashed circle) or electrical stimulation with a tungsten electrode (inserted 300um deep). Vascular maps from two representative ferrets reveal the location of the stimulation sites, one for each stimulation methodology. (e) Both stimulation methodologies are able to evoke strong intrinsic signal responses at the sites of cortical stimulation (average of 5 trials shown).

4.3.2 Pairing-Induced Modification of the Orientation Preference Map

In accordance with previous work in the cat visual cortex (Schuett et al., 2001), the pairing protocol was capable of inducing large modifications in the ferret orientation preference map as assessed by block-wise intrinsic signal imaging (Figure 2). We provide two examples of pairing in Figure 2, one using optical stimulation (Figure 2a-c, g-i) and the other electrical stimulation (Figure 2d-f, j-l). In both cases, enlarging activation areas (Figure 2c,f) and shifts toward paired orientation (Figure 2i l) were observed, as indicated by hot color pixels. In order to quantify these visual inspections, data were analyzed by annular ROIs around the stimulation site (Figure 2m). There was a weakening of cortical response to the orthogonal orientation near the stimulation site (green lines in Figure 2n), and a corresponding enhancement of the paired orientation's response in the electrical stimulation example (dashed red line in Figure 2n). The net effect was a local pairing-induced shift in orientation preference towards the paired orientation near the stimulation site (Figure 2o). As an internal control for inter-trial variability, the pairing effect vanished when the pre-pairing imaging dataset was split into even and odd trials and then cross-compared against itself (Figure 2o).

In the group data (n = 17, includes both electrical and optical stimulation), we observed a non-significant shift towards the paired orientation (Figure 3b, n = 17) for ROIs located close to the stimulation site (i.e. within 0.5mm of the stimulation site). However, the overall magnitude and direction of the map modifications was variable from one orientation map to the next. In both optical and electrical stimulation experiments, maps often showed modest-to-high enhancement, while in a few cases there was suppression of

the cortical response to the paired orientation.

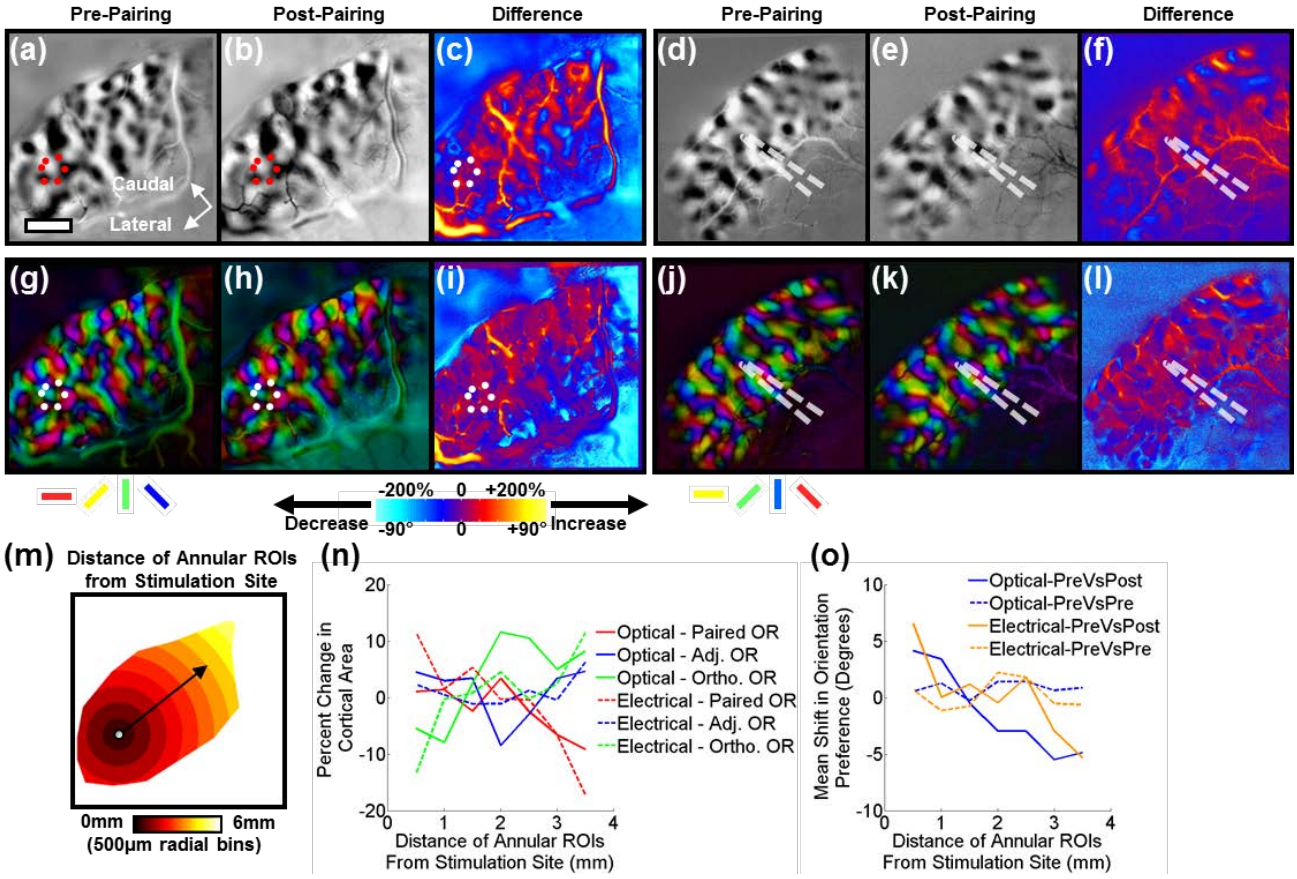

Figure 4-2: Examples of pairing-induced modification in the ferret orientation preference map using either optical stimulation (a-c, g-i) or electrical stimulation (d-f, j-l).

(a, b, d, e) The block-averaged single condition response maps for the paired orientation are shown prior to pairing (a, d) and after pairing (b, e). **(c, f)** Differential maps of the pre-pairing versus post-pairing single condition response maps are also shown. Warmer colors indicate an increase in cortical response to the paired orientation, while cooler colors indicate a weakening in cortical response, and purple indicates no change. **(g, h, j, k)** The orientation preference map is shown prior to pairing (g, j) and after pairing (h, k). Hue denotes the preferred orientation according to the legends below (g) and (j)

respectively, while saturation indicates response magnitude. The paired orientation is denoted by red, and is 0˚in the optical stimulation example (g-i) and 135˚ in the electrical stimulation example (j-l). **(i, l)** The difference map of orientation preference between the pre-pairing versus post-pairing orientation maps are also shown. Warmer colors indicate an attractive shift towards the paired orientation, while cooler colors indicate a repulsive shift, and purple indicates no change. **(m-o)** Cortical areas were segregated into 500μm annular ROIs relative to the stimulation site (m). We found that local ROIs, within 1mm of the stimulation site, displayed pronounced pairing-induced changes in the amount cortical area preferring the paired and orthogonal orientations (n) ("OR" = orientation, "Adj." = adjacent orientation [22.5 – 67.5° from paired angle], "Ortho" = orthogonal orientation), as well as orientation preference tuning (o)**.** However, these changes are observed only in an analysis of pre-pairing vs. post-pairing maps (blue and yellow solid lines), but not when the pre-pairing map dataset, split into even and odd trials, is compared against itself (blue and yellow dotted lines). Scale bar in (a) is 1mm and applies to all images in this figure.

4.3.3 Relationship of Pairing-Induced Shift in Orientation Preference to Functional Architecture

To understand the source of the variability in the pairing-induced shifts, we examined the relative location of the stimulation site within the animal's orientation preference map (Figure 3a, left image), specifically the stimulation site's Euclidean distance to its nearest-neighbor pinwheel center or fracture line (DNP). A high DNP indicates stimulation sites that are located far from pinwheel centers, while a low DNP indicates

the stimulation site is in close proximity to a pinwheel center (Figure 3a, right image). We found pairing-induced shifts were greatest when the stimulation site's DNP was high, which meant local cortical activation far from pinwheel centers evoked stronger pairing-induced shifts (Figure 3c). This effect was quantified by measuring the Pearson's correlation coefficient of each map's mean shift in orientation preference versus the stimulation site's DNP. For pixels located within 0.5mm of the stimulation site, we found there to be a large and significant correlation: r = 0.79 for all intrinsic signal imaging experiments ($p < 0.001$), r = 0.84 for optical stimulation experiments ($p < 0.05$), and r = 0.83 for electrical stimulation experiments ($p < 0.01$). The correlation maintained significance for map locations within ~1mm of the stimulation sites (Figure 3d). This suggests that the variability in the pairing-induced shifts can be largely explained by local functional architecture.

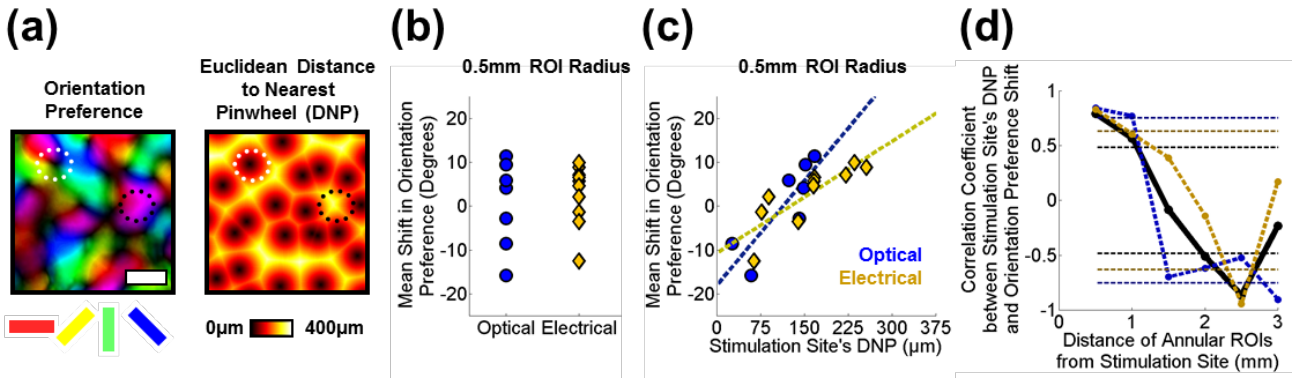

Figure 4-3: Pairing-induced shifts in the ferret orientation preference map depends strongly on local geometric map structure, specifically the distance of the stimulation site to regions of the visual cortex with abrupt changes in orientation preference.

(a) An example orientation preference map (*left image*) with a corresponding image denoting the Euclidean distance of each pixel from its nearest-neighbor pinwheel center

or linear fracture (DNP, *right image*). Scale bar length is 400um. **(b)** We found substantial case-to-case variability in both experimental groups with respect to the mean pairing-induced shift in orientation preference of pixels located within 0.5mm of the stimulation site (blue circles = optical stimulation experiments [n= 7], yellow diamonds = electrical stimulation experiments [n = 10]). **(c)** However, the mean pairing-induced shift in orientation preference in both experimental groups was strongly predicted by the stimulation site's DNP ($r = 0.79$, $p < 0.001$ [all intrinsic signal imaging experiments]; $r = 0.84$, $p < 0.05$ [optical stimulation experiments]; $r = 0.83$, $p < 0.01$ [electrical stimulation experiments]). The best fit line for each experimental group is shown. For optical stimulation experiments the stimulation site ROI was centered around the centroid of the site of viral transfection, while the tip of the stimulation electrode was used for electrical stimulation experiments **(d)** For both experimental groups, the correlation between the pairing-induced shift and the stimulation site's DNP declines with annular ROI distance from the stimulation site (black – all intrinsic signal imaging experiments, blue – optimal stimulation experiments, yellow – electrical stimulation experiments). The corresponding dotted horizontal lines indicate the threshold for the correlation coefficient's significance. All statistical tests on the correlation coefficient were done with Student's t-test.

We further investigated the local functional structure versus shift in orientation preference, by splitting the experimental data into two groups. The grouping was based on how far the stimulation site was pinwheel centers. We specifically used a 150μm threshold with respect to the stimulation site's DNP. The group where the stimulation site's DNP was high (n = 8) exhibited a significant, pairing-induced shift in orientation

preference towards the paired orientation within 1mm of the stimulation site (~2-7˚ shift in orientation preference, Figure 4a). These changes were accompanied with an areal enlargement in the cortical area preferring the paired orientation, and with a concomitant decrease in cortical area preferring the orthogonal orientation (Figure 4b). In contrast, the second group, where the stimulation site's DNP was low (n = 9), failed to display any significant orientation preference shifts or areal changes (Figure 4a, c).

Next, we performed control experiments to ensure that the pairing-induced effects did not simply arise from non-specific, inter-trial variation or from repeated visual stimulation (Figure 4a). First, we did not observe significant pairing effects when the pre-pairing imaging dataset was split into even and odd trials and then cross-compared against itself (n = 23). These results indicate that the pairing-effects are not likely due to inter-trial fluctuations in orientation preference. Secondly, a set of sham experiments (n = 3) were also performed to assess the possibility that the visual stimulation paradigm alone might have an effect on orientation responses. These animals experienced repeated visual stimulation for 3 hours, but not direct cortical stimulation. We detected only small changes in the orientation preference of pixels after visual stimulation only (Figure 4a). Moreover, the absence of enhancement to the unpaired orthogonal orientation angle in the pairing experiments suggested repeated visual stimulation did not by itself enhance the cortex's response to a visual stimulus. Thus, each of these control experiments demonstrated stability in the orientation preference map in the *absence* of pairing with cortical stimulation.

4.3.4 Modification is Independent of Orientation Preference

Although we show that pairing-induced shifts depend on the local functional architecture, this observation might be simply explainable by an initially weak cortical response to the paired orientation near pinwheels. If this hypothesis were, we would then anticipate that cells only shift their responses towards the paired-orientation if a cell's initial orientation preference most closely matched the paired visual stimulus. To assess whether pairing-induced shifts depended on the initial orientation preference tuning of cells (relative to the paired orientation), pixels in the group where the stimulation site's DNP was high (n = 8, same as the preceding section) were segregated into three orientation preference sub-groups (0-30˚, 31-60˚, and 61-90˚ relative to the paired orientation preference). We found that the resultant orientation shift was still significant for all tested sub-groups within 0.5mm of the stimulation sites (Figure 4d), suggesting the pairing-induced changes were actually independent of each pixel's initial orientation tuning. In a similar manner, the group where the stimulation site's DNP was low (n = 9) did not show significant changes across all three orientation preference groups (*data not shown*).

We also tested whether the stimulation site's orientation preference was important. In Figure 4e, we plot the orientation preference of the stimulation site (relative to the paired orientation) versus the pairing-induced shifts local to the stimulation site (i.e. the mean shift in orientation preference for all pixels within 0.5mm of the stimulation sites). The flatness of the curves indicates independence of the stimulation's site orientation preference with the mean pairing induced shifts. We observed this independence across electrical and optical stimulation paradigms, as well as when the stimulation site's DNP

was high or low. Together the data in Figure 4d-e demonstrate pairing-induced plasticity is independent of a cell's orientation. And thus the weaker pairing-induced shifts observed in animal experiments with low DNP values cannot simply be explained away by weak cortical responsiveness to the paired visual stimulus.

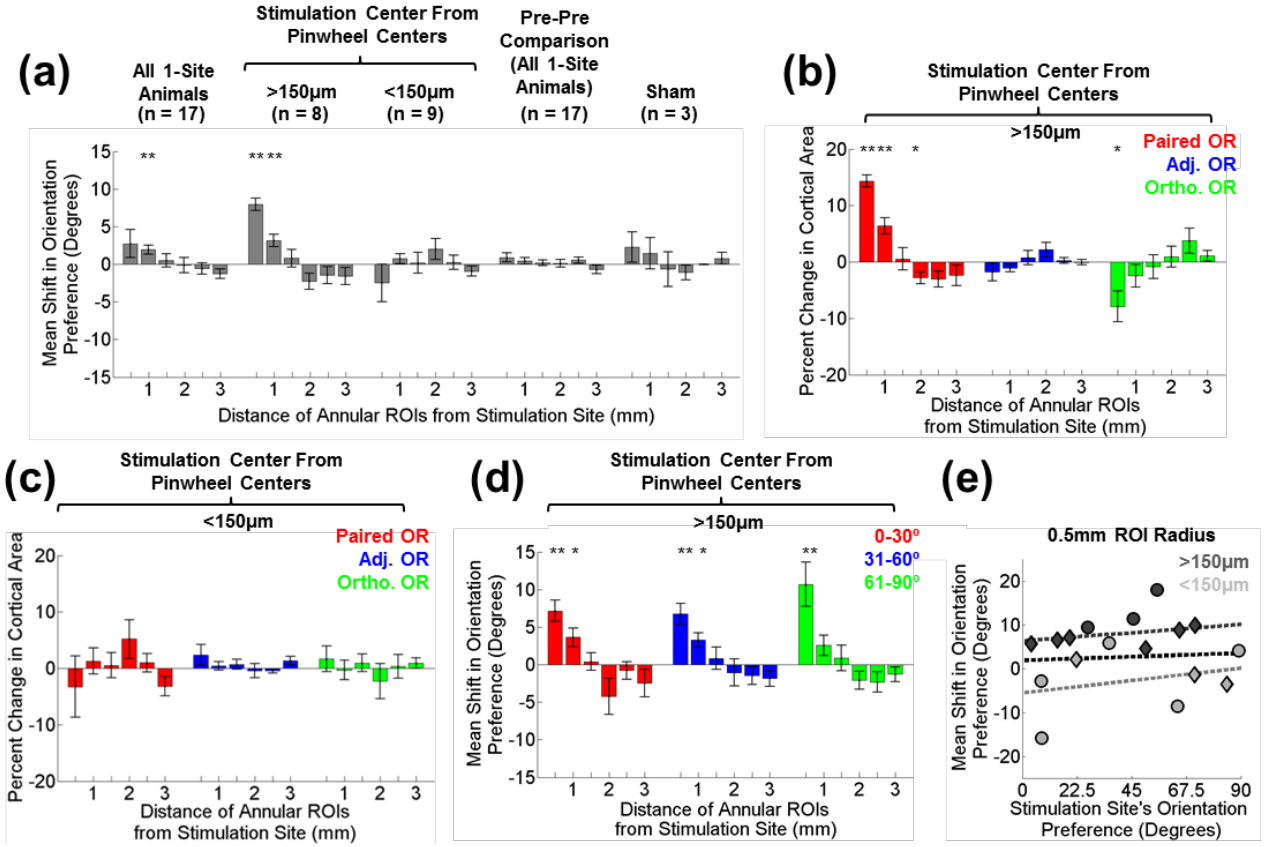

Figure 4-4: Pairing-induced shifts in the ferret orientation preference map are strongest at the stimulation site; however, the shifts do not strongly depend on a pixel's initial orientation preference.

(a) The mean shift in orientation preference towards the paired orientation showed a non-significant trend across imaging experiments (optical and electrical stimulation, n = 17). The effect was significant for distances of 1mm or less for experiments in which the

stimulation site's DNP was further than 150μm (n = 8), but not at all for experiments in which the stimulation site's DNP was closer than 150μm (n = 9). The mean pre-stimulation orientation preference across imaging experiments was stable, as a pre-pairing vs. pre-pairing comparison did not show significant changes in orientation preference (n = 17). Sham experiments (n = 3), in which the visual stimulus was presented for 3-4 hours without cortical stimulation showed no changes. **(b)** For experiments in which the stimulation site's DNP was further than 150μm, there was a significant increase in cortical area preferring the paired stimulus within 1mm of the stimulation site ($p<0.01$) and a decrease in cortical area preferring the orthogonal stimulus within 500μm of the stimulation site ($p<0.05$). **(c)** We did not observe any significant changes in the overall cortical area if the stimulation's site DNP was closer than 150μm. **(d)** For experiments in which the stimulation site's DNP was further than 150μm, splitting pixels from each animal experiment into three groups, based on their initial orientation preference bias with respect to the paired orientation (0-30˚ - red, 31-60˚ - blue, and 61-90˚ - green), did not suggest that a pixel is more likely to shift towards the paired orientation by virtue either of its initial orientation preference or distance from the paired orientation. **(e)** The local orientation preference of the stimulation site (relative to the paired orientation) also was not correlated with the pairing-induced shifts in orientation preference ($r = 0.07$, $p >0.05$ [black - for all intrinsic signal imaging experiments]; $r = 0.45$, $p >0.05$ [dark gray- sites with DNP >150μm]; $r = 0.30$, $p >0.05$ [light gray- sites with DNP <150μm]; $r = 0.29$, $p >0.05$ [light/dark gray circles - optical stimulation experiments]; $r = -0.33$, $p >0.05$ [light/dark gray diamonds - electrical stimulation experiments]). The best fit lines for three experimental groups are shown

(black - all intrinsic signal imaging experiments; dark gray- sites with DNP >150μm; light gray- sites with DNP <150μm). For all panels, error bars are SEM. All statistical testing was done with Student's t-test. For denoting significance, '**' denotes $p<0.01$ and '*' denotes $p<0.05$.

4.3.5 Dependence of Cortical Stimulation on Multiple Stimulation Sites

In order to explore spatial interactions related to our plasticity paradigm, we optically activated two non-overlapping, but adjacent transfected sites (n = 7; Figure 5). We were interested in whether co-activation of two close sites in the orientation preference map might nonlinearly influence, through interareal interactions, pairing-induced modification at either stimulation site. The average distance between stimulation sites was ~725μm, or roughly the order of one hypercolumn in ferret visual cortex (Kaschube et al., 2010). The distance was chosen for a number of reasons: a.) the sites were close enough for local horizontal connections to play a modulatory role, b.) there was sufficient distance, so that the two stimulation sites would be non-overlapping and c.) our previous experiments indicated that pairing-plasticity induced significant map changes up to 1mm. An example two-site stimulation pairing-experiment is shown in Figure 5. In this example, we induced a local pairing-induced shift in orientation preference towards the paired orientation (Figure 5d,e).

In figure 5f, we first evaluated in the group data (n = 7) whether there was a difference in pairing-induced plasticity if the annular ROIs were centered on both stimulation sites (purple group) or just centered on a single stimulation depending on its DNP (site with

lowest DNP: blue; site with larger DNP: red). For all three ROI groupings, we observed a similar non-significant shift in orientation preferences towards the paired orientation. A 1-way ANOVA test showed there was no significant difference between the groups ($p < 0.05$). Thus, this means pairing-induced plasticity at the two stimulation sites was indistinguishable. For the remaining analysis of the two-site stimulation experiments in this paper, we center the annular ROIs on both stimulation sites.

Next we investigated whether the mean pairing-induced shifts were still well predicted by the location of a stimulation site in the orientation preference map (Figure 5g, h). We still found a dependence in the two-site stimulation experiments, but this dependency was driven by the stimulation site that was closer to a nearby pinwheel center ($r = 0.88$, $p<0.01$), and not for the stimulation site that was farther away from its nearest pinwheel center ($r = -0.42$ $p > 0.05$) or the mean/summed distance ($r = 0.40$, $p >0.05$). Overall, these results suggest an inter-dependent interaction between the two stimulation sites that could be mediated by local intracortical connections.

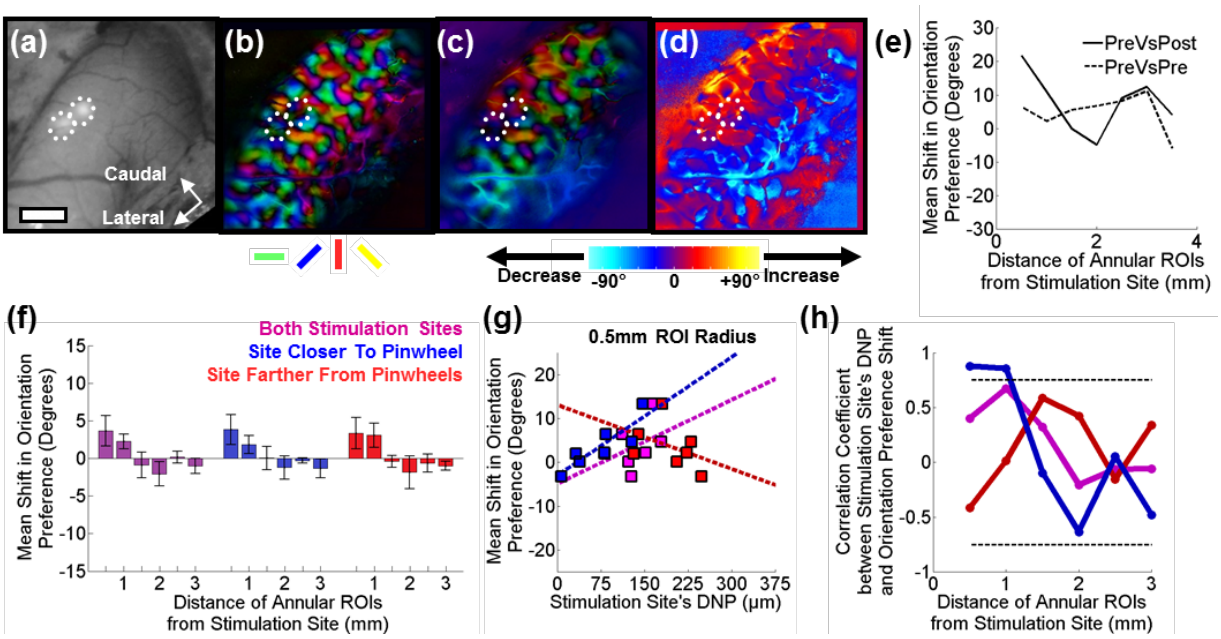

Figure 4-5: Pairing-induced modification of the ferret orientation preference map using two-site optical stimulation (n = 7).

(a) Layer 2/3 neurons at both stimulation sites were co-activated together by optically activating cells transfected with ChR2/YFP via two injection sites using 473-nm light (see the YFP fluorescence in dashed white circles). **(b-c)** The orientation preference map is shown prior to pairing (b) and after pairing (c). As in Figure 2, hue denotes the preferred orientation according to the legends below (b), while saturation indicates response magnitude. The paired orientation is 90˚ and denoted by a red color**. (d)** The difference map of orientation preference between the pre-pairing versus post-pairing orientation maps. As in Figure 2, warmer colors indicate an attractive shift towards the paired orientation, while cooler colors indicate a repulsive shift, and purple indicates no change. **(e)** We found that local annular ROIs, within 1mm of the stimulation site, displayed pronounced pairing-induced changes in orientation preference tuning. However, the changes are observed only in an analysis of pre-pairing vs. post-pairing

maps (solid line), but not in the control analysis where the pre-pairing map dataset, split into even and odd blocks, is compared against itself (dashed line). **(f)** Overall there was a non-significant trend at both stimulation sites for the orientation preference of cells to shift towards the paired orientation (purple, when considering both stimulation sites together; blue – only considering the stimulation site whose DNP was smaller; red – only considering the stimulation site whose DNP was larger). Statistical tests were done with Student's t-test. Color code in (f) applies to (f-h) **(g)** Within 0.5mm of both stimulation sites, the mean pairing-induced shift in orientation preference was only predicted by the stimulation site's DNP that was smaller ($r = 0.40$, $p > 0.05$ [mean DNP of both stimulation sites, purple]; $r = 0.88$, $p < 0.01$ [smaller of the two stimulation site's DNP, blue]; $r = -0.42$, $p > 0.05$ [larger of the two stimulation site's DNP, red]). The best fit line for each experimental group is shown. **(h)** Only the correlation between the pairing-induced shift and the smaller of two stimulation site's DNP (blue) most resembled the correlation seen in the one-site simulation experiments. The corresponding dotted horizontal lines indicate the threshold for the correlation coefficient's significance. All statistical tests were done with Student's t-test.

4.3.6 Pairing-Induced Plasticity is Weaker at Pinwheel Centers

The pairing effect's dependency on the stimulation site's DNP indirectly implies that that pairing-induced plasticity near pinwheel centers is weaker than in iso-orientation domains. However, the present analyses do not conclusively demonstrate that. Instead they show that intracortical stimulation near pinwheel centers (ie a low DNP) prevents plasticity in the orientation map, but they don't rule out the possibility that pinwheel

centers might also be plastic if the stimulation site's DNP is high.

To test this hypothesis, we computed the two-dimensional spatial derivative of the orientation preference map. In regions of low spatial gradient (iso-orientation domains), we found a significant pairing-induced change for experiments in which the stimulation site's DNP was high: ~10˚ shift in single-site stimulation experiments and a ~7 ˚ shift in two-site stimulation experiments. These results are harmonious with the previous results concerning one-site and two-site optical imaging experiments (Figure 6a, b). However, in regions of high spatial gradient (pinwheels or line fractures), we failed to observe significant changes in orientation preference, regardless of whether the stimulation site's DNP was high (Figure 6a, b). Thus, pinwheel centers really do seem to reflect areas in the orientation preference map that resist pairing-induced alterations in their orientation preference. Consistent with the idea that pinwheel centers may reflect stable singularities in the orientation preference map, we also show the location of the stimulation site's DNP was highly consistent between the pre-pairing and post-pairing orientation maps with a mean variation of 0.45±7.52μm (Figure 6c).

Reduced pairing-induced plasticity at pinwheel centers has been previously reported in cat visual cortex (Schuett et al., 2001). Schuett et al. suggested the lower plasticity at pinwheel centers may be due to pinwheel centers being co-localized at the centers of cat and primate ocular dominance columns (Bartfeld and Grinvald, 1992; Obermayer and Blasdel, 1993; Crair et al., 1997b; Hubener et al., 1997). This hypothesis was feasible as Crair et al. demonstrated that the centers of ocular dominance columns for the deprived

eye are less plastic and maintain their responsiveness even after MD (Crair et al., 1997a). An advantage of the ferret model is that pinwheel centers and ocular dominance columns have been shown to be not co-localized in ferret visual cortex (Issa et al., 1999; White et al., 2001a; Yu et al., 2005). Indeed in our experiment data, we show the position of pinwheels centers (dots in Figure 6d-f) was not biased towards regions of high ocular dominance (dark and bright region in Figure 6f). Our Monte Carlo simulation also indicated that the position of pinwheel centers was indistinguishable from pinwheels being randomly located across the ocular dominance map (1-way ANOVA, $p > 0.05$). Thus, the reduced pairing-induced plasticity at pinwheel centers in ferret visual cortex suggests there may not be a clear-cut relationship between pairing-induced plasticity in the orientation preference map and ocular dominance plasticity.

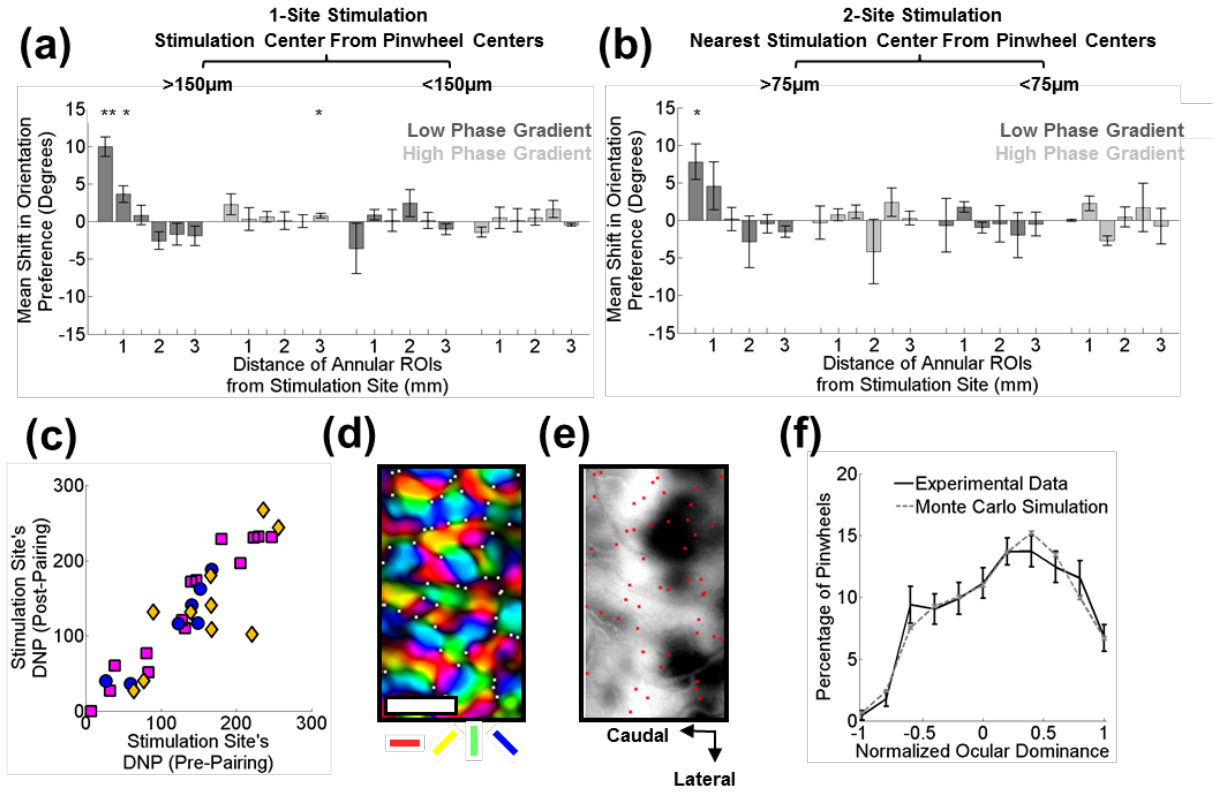

Figure 4-6: Pairing-induced shifts are weaker near pinwheel centers, but this property does not appear to be due to the local heterogeneity in orientation preference and ocular dominance around pinwheel centers.

(a, b) Unlike iso-orientation domains (low phase gradient), the mean pairing-induced shift in orientation preference is not significant in regions of the orientation preference map exhibiting abrupt changes in orientation preference, such as pinwheel centers and fractures. This was observed in both 1-site stimulation (a) and 2-site stimulation (b) experiments. Statistical tests were done with Student's t-test. For denoting significance, '**' denotes $p<0.01$ and '*' denotes $p<0.05$. **(c)** The location of the nearest neighbor pinwheel center or fracture was stable between pre-pairing and post-pairing imaging experiments with a mean variation of 0.45±7.52µm ($r = 0.90$, $p<<0.01$ (for all experiments); $r = 0.96$, $p << 0.01$ (for optical stimulation experiments); $r = 0.80$, $p < 0.01$

(for electrical stimulation experiments). These results indicate that location and presence of pinwheel centers near the stimulation site could be reliably assessed and that pinwheel centers exhibited stability throughout the pairing experiments. **(d)** An orientation preference map is shown. Pinwheel centers are labeled with white circles. Scale bar is 1mm. **(e)** For the same animal, the ocular dominance map is also shown. Contralateral eye bias is denoted by bright pixels and ispsilateral eye bias indicated by dark pixels. The same pinwheel centers labeled in (d) are shown as red circles. **(f)** The position of pinwheels centers across the experimental data (n = 24) was not found to be biased towards the center of ocular dominance columns. A value of +1 for the normalized ocular dominance represents a maximal contralateral eye bias, while -1 is an ipsilateral eye bias. A Monte Carlo simulation (n=100) also indicated that the position of pinwheel centers is indistinguishable from pinwheels being randomly assigned across the ocular dominance map (1-way ANOVA, $p>0.05$). Error bars are SEM.

4.3.7 Modifications in Population Responses of Neurons and Astrocytes

In order to confirm the findings based on indirect measurements of neural activity using intrinsic signal optical imaging, we performed two-photon calcium imaging experiments at depths of 150-200μm with single cell resolution. Imaging ROIs were within 1.5mm of the stimulation site, and pairing was done with electrical stimulation. For the example imaging ROI in Figure 7, the stimulation site's DNP was greater than 150μm and the displayed cells were located within 0.5mm of the stimulation site. The pre-pairing and post-pairing tuning curves of six example cells exhibited orientation preference shifts towards the paired orientation (Figure 7b). Furthermore, the overall change in the post-

pairing population responses of neurons and astrocytes in this imaging ROI showed a marked shift in orientation preference towards the paired orientation (~9˚ shift, Figure 7c-f). These observations are consistent with the modifications observed in the intrinsic signal functional maps.

Across the cellular responses of twelve ROIs imaged (n = 4 animals), we found pairing-induced shifts in orientation preference (Figure 6g). These changes were localized within 0.5mm of the stimulation site, but not greater than 1mm (Figure 6g, *left and center images*). The pairing-shifts were also independent of the cell's orientation preference and cell type (neuron versus astrocyte). Though like the intrinsic signal experiments, there was an elevation in the mean orientation preference shift for cells with an initial orientation preference most dissimilar to the paired orientation (Figure 4d and Figure 6g, *left image*). Moreover, the stimulation site's DNP still predicted whether cells would shift their orientation preferences. Only cells recorded in imaging experiments where the stimulation's site DNP was high (>150μm, n = 2) showed strong pairing-induced shifts towards the paired orientation. For stimulation sites with a low DNP (n = 2), we did not find strong shifts in orientation preference and instead observed small repulsive shifts away from the paired orientation.

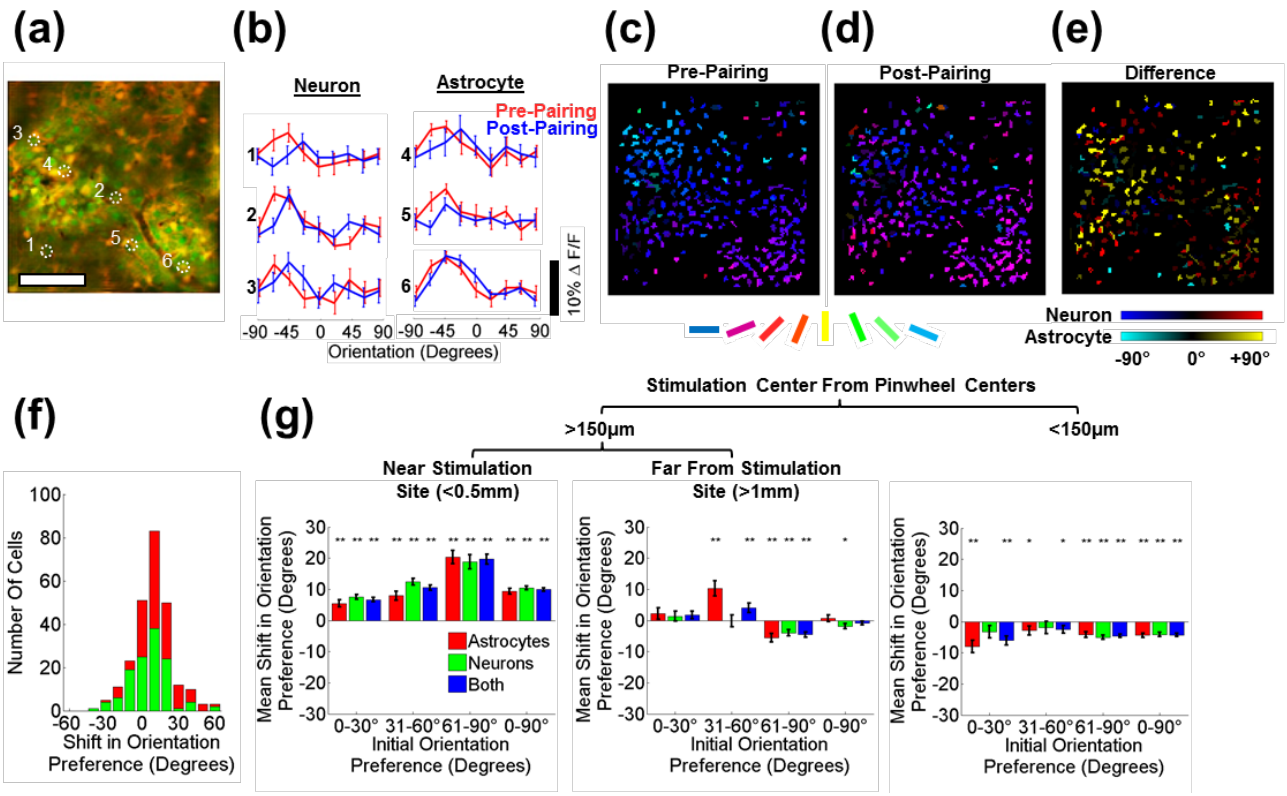

Figure 4-7: Pairing-induced shifts were observed in layer 2/3 cells of the primary visual cortex with two-photon calcium imaging.

(a) Cells at a depth of ~150µm were loaded with the calcium dye, Oregon Green 488 BAPTA-1 acetoxymethyl ester, and Sulforhodamine 101, an astrocyte-specific marker. In this imaging ROI, cells labeled green are neurons, while cells labeled red or double labeled (yellow) are astrocytes. Scalebar is 100µm and applies also to (c-e). (b) The average change in fluorescence ($\Delta F/F$) in response to different orientations is shown for the six circled cells in (a) over 15-45 repetitions of visual stimulation. The red and blue traces are respectively the pre-pairing and post-pairing responses. The mean shifts in orientation preference for the six presented cells are 33.7˚, 12.8˚, 19.38˚, 26.3˚, 11.7˚, and 18.2˚. (c, d) The cellular orientation preference map is shown prior to pairing (b) and after pairing (c). The phase of the orientation preference map has been rotated, such that

the paired orientation is denoted by red. The paired orientation is 45˚. (e) The difference map of orientation preference between the pre-pairing versus post-pairing orientation cellular maps shown in (c) and (d). Warmer colors indicate an attractive shift towards the paired orientation (red for neurons and yellow for astrocytes), while cooler colors indicate a repulsive shift (dark blue for neurons and light blue for astrocytes). (f) A histogram of the shift in orientation preference for the cells show in the above ROI. The mean shift in orientation preference was 5.83˚ for neurons (n = 124; green), 12.19˚ for astrocytes (n=128; red), and 9.06˚ across both cell types (n = 252). (g) The overall shifts in orientation preference across calcium imaging experiments (n = 4 animals / 12 ROIs), are shown as a function of either cell type (green – neurons, red – astrocytes, and blue – both cell types) and binned based on initial orientation preference (0-30˚, 31-60˚, 61-90˚, and 0-90˚). The stimualtion site's DNP was >150μm in two animal experiments (7 ROIs, *left* and *center* image), while it was <150μm in the other two imaging experiments (5 ROIs, *right* image). For the two experiments where the stimulation site was >150μm, cells were split into two groups based on being either close (<500μm) or far (>1mm) from the stimulation site. *Left Image:* The numbers of cells included were 504 neurons and 398 astrocytes, and the initial orientation preference distribution of cells was 53% (0-30˚), 31% (31-60˚), and 16% (61-90˚). *Center Image:* The numbers of cells included were 700 neurons and 441 astrocytes, and the initial orientation preference distribution of cells was 25% (0-30˚), 23% (31-60˚), and 52% (61-90˚). *Right Image:* The numbers of cells included were 766 neurons and 695 astrocytes, and the initial orientation preference distribution of cells was 17% (0-30˚), 23% (31-60˚), and 60% (61-90˚). Error bars are SEM. Statistical tests for significant shifts in orientation preference were done with

Mann-Whitney test by comparing the pre-pairing and post-pairing distribution of orientation preferences. For denoting significance, '**' denotes $p<0.01$ and '*' denotes $p<0.05$.

4.3.8 Comparison between calcium imaging and intrinsic signal optical imaging data:

The changes observed in two-photon calcium imaging experiments were directly compared with those of the intrinsic signal imaging experiments. We excluded one animal in these comparisons, due to the poor quality of the intrinsic signal maps. For three out of the four calcium imaging experiments, the mean orientation preference of cells at each of the imaged ROIs (n = 10), as measured with two-photon calcium imaging, was strongly correlated with the orientation preference measurements of the intrinsic signal maps (Figure 8a). The mean pairing-induced shifts in orientation preference were also correlated (Figure 8b). Additionally, we found that the mean orientation preference shift of cells in the two-photon calcium imaging experiments were similar to the mean orientation preference shifts measured in the one-site stimulation intrinsic experiments, (Figure 8c). Overall, across all imaging modalities and stimulation paradigms, we observed a strong correlation between the pairing-induced changes of orientation preference and the stimulation site's DNP (Figure 8d).

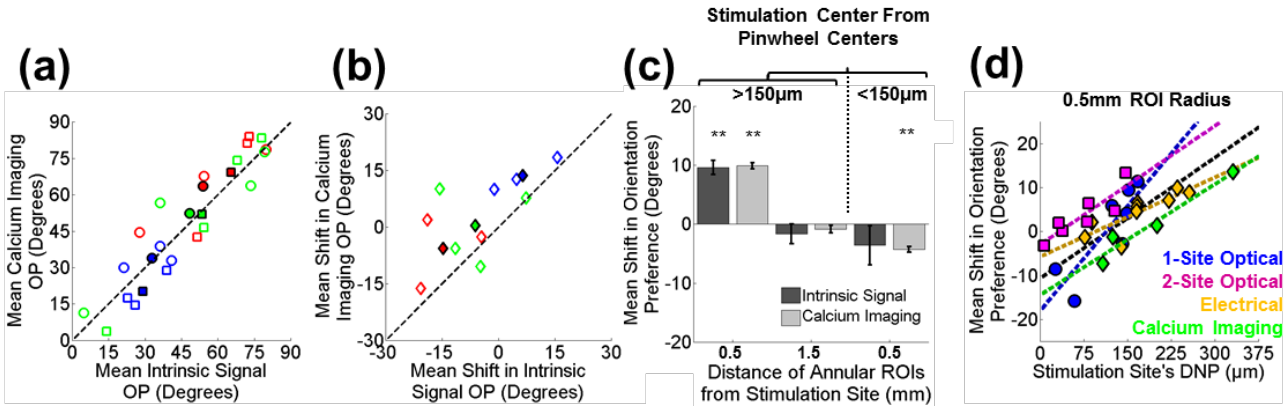

Figure 4-8: There was close agreement in the orientation preference across both imaging modalities.

(a) A plot of the mean orientation preference (OP) at each imaging ROI for three animal experiments (n = 3 animals / 12 calcium imaging ROIs). Here we compare blockwise two-photon calcium imaging with Fourier-based intrinsic imaging ($r = 0.92$, $p << 0.01$ for individual imaging ROIs and $r = 0.96$, $p < 0.01$ for the mean orientation preference for an animal experiment). Circles indicate the pre-pairing orientation preference, while squares indicate the post-pairing orientation preference. The data point color indicates a distinct animal experiment. The open circles/squares indicate the orientation preference measured at an imaging ROI, while the filled circles/squares indicate the mean orientation preference for an animal experiment (across all imaging ROIs). (b) A plot comparing the mean pairing-induced shift in orientation preference (OP) at each imaging ROI for three animal experiments, as measured by either blockwise two-photon calcium imaging or Fourier-based intrinsic imaging ($r = 0.66$, $p < 0.05$ for individual imaging ROIs and $r = 0.99$, $p = 0.06$ for the mean orientation preference for an animal experiment). Data point color indicates a distinct animal experiment. The open diamonds indicate the orientation preference measured at an imaging ROI, while the closed diamonds indicate the mean

orientation preference for an animal experiment (across all imaging ROIs). (c) Comparison of the mean shift in orientation preference from the blockwise intrinsic signal functional maps (n = 9 for site's DNP <150μm and n = 8 for site's DNP >150μm) and the blockwise calcium imaging experiments (n = 902 cells for site's DNP <150μm and 0.5mm annular ROI; n = 1141 cells for site's DNP <150 μm and 1.5mm annular ROI; n = 1461 cells for site's DNP >150μm and 0.5mm annular ROI). Error bars are SEM. The Student's t-test was used on intrinsic signal experiments, while the Mann-Whitney test was applied to calcium imaging experiments. For denoting significance, '**' denotes $p<0.01$ and '*' denotes $p<0.05$. (d) In all experimental groups, the mean pairing-induced shift in orientation preference was strongly predicted by the stimulation site's DNP ($r = 0.54$, $p < 0.01$ (for all intrinsic signal imaging experiments); $r = 0.84$, $p < 0.05$ (1-site optical stimulation experiments); $r = 0.89$, $p < 0.01$ (2-site optical stimulation experiments); $r = 0.83$, $p < 0.01$ (electrical stimulation experiments); $r = 0.97$, $p < 0.05$ (electrical stimulation experiments, but with two-photon calcium imaging)). The best fit line for each experimental group is shown, as well as the best fit for all intrinsic signal imaging experiments (black line).

4.4 DISCUSSION

Most previous plasticity studies in the visual cortex have used plasticity-inducing paradigms in which an animal's normal visual experience is disrupted through abnormal visual experience (e.g. monocular/binocular deprivation, dark rearing, or stripe rearing) (Blakemore and Cooper, 1970; Hubel and Wiesel, 1970; Sengpiel et al., 1998; Issa et al., 1999; White et al., 2001b; Yu et al., 2011). While disruption of normal visual experience

has been particularly fruitful in improving our understanding how neurons alter the functional responses *in vivo*, these experiments by their nature modulate neural activity across entire functional areas. Selective activation of local micro-circuits is thus necessary to begin elucidating the role that local functional architecture has on neural plasticity by creating the opportunity to contrast regions within a single cortical area. In this study, we combined a plasticity-inducing paradigm that combines the presentation of a visual stimulus with direct cortical stimulation of select neural populations in the ferret visual cortex. Consistent with other imaging studies, we have found that visual cortex neurons are plastic, but that this capability is not uniformly displayed across the orientation preference map (Dragoi et al., 2000; Dragoi et al., 2001; Schuett et al., 2001; Godde et al., 2002).

4.4.1 Stability of orientation preference maps

The stability of functional maps in the visual cortex has been widely reported in multiple intrinsic signal imaging studies, either across longitudinal imaging studies or studies where visual experience was manipulated (Chapman et al., 1996; Godecke et al., 1997; Sengpiel et al., 1998; Shtoyerman et al., 2000; Yu et al., 2011). A few studies however have suggested larger scale map modifications are possible or that pinwheel position is not invariant (Dragoi et al., 2000; Godde et al., 2002). In this study we found that the orientation preference map does not change substantially after pairing, which is also consistent with Schuett et al. (Schuett et al., 2001). Most of the plastic changes we observed were confined within 1mm of the stimulation site. And even close to the stimulation site, the location of pinwheel centers and line fractures remains similar after

pairing (Figure 6c). Most changes we observed tended to be uniform shifts in the orientation preference map, in which cells shift their orientation preference towards the paired orientation. The process results in an overrepresentation of cortical cells preferring the paired visual stimulus at the expense of less cells responding to the orthogonal stimulus.

4.4.2 Dependence of initial orientation preference tuning

The dependence of a neuron's orientation preference and its impact on neural plasticity has so far proven inconclusive. Dragoi et al. and Godde et al. respectively each suggested that the neural plasticity observed in their studies was dependent on a neuron's initial orientation preference, while Schuett et al. and our study failed to find a relationship (Dragoi et al., 2000; Schuett et al., 2001; Godde et al., 2002). Dragoi et al. used a habituation approach in which an adapting visual stimulus was presented to animal, while Godde et al. utilized cortical stimulation with a stimulating electrode. Crudely speaking, the studies conducted by Dragoi et al. and Godde et al. are each one half of the protocol of Schuett and the current study: visual stimulation and cortical stimulation respectively.

At first glance it is difficult to explain this discrepancy with a biological explanation, despite the methodological differences in the studies. However, one concern is that Dragoi et al. and Godde et al. employed a similar analytical measure to estimate changes in orientation preference. As orientation preference measurements are circular, rather than linear qualities, an intuitive measure is to estimate the absolute value of the orientation preference of each pixel/cell relative to the referenced orientation (i.e. the

orientation of the adapting stimulus in Dragoi et al. and the orientation preference of the stimulation site in Godde et al.). This operation is performed on both the orientation preference measurement before and after the experimental manipulation. And then the difference in orientation preference between the two quantities is taken as the degree of plasticity. Thus, this analytic has the desirable quality of eliminating the ambiguity of whether a pixel shifted counter-clockwise or clockwise, which could inadvertently reverse the direction of change relative to the referenced orientation (Figure 9).

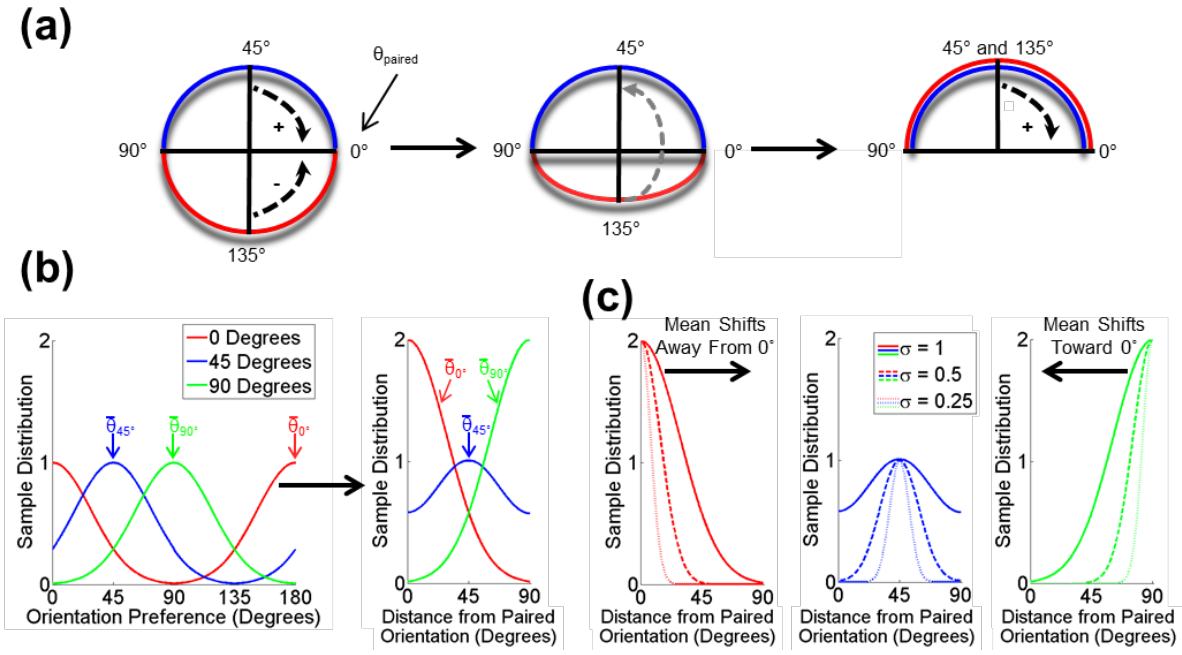

Figure 4-9: Circular dispersion (i.e. absolute value function in this example) provides information about how orientation preference measurements are distributed relative to the paired orientation.

(a) As orientation preference measures are circular quantities and not linear quantities, both counter-clockwise (-) and clockwise (+) changes in orientation preference can result in shifts towards the paired orientation. Measurement ambiguities can result when these

signed values are summed, as positive and negative rotations would tend to cancel each other out (left image). Circular dispersion eliminates the ambiguity by estimating the distance of each orientation preference measurement from the paired orientation in degrees (right image). In essence, this process graphically involves projecting elements on the bottom half of the circular distribution upward onto the upper half of the circular distribution (middle image). (b) Graphs showing how Gaussian distributions (left image, $\sigma = 1$) centered on 0˚ (red line), 45˚ (blue line), and 90˚ (green line) respectively are transformed with circular dispersion (right image). Unfortunately the benefit of circular dispersion is also a potential liability and can lead to systematic errors if left uncorrected. The sample mean tends to shift after applying circular dispersion; however, the sample mean only shifts if the mean population value is close to the real axis, such as 0˚ or 90˚, but not for 45˚ (center image) that is orthogonal to the real axis. The sample means for each distribution ($\bar{\theta}$) are shown in both plots. Shifts in the sample mean (particularly for the 0˚ or 90˚ distributions) become problematic because they can propagate a systematic, orientation preference-dependent bias. (c) We show that with progressively larger uncertainty (ie larger σ values), the systematic shifts in the population mean are more pronounced and, thus, are dependent on measurement uncertainty. Data in this panel was generated using simulated orientation preference data drawn from normal distributions with either σ=0.25, 0.5, or 1.

And generally speaking this approach is quite reasonable and, in fact, is very similar to our analytical measure. Unfortunately, standard measures of circular dispersion about a referenced orientation suffer from the population not being symmetric about the sample

mean (ie the absolute value or cosine function, see (Mardia and P., 2000)). This can lead to biasing the mean of the population artifactually towards or away from the referenced orientation, depending on a pixel's/cell's initial orientation preference (Figure 9b,c). Specifically, this artifact leads to shifts away from the referenced orientation if the orientation preference is very similar to the referenced orientation, while there is an artifactual shift towards the referenced orientation if it's very different to the referenced orientation (Figure 10). Indeed, Dragoi et al. observed that that the *repulsive* orientation preference shifts were maximal if a neuron's orientation preference was very similar to the adapting stimulus, while Godde et al. found that *attractive* shifts towards the stimulation site's orientation preference were greatest if a cell's or pixel's orientation preference was maximally dissimilar. To correct for this artifact, we developed a correction factor that takes into account how much the population mean shifts when a circular dispersion method is used (see Methods section). When we corrected for this artifact our results were more in-agreement with Schuett et al., such that a neuron's initial orientation preference did not appear to be a contributing factor in whether the cells were more plastic (Figure 11).

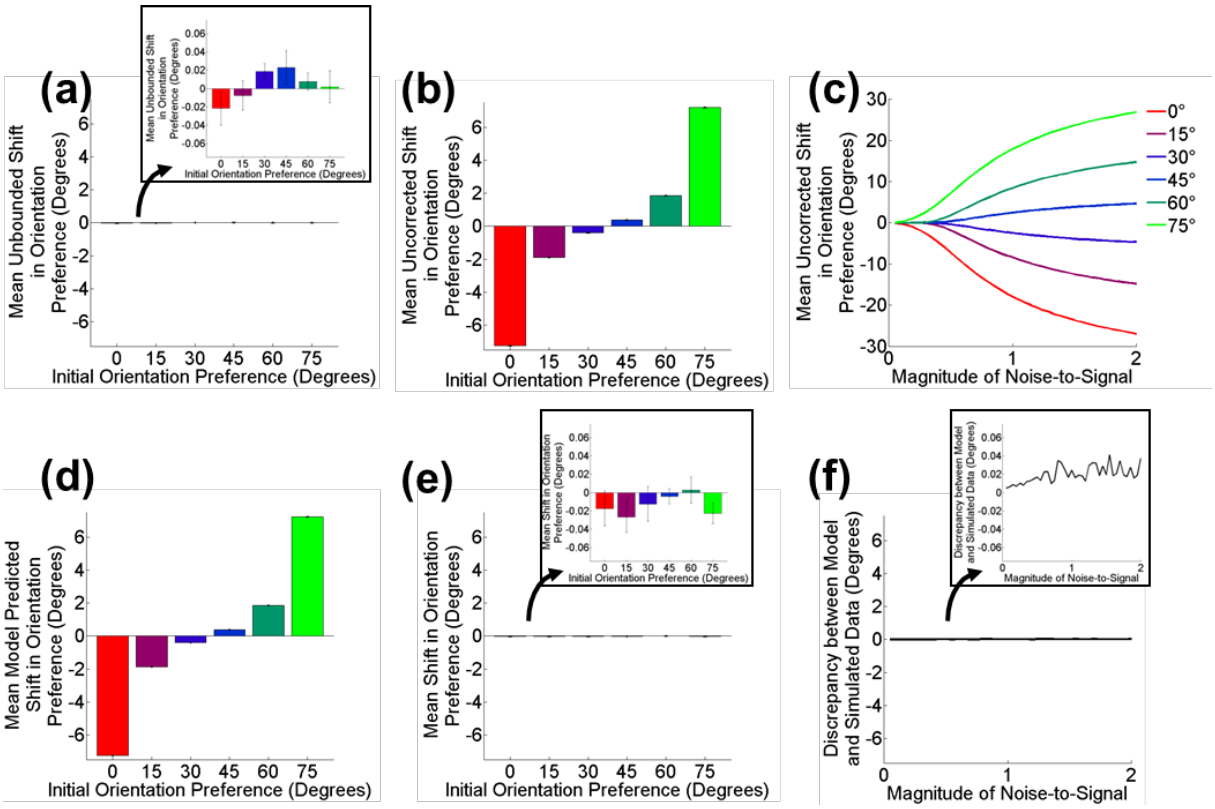

Figure 4-10: A model of simulated orientation preference data.

This model can illustrate how the mean shift in orientation preference, using a circular dispersion measure, exhibits a repeatable orientation-specific bias. To simulate the artifactual orientation-specific bias, we generated a “signal” group with a random distribution of orientation responses and a magnitude of 1 (z1). In the second “signal + noise” group (z2), we simulated the impact of adding random noise by combining the original distribution of orientation responses in the “signal” group with a second “noise“ group. The “noise” group also had a random distribution of orientation preferences, but it’s magnitude relative to “signal” group was varied between 0.05-2x . (a) The mean difference in orientation preference between the “signal” and “signal+noise” group was found to be very small and did not depend on the initial orientation preference in the “signal” group. This was only true if the orientation preference difference was

"unbounded" and not relative to a referenced orientation (i.e. arg[z1] – arg[z2]). The panel inset is a magnified version of this panel figure, in which the y-axis range is decreased by a factor of 100x (similar panel insets are used in panels (e) and (f)). Error bars are SEM and indicate the error from repeated simulations (n=5). The noise level in this panel was 0.5x. (b) However, if instead a circular dispersion measure was used (ie |arg[z1]| – |arg[z2]|), the mean difference in orientation preference between the "signal" and "signal+noise" group was found to exhibit large orientation preference-dependent shifts. (c) The magnitude of mean orientation-specific bias increased as the magnitude of noise-to-signal grew in the "signal+noise" group. (d, e) Our model (see Methods section) closely approximated the mean orientation-specific bias in (b), which we used to eliminate the artifactual orientation-specific bias (e). The noise levels in these panels were 0.5x. (f) The discrepancy between our model approximation and the simulated data remained continually low, even if the noise-to-signal ratio increased. Thus, the model robustly predicts the orientation-specific bias independent of noise.

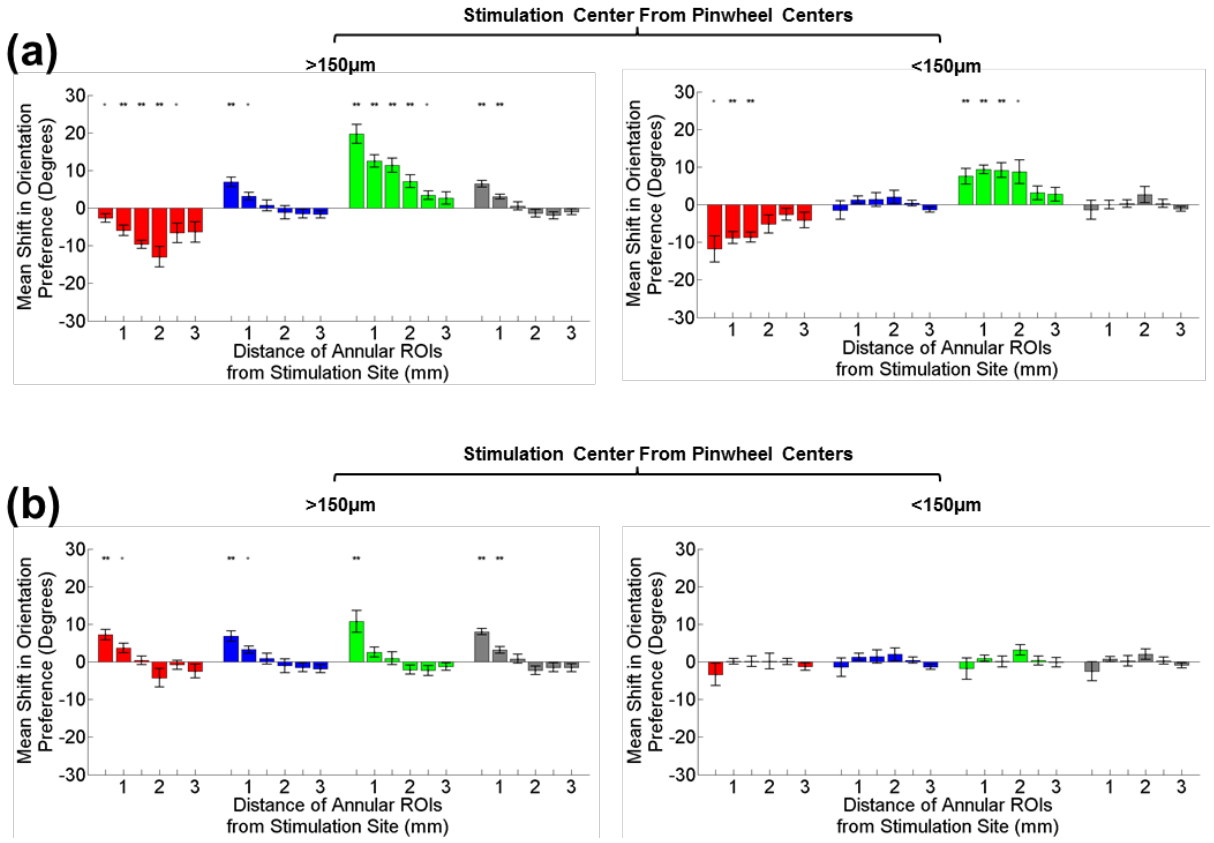

Figure 4-11: Pairing-induced shifts in the ferret orientation preference map only depend on a pixel's initial orientation preference if the results have not been corrected for the intrinsic orientation-preference dependent bias.

(a) The orientation preference map data left uncorrected and (b) the same data corrected by the model (*left panel is part of figure 4d*). Experiments were split into two groups based on whether the stimulation site's DNP was either closer or further than 150µm (left images – farther than 150µm and right images – closer than 150µm). Pixels were split from each animal experiment into three groups, based on their initial orientation preference bias with respect to the paired orientation (0-30˚ - red, 31-60˚ - blue, and 61-90˚ - green). Error bars are SEM. All statistical tests were done with Student's t-test. For denoting significance, '**' denotes $p<0.01$ and '*' denotes $p<0.05$.

4.4.3 Pairing-Induced Plasticity at Pinwheel Centers

Perhaps the most striking effect in this study is that neurons nearer to pinwheel centers are “less plastic” to pairing than neurons located in iso-orientation domains. Schuett et al. reported similar findings in cat visual cortex (Schuett et al., 2001). However, we have also extended these findings in the ferret visual cortex. We show that not only are pinwheels less susceptible to pairing-induced plasticity, but also that cortical stimulation progressively nearer to pinwheel centers weakens the overall pairing-induced changes for all neurons located within 0.5-1.0mm of the stimulation site. For two-site stimulation experiments, the stimulation site nearest to a pinwheel center also seemed to better predict the pairing-induced changes in the functional maps. This latter finding suggests an interaction between the two stimulation sites that may not merely be a simple summation of activation by the two sites.

Also cortical stimulation very close to pinwheel centers appears to shift a cell’s orientation preference away from the paired orientation. Curiously the “repulsive” shift away from the paired-orientation resembles the reported neural plasticity by Dragoi et al. Dragoi *et al.* exposed adult cats to a particular adapting visual stimulus and observed repulsive shifts in the orientation preference of visual cortex neurons away from the adapting orientation; however this effect was most pronounced at pinwheel centers(Dragoi et al., 2000; Dragoi et al., 2001).

4.4.4 Potential Mechanisms of Pairing-Induced Plasticity

The simplest explanation for these effects is that successful induction of neural plasticity

in cortical cells is consistent with Hebbian theory. In this model postsynaptic responses are strengthened via long-term potentiation when post-synaptic spiking activity closely follows the presynaptic input (Zhang et al., 1998; Schuett et al., 2001). While this mechanism is appealing for its simplicity, the model is difficult to reconcile with the observation that pinwheel centers appear less plastic. One possible explanation is that the input-output transformation of neurons at pinwheel centers is different than for neurons in iso-orientation domains. Indeed, Schummers et al. (2002) found that most visual cortex neurons exhibited sharp orientation tuning curves, despite neurons near pinwheel centers receiving more broadly-tuned, sub-threshold input (Schummers et al., 2002). This difference was interpreted as pinwheel neurons having a higher spiking threshold. If true, this difference could suggest why pinwheel neurons are less plastic than iso-orientation domain neurons. A higher spike threshold then might prevent post-synaptic neurons from receiving sufficient pre-synaptic drive to facilitate LTP.

So far this discussion has assumed that plasticity is merely a strengthening of geniculo-cortical afferents without taking into account the role lateral connections might play in gating neural plasticity. But this is likely not the case, as Schuett et al. found interocular transfer of pairing-induced plasticity(Schuett et al., 2001). This finding suggests pairing-induced plasticity is not purely a synaptic reweighting of thalamo-cortical inputs. And instead implies plasticity of intracortical connections, since primary visual cortex is the first area along the visual pathway where neural responses become binocular.

It has been also shown that orientation-selective neurons in the visual cortex respond

maximally to visual stimuli that are present within the cell's classical receptive field (CRF) and at the cell's preferred orientation; however, neural responses are also modulated by the presence of visual stimuli that are outside the cell's CRF, or extra-classical surround (Hubel and Wiesel, 1962; DeAngelis et al., 1993). Two recent studies have shown that neurons at pinwheel centers tend to exhibit less extra-classical contextual modulation and more faithfully reflect the geniculo-cortical input, whereas neurons in iso-orientation domains are more sensitive to visual stimuli in the extra-classic surround (Hashemi-Nezhad and Lyon, 2011; Okamoto et al., 2011). These above studies are relevant, because it's been shown that a neuron's short-range connections tend to be isotropic (Bosking et al., 1997; Das and Gilbert, 1999; Stettler et al., 2002). These local connections project up to 1mm, which is consistent with the spatial extent of neural plasticity we observed in this study. Moreover, it's been shown that short-range connections play an important role in contextual modulation (Das and Gilbert, 1999), as cortical neurons that share dissimilar orientation preferences tend to suppress each other's activity through cross-orientation suppression (Morrone et al., 1982).

It is then interesting to speculate whether pinwheels are merely less plastic, or if pairing-induced plasticity at pinwheel centers might instead behave differently than in iso-orientation domains. Cortical stimulation near pinwheel centers very likely co-opts neural circuitry with heterogeneous orientation preferences, that when simultaneously activated could suppress neural activity in a manner similar to cross-orientation suppression. Thus, this might explain the suppression of the paired orientation whenever the stimulation site is very close to pinwheel centers. The effect would likely diminish as the stimulation site

is located further from a pinwheel center.

4.5 METHODS

4.5.1 Basic Experimental Procedures

Imaging experiments were performed in 6- to 10-week-old ferrets (n = 28). For optical stimulation experiments, a viral vector containing Channelrhodopsin -2/YFP was injected into the visual cortex 2-4 weeks prior to imaging experiments. Experimental procedures were approved and carried out in accordance with protocols approved by the local IACUC of University of Pittsburgh and Carnegie Mellon University. For all experiments, animal anesthesia was induced with an i.m. injection of ketamine (30mg/kg) and maintained under isoflurane (1.5-2.5% for surgery and 0.75-1.0% for imaging experiments; in a 1:1 mixture of O2 and N_2O). The animal's vital signs were monitored and maintained at all times during experiments: a rectal probe for animal temperature (38°C), EKG for heart-rate (270-300bpm), and a capnometer for expired CO_2 (3-4%). Routine application of either saline eye drops or silicone oil was used to keep a ferret's eyes moist.

4.5.2 Viral Injections

We made 1-2 microinjections into a ferret's visual cortex with a viral vector construct: Lentivirus (HIV-1)) under the Synapsin-1 promoter, containing genes for the expression of ChannelRhodopsin-2 and YFP provided by Mike Ehlers. After anesthesia induction, we placed anesthetized ferrets into a stereotaxic instrument and performed a sterile

midline scalp incision, subsequently followed by a craniotomy over the ferret visual cortex. Afterwards, a small dural incision exposed the underlying brain. A small amount of virus (~5µL) was pressure injected (20 PSI) into the visual cortex at a depth of ~300µm. Artificial dura (made of transparent, soft thermoplastic polyurethane) was placed between the cortex and resected dura. The skull was replaced and affixed with tissue acrylic cement before the scalp was closed with surgical suture. After the surgery was completed, isoflurane was discontinued and the animal recovered. Animals received antibiotics for 5 days to prevent post-surgical infection. All steps in this procedure followed standard aseptic practices.

4.5.3 Imaging Experiments

After anesthesia induction, ferrets were tracheotomized and artificially ventilated. Each ferret was then placed in a stereotaxic device to stabilize the head. This step was followed by a midline scalp incision and a craniotomy over the visual cortex. The dura was then resected to expose the visual cortex. If the imaging experiment involved two-photon calcium imaging, Oregon Green 488 BAPTA-1 AM (*Invitrogen*) and Sulfarhodamine-101 (*Invitrogen*) were then pressure injected (20PSI) into multiple locations of the visual cortex at a depth of ~300µm (Stosieck et al., 2003; Reid et al., 2005). 2% agarose was placed between the arachnoid membrane's surface to stabilize the preparation. Afterwards, a small glass window was then fastened to the ferret's skull with dental acrylic to secure the agarose. For experiments where electrical stimulation was used, we removed the glass coverslip before inserting the stimulation electrode into the visual cortex. The glass coverslip was replaced at the termination of the pairing procedure. For

two-photon calcium imaging experiments, a head-mount was also fastened to the ferret's skull with dental acrylic. The ferret's head was then rotated, so that the surface of the visual cortex was parallel to the fixed imaging plane. This head-mount was unnecessary in blockwise-intrinsic signal experiments, as the imaging camera was instead rotated. At the termination of imaging experiments, animals were euthanized with an overdose of sodium pentobarbital.

Blockwise-intrinsic signal images were acquired using software and hardware from Optical Imaging Inc. (Imager 3001). We recorded the surface blood vasculature map under illumination with green light (595nm) and measured intrinsic signal changes with red light (620nm or 700nm) with a Dalsa M60 CCD camera. For each trial, we captured six frames of 1.4s duration at a spatial resolution of 6.4μm/pixel. For two-photon calcium imaging experiments, intrinsic signal maps were generated using a temporally encoded approach (Kalatsky and Stryker, 2003). Temporally encoded maps were continuously acquired at 30Hz and at a spatial resolution of 9.4-15μm/pixel (Moon et al., 2004). Cells in two-photon calcium imaging experiments were imaged at the desired focal plane with a tunable, ultra-fast Ti:Sapphire laser (*SpectraPhysics* Mai Tai DeepSee HP) with 900nm laser light and a 16X water immersion objective (Nikon, 0.8NA). Calcium imaging data was acquired at 3-10Hz and a spatial resolution of 2.28-5.10μm/pixel. The laser was controlled with Prairie View Acquisition Software (ver. 4.0).

4.5.4 Visual Stimulation

Visual stimuli were binocularly presented on a 24” monitor using a visual stimulus generator (*Cambridge Systems*). Visual stimulation involved the presentation of 100% contrast, square-wave gratings (0.125 cycles/°) that drifted at a rate of 2.5 cycles/s with the direction of motion being reversed 1/s. The visual stimulus lasted 8s/2s with an interstimulus interval of 8s/4s in intrinsic signal and two-photon calcium imaging experiments respectively. We presented gratings at four different orientations in blockwise intrinsic signal experiments (0°, 45°, 90°, and 135°) and eight different orientations in the blockwise two-photon calcium imaging experiments (0°, 22.5°, 45°, 67.5°, 90°, 112.5°, 135°, and 157.5°). During the inter-stimulus period, the screen was blank (black). The temporally encoded stimulus used to generate intrinsic signal maps in two-photon calcium imaging experiments was rotated clockwise or counter-clockwise (60s cycle) and drifted at a rate of 2.5 cycles/s. The pairing protocol consisted of repeatedly flashing a stationary grating, either at the paired or orthogonal orientation, for 20ms at a rate of 7Hz across a 3s period. Each 3s presentation period was followed by a 3s interstimulus period of no visual stimulation. Presentation of the paired and orthogonal orientation was alternated and repeated over the course of 2-4 hours. For the generation of ocular dominance maps, eye-specific responses were measured by covering one eye with mechanical shutters.

4.5.5 Cortical Stimulation

Neural tissue was activated either by optical stimulation of cells transfected with ChannelRhodopsin-2 or electrical stimulation with a stimulating electrode. Optical

stimulation was achieved by illuminating the brain's surface with 473-nm laser light (Stabilized Violet-Blue 473nm, *CrystaLaser*) at 5-20mW/mm^2 and for a duration 10-40ms. To activate cells electrically in the visual cortex, we inserted a 2MΩ tungsten electrode into the brain at a depth of 300µm. Current was either delivered in 1 pulse, or a short 300-Hz burst over a 10ms period (3 pulses), at 60-300µA per pulse (typically 180µA). For the pairing protocol, the latency between visual stimulation and cortical stimulation was 30-60ms for optical stimulation (typically 60ms) and 40-65ms for electrical stimulation (typically 65ms). Across the variation in cortical stimulation parameters, we didn't observe any systematic differences.

4.5.6 Data Analysis

For each blockwise-intrinsic signal imaging session (pre-pairing and post-pairing), we imaged for ~2-3 hours and averaged together the trial reflectance measurements. Next to calculate the single-condition evoked response for each pixel ($\Delta R/R$), we applied two blank subtraction methods to suppress biological fluctuation and non-specific visual responses. First, the averaged reflectance measurements were "first-frame subtracted" with the baseline reflectance (1.4s prior to the presentation of the visual stimulus) being subtracted from the reflectance during the presentation of the visual stimulus. Secondly, the single-condition responses (0°, 45°, 90°, and 135°) were "cocktail-blank subtracted" (ie the mean response to all stimuli presented was subtracted from each single-condition map). After applying the blank subtraction methods, the imaging data was then range-fitted, such that the 1.5% most-responsive pixels were set as the maximum response. Each single-condition map was "z-scored" with the image mean being subtracted and

then divided by the standard deviation of response across all stimuli presented. Image registration of the pre-pairing images to the post-pairing images was done via a 2-d affine transform with penetrating blood-vessels used as landmarks.

For generating Fourier-intrinsic signal orientation preference maps from a temporally encoded stimulus (either clock-wise or counter-clockwise stimulation), we used the discrete Fourier transform at the stimulation frequency (1/30s) to extract the orientation-specific response (z) from the raw reflectance measurements. This step was performed for each trial and then the trial data was averaged. The orientation response map was z-scored with the image mean being subtracted and then divided by the standard deviation of response. Image registration of the pre-pairing images to the post-pairing images was done via a 2-d affine transform with penetrating blood-vessels used as landmarks. The hemodynamic phase-delay was estimated and then subtracted from each orientation preference map. The hemodynamic delay, $\theta_{delay}$was computed as:

$$\theta_{delay} = \arg[(\sin\theta_{CW} + i\cos\theta_{CW}) \times (\sin\theta_{CCW} + i\cos\theta_{CCW})]/2$$

where θ_{CW} is a pixel's preferred orientation for clockwise stimulation, θ_{CCW} is the pixel's preferred orientation for counter-clockwise stimulation, and arg is the argument (complex-analysis).

For each imaging ROI in the block-wise calcium imaging sessions, we recorded a cell's fluorescence across multiple timestacks (~15-45 minutes total). The fluorescence changes ($\Delta F/F$) in individual trial responses were then averaged together, unless orientation tuning curves were being generated. Due to the presence of some biological motion, we

used sub-pixel image-registration via 2-d cross-correlation to align all images to the first timestack image (Guizar-Sicairos et al., 2008). The fluorescence data was then "first-frame subtracted" with the baseline response (2s prior to the presentation of the visual stimulus) being subtracted from the responses during the presentation of the visual stimulus. Individual cells were automatically identified by applying a 2-d spatial, bandpass filter to the raw fluorescence image (fermi-filter):

$$Filter(\lambda_{cutoff}, \lambda) = \frac{1}{1 + e^{-\frac{\lambda_{cutoff}}{T}(\frac{1}{\lambda_c} - \frac{1}{\lambda})}}$$

$$\mathcal{F}^{-1}(\mathcal{F}(Image) \times Filter(\lambda_{lp}, \lambda)) \times (1 - Filter(\lambda_{hp}, \lambda)))$$

, where $\mathcal{F}$ is the Fourier Transform, λ is the spatial wavelengths present in the image, λ_{cutoff} is the filter cutoff (low-pass cutoff (λ_{lp}): 4μm; high-pass cutoff (λ_{hp}): 40μm), and T is the "temperature" parameter of the fermi-filter (T = 0.05). The filtered image was then thresholded and cells were automatically identified from the binarized image. Any cells that were either too large or small were discarded. Like the intrinsic signal imaging data, image registration of the pre-pairing images to the post-pairing images was done via a 2-d affine transform with the soma of cells being used as landmarks.

For each of the previously discussed imaging techniques, we computed the orientation preference of each pixel/cell (θ_{pref}). For blockwise-imaging experiments, the vector addition approach was used to compute orientation preference by summing up the single-condition orientation responses, using the following formula:

$$z = \sum_{\theta=0^\circ}^{180^\circ} \left(\frac{\Delta Y}{Y}\right)_\theta \times e^{\frac{2\pi i \times \theta}{180}}$$

$$\theta_{pref} = z/\left(\sum_{\theta=0^{\circ}}^{180^{\circ}} \left(\frac{\Delta Y}{Y}\right)_{\theta}\right)$$

, where θ is the orientation of the presented visual stimulus, z is the orientation response (complex-field), and ($\frac{\Delta Y}{Y}$) is the visual stimulus-evoked changes (either reflectance from intrinsic signal imaging experiments ($\frac{\Delta R}{R}$) or fluorescence from two-photon calcium signal experiments ($\frac{\Delta F}{F}$)). For Fourier intrinsic signal maps, the orientation preference was computed by taking the argument of the orientation response (z). For measuring changes in orientation preference, we computed the change in a pixel's/cell's orientation preference, relative to the paired orientation:

$$\Delta\theta(n) = \left|\theta_{pre-pairing}(n) - \theta_{paired}\right| - \left|\theta_{post-pairing}(n) - \theta_{paired}\right| + Correction\ Factor(n)$$

$$Correction\ Factor(n) = \frac{\sum_{\Theta=0}^{180^{\circ}}(Offset(\Theta, n) - Offset(\pi - \Theta, n))}{\sum_{\Theta=0}^{180^{\circ}} PDF(\Theta)}$$

$$Offset(\Theta, n) = (|\Theta + \theta(n)| - \Theta) \times PDF(\Theta)$$

, where *n* denotes the current pixel/cell, θ_{paired} is the paired orientation, $\theta_{pre-pairing}$ and $\theta_{post-pairing}$ are respectively a pixel's/cell's pre-pairing and post-pairing orientation preference, Θ is the current orientation preference bin (100 bins, evenly spaced between -180˚ and +180˚), and PDF is the probability density function for the current orientation preference bin. We estimated the correction factor by first computing the unreferenced change in orientation preference across the measured population (pixels or cells):

$$\Delta\theta_{unreferenced} = \theta_{pre-pairing} - \theta_{post-pairing}$$

From this distribution, we computed a discrete probability density function (100 bins, ranging from 180˚ and +180˚), which we then used to estimate the expected offset for

each pixel/cell (see above). In addition to computing shifts in a pixel's orientation preference, we also estimated the change in cortical area preferring a visual stimulus for intrinsic signal maps. For this measure, we counted the number of dark pixels biased towards the visual stimulus (pixels with values below 0) and normalized this number by the total number of pixels.

The stimulation sites in optical stimulation experiments were identified by the YFP fluorescence of cells transfected with ChR2, while in electrical stimulation experiments the stimulation site was identified by the tip of the stimulating electrode (illuminated under 620nm or 700nm light). Pinwheels were identified by the crossing of zero contours in the real and imaginary parts (Kaschube et al., 2010). Regions of abrupt orientation preference changes (high-phase gradient), which include both pinwheels and line fractures, were identified by estimating two-dimensional spatial derivative of the orientation preference map and thresholding at 1.5 times the mean. The low-phase gradient (iso-orientation domains) was defined as the inverse mask of the high-phase gradient (Schuett et al., 2001).

5 DISCUSSION OF DISSERTATION RESULTS

In this final chapter, I will highlight the scientific findings from the previous data chapters, and discuss their relevance in the context of the literature. The encompassing goal of this dissertation work was to study whether columnar organization and plasticity in the ferret visual cortex depends on age and local functional architecture. My hope is that this dissertation work should influence our collective understanding how neural circuits organize together and adaptively alter their functional responses, particularly in face of: a.) gross morphological changes in the structure of the brain (i.e. early postnatal growth of the neocortex) and b.) alterations in an animal's visual experience.

But what is the rationale for studying functional maps in this dissertation? One of the main justifications for this scientific work is a growing body of computational studies investigating the self-organization of neural circuits (von der Malsburg, 1973; Singer, 1983; Durbin and Mitchison, 1990; Obermayer et al., 1990; Santini, 1996; Swindale, 1996; Wolf and Geisel, 1998; Goodhill and Cimponeriu, 2000; Swindale et al., 2000; Koulakov and Chklovskii, 2001; Tanaka et al., 2004; Yu et al., 2005; Wright et al., 2006; Schnabel et al., 2008; Wright and Bourke, 2008; Kaschube et al., 2010; Keil et al., 2010; Keil and Wolf, 2011; Reichl et al., 2012b, a). A particularly successful model has been the dimension reduction model. In this model, functional properties of visual stimuli are represented in a higher-dimensional stimulus space that "twists" to cover uniformly as many stimulus properties as possible (Durbin and Mitchison, 1990). However, to test the validity models, predictions made by computational studies need to be carefully evaluated with actual experimental data.

A common prediction made by computational studies is that substantial functional reorganization of neural connections should occur in functional maps (Wolf and Geisel, 1998; Shouval et al., 2000; Koulakov and Chklovskii, 2001; Lee et al., 2003; Alexander et al., 2004; Wolf, 2005; Oster and Bressloff, 2006; Wright et al., 2006; Schnabel et al., 2008; Wright and Bourke, 2008; Kaschube et al., 2009; Kaschube et al., 2010; Keil et al., 2010; Keil and Wolf, 2011; Reichl et al., 2012b, a), which has proven puzzling as the functional layout of experimentally measured functional maps, at least over short-timescales, have been shown to be stable (Chapman et al., 1996; Godecke et al., 1997; Sengpiel et al., 1998). I set out with my advisor, Justin Crowley, to test this hypothesis by observing whether functional maps of the ferret visual cortex exhibit any functional reorganization, or remain stable structures. Broadly speaking we investigated this topic from two different angles: either with and without plasticity-inducing paradigms. In the first set of experiments, we simply studied early map development when animals are initially exposed to normal visual experience (Chapter 2). This set of experiments was intended to provide insight into the natural, development progression of neural circuits. And then secondly, we used plasticity-inducing paradigms to test the extent of map modification in the ocular dominance map (Chapter 3) and orientation preference map (Chapter 4).

A brief summary of the findings in my thesis work are:

- **FINDING 1:** The functional organization of ferret visual cortex maps remains stable throughout life (i.e. ocular dominance, orientation preference, and direction

preference). Our longitudinal imaging data in Chapter 2 strongly suggests that neural circuits in ferret visual cortex don't functionally reorganize and form new cortical columns, despite considerable growth and shrinkage of the visual cortex. Additionally, we see in Chapter 3 that even after relatively long 14 day monocular deprivation experiments, ferret ocular dominance maps largely recover their original structure and shape after 1 hour. Likewise in Chapter 4, pairing-induced plasticity experiments did not perturb the location of pinwheel centers and the functional arrangement of orientation hypercolumns.

Significance: Our findings when taken in context with other longitudinal imaging studies (Chapman et al., 1996; Godecke et al., 1997; Sengpiel et al., 1998; Shtoyerman et al., 2000) demonstrate that the functional organization in maps and neural circuits are not significantly modified either by visual experience or plasticity inducing paradigms. Thus, functional organization seems "frozen" in its final organizational state at eye-opening, at least in the visual cortex of cats and ferrets. This stability has important ramifications on the timescale that self-organization of functional maps might take place, which must then operate well before eye-opening.

- **FINDING 2:** While functional organization is stable, the size of cortical columns can dynamically change either through gross structural changes in the visual cortex itself (see Chapter 2) or through plasticity-inducing protocols (see Chapter 3 and 4). In the case of plasticity, most changes are pronounced as expansions or erosions of a column's borders (e.g. for ocular dominance columns see the MD experiments in Figure 3 of Chapter 3 or see orientation column expansion in the pairing experiments in Figure 2 of Chapter 4).

Significance: Recent studies indicate the scale of cortical columns does not change during early postnatal development (Muller et al., 2000; Rathjen et al., 2003; Kaschube et al., 2009; Keil et al., 2010). However, the work I show in Chapter 2 is one of the first studies demonstrating that the spacing of cortical columns can systematically change (but see Blasdel et al., 1995). In conjunction with finding 1, this suggests the "balloon model" (i.e. expansion/shrinkage of cortical columns tracks areal changes in the expansion/shrinkage of visual cortex) can correctly predict how functional maps react to gross structural changes in the visual cortex.

- **FINDING 3:** As we show in Chapter 3, ocular dominance plasticity in the visual cortex is not just confined to the first month after eye opening (PD35-PD60), but exhibits an age-dependent decline. With two week monocular deprivations, we show ocular dominance plasticity is absent however in fully mature animals. We also show rapid recovery of deprived eye responses after monocular deprivation (within 1 hours), suggesting homeostatic processes.

  Significance: Recent studies show that the rodent visual cortex exhibits "post-critical period" plasticity (Sawtell et al., 2003; Pham et al., 2004; Tagawa et al., 2005; Hofer et al., 2006; Lehmann and Lowel, 2008; Sato and Stryker, 2008). Our study shows that adult ocular dominance plasticity is not merely a peculiar feature of rodent visual cortex, but also is present in carnivores, suggesting the possibility that adult ocular dominance plasticity is a general feature of the mammalian visual system.

- **FINDING 4:** In Chapter 3, we show chronic fluoxetine treatment in ferrets does not reinstate ocular dominance plasticity in adult ferret visual cortex. However, chronic fluoxetine treatment in young adult ferrets appears to promote a "reverse" ocular dominance shift as cells become more responsive to the deprived eye, than the spared eye.

  Significance: Chronic treatment with fluoxetine (a SSRI) has been demonstrated to reactive plasticity in the adult rat visual system (Bastos et al., 1999; Maya Vetencourt et al., 2008; Maya Vetencourt et al., 2011). The failure of fluoxetine treatment to re-open ocular dominance plasticity in adult ferrets then suggests the action of fluoxetine is not-straightforward, and is likely species-specific. The impact of fluoxetine, as well as other pharmacological drugs modulating major neurotransmitter systems, must then be evaluated carefully on a species-specific basis.

- **FINDING 5:** In Chapter 4, we show pairing-induced plasticity depends on the local functional architecture of the orientation preference. We determined that neurons located near pinwheel centers are less plastic than neurons located in iso-orientation domains. We interpret these findings as pairing-induced plasticity is greatest whenever co-activated cell populations share similar functional properties.

  Significance: Our results show that plasticity is not uniformly expressed across cell populations. Similar observations have been made that pinwheel centers are less sensitive to extraclassical surround modulation (Hashemi-Nezhad and Lyon, 2011; Okamoto et al., 2011). Thus, homogeneity in the functional properties of cell populations might lead cells in iso-orientation domains to be more sensitive to

modulation by top-down influences (such as attention) or from visual output outside a cell's receptive field, while cells at pinwheel centers more faithfully relay geniculo-cortical input into the visual cortex. Thus, the computational function of cells located in pinwheel centers and iso-orientation domains may serve distinct purposes.

5.1 REVIEW AND IMPLICATION FOR FUTURE RESEARCH

In this section, I review each finding in more detail, and suggest future experiments to investigate unanswered questions of my dissertatoin research. For the sake of simplicity, we will consolidate the discussion of findings 1 and 2 together, as well as findings 3 and 4.

5.1.1 Finding 1 and 2: Cortical columns can dynamically change in size, while the functional organization of ferret visual cortex maps remains stable throughout life

In Chapter 2, we demonstrate that the spacing between cortical columns in ferrets initially increases isotropically from eye-opening and peaks around PD50-60. And thereafter the column spacing deceases, but in anisotropic manner (ie column shrinkage is most pronounced along the media/lateral axis). Despite these changes, the functional organization of maps remains stable and does not undergo reorganization. Our results strongly imply that the length of neuronal processes, such as axons and dendrites, scale linearly with neocortical growth. Thus, functional reorganization of synaptic circuits

seems unnecessary to accommodate gross areal expansions of cortical areas, such as when the brain grows during early postnatal development.

Our results in ferrets however are in stark contrast to what appears to occur in cats, another carnivore. In cats, the column spacing in ocular dominance and orientation maps does not systematically change with age (Kaschube et al., 2009; Keil et al., 2010), which implies functional reorganization of neural connections must take place. Indeed, one study demonstrates that "zig-zag" reorganization is a candidate model to explain what happens in cat ocular dominance maps (Keil et al., 2010). The model correctly predicts that cat ocular dominance columns are initially more stripe-like in appearance at young ages, but through "zig-zag" reorganization ocular dominance columns become less banded and more isotropic (ie patchy) in appearance. Thus, a constant column spacing can be maintained, while new cortical columns are inserted into the functional map to compensate for the increased size of the visual cortex.

Analysis of cat ocular dominance maps shows that "zig-zag" reorganization appears to occur between the postnatal ages of 30-60. While cats and ferrets share similar developmental milestones, ferrets appear to be delayed by 21 postnatal days due to a cat's longer gestational period (a brief overview can be found in Issa et al., 1999). Hence "zig-zag" reorganization in cats appears to occur around the equivalent of postnatal day 50 in ferrets, which is when we start seeing a drop in the column spacing in ferrets. And to make matters more interesting, cat visual cortex expands by a factor of 30% during this same period (Keil et al., 2012). Thus, cat visual cortex is still growing, while ferret visual

cortex begins shrinking. This difference in areal expansion/shrinkage might point to why there is such a discrepancy between the presence of functional reorganization in cats, and not in ferrets.

An interesting prediction was made in the aforementioned study of "zig-zag" reorganization (Keil et al., 2010). This group showed that zig-zag type reorganization only occurs in a model system where the areal boundaries expand and the length of the lateral connections remains constant. Conversely, when the group allowed the length of lateral connections to grow at the same rate as the areal expansion, the model closely resembled the "balloon" model. In the balloon model, cortical columns expand in an isotropic manner, tracking the areal expansion of visual cortex. This behavior is in fact very similar to what we observed in ferret visual cortex between eye-opening and PD50-60.

Another facet to these results is that the expansion and shrinkage of the visual cortex appears to strikingly parallel GABA levels in the ferret visual cortex. One group has shown that the proportion of immuno-reactive labeled GABA neurons compared to overall number of Nissl-stained cells in the ferret visual cortex (ie the ratio of GABA to all other cells) fluctuates with an eerily similar timecourse to the column spacing measurements we report here (Gao et al., 1999). I show this timecourse in Figure 1 (see below). Interestingly, another paper provides some evidence that this relationship might not be merely correlated (Hensch and Stryker, 2004). In this study, the benzodiazepine diazepam (a GABA agonist) was chronically infused into the developing cat visual

cortex. The group found that the local column spacing in ocular dominance maps increased at the infusion site. Conversely, the local column spacing decreased when they infused the inverse-GABA agonist DMCM (methyl-6,7-dimethoxy-4-ethyl-β-carboline). These results when taken together with our study and Gao et al. (Gao et al., 1999) imply that increasing levels of GABA result in a larger local column spacing, while lower levels of GABA result in smaller column spacings. An important caveat to these results is that alteration of cortical inhibition may not necessitate a function reorganization of cortical columns. The longitudinal imaging data in this paper and Chapman et al. (Chapman et al., 1996) demonstrates that the functional layout of ferret orientation columns does not change substantially, despite changing levels of GABA in ferret visual cortex (Gao et al., 1999). Rather it seems conceivable that the perturbation of GABA circuits could instead be altering the gross structure of the visual cortex itself.

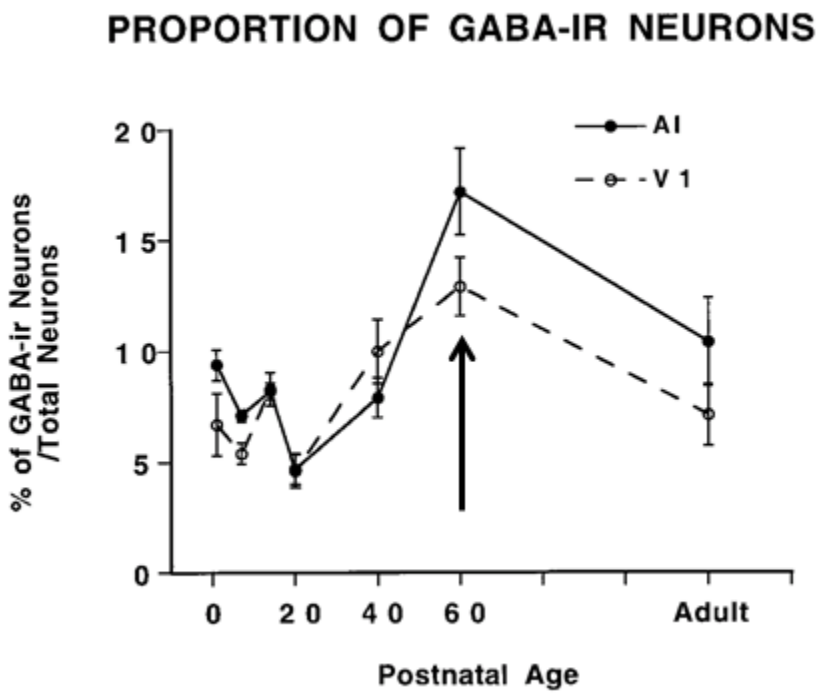

Figure 5-1: Proportion of immune-stained GABA cells to Nissl-stained neurons in ferret visual cortex.

Each data point is the average of a number of animal cortices and the error bars are SEM. Notice how the proportion of GABA cells to total number of cells peaks at PD60 in both A1 (auditory cortex) and V1 (visual cortex). This is the same peak we observed in Figure 2a and 2b in Chapter 2. This figure was taken from Gao et al. (Gao et al., 1999)

5.1.2 FUTURE EXPERIMENT - Visualize the Growth of Layer 2/3 Lateral Connections

My dissertation work, along with our studies (Muller et al., 2000; Rathjen et al., 2003; Kaschube et al., 2009; Keil et al., 2010), have characterized much of the developmental changes in functional maps of cat and ferret visual cortex. The next natural step is

seeking a structural correlate. A central prediction of the "zig-zag" reorganization model is whether lateral connections in layer 2/3 are constant or grow in young cats and ferrets. To do these experiments, I would advocate making small iontophoretic injections of an anterograde tracer, biocytin (Horikawa and Armstrong, 1988), into iso-orientation domains of ferret and cat visual cortex. Biocytin injections have become a standard tool to visualize the extent of lateral connections (Darian-Smith and Gilbert, 1994; Durack and Katz, 1996; Bosking et al., 1997; Kisvarday et al., 1997; Yousef et al., 2001). These injections would be used to visualize both short-range and long-range lateral projections. Long-range lateral connections (ie those that project between 1-3mm) should be particularly informative, as these connections are known to connect iso-orientation domains of the same orientation preference (Gilbert and Wiesel, 1983; Das and Gilbert, 1995; Bosking et al., 1997; Trachtenberg and Stryker, 2001; Stettler et al., 2002). Thus, we should observe a close relationship between the local column spacing in the orientation preference map and the extent of long-range lateral connections.

I would make injections in animals in the following age-ranges: PD30-180 in ferrets and PD5-150 in cats. These ages would provide a comprehensive look across early development, which encompasses eye-opening, the development of horizontal connections, the critical period, and early adult-hood (Callaway and Katz, 1990; Durack and Katz, 1996; Gao et al., 1999; White et al., 2001b; Keil et al., 2010). Before making injections, I would visualize the animal's orientation preference map with optical imaging of intrinsic signal and take pictures *in vivo* of the surface blood vessel map. Imaging the blood vessel map *in vivo* has the advantage that we could later align the post-mortem

blood vessel map back to its actual scale, as well as being able to overlay the lateral projections onto orientation preference maps. Indeed tissue shrinkage or warping, if not accounted for, could seriously hamper quantitative measurements on the extent of lateral connections; thus, this proposed setup would mitigate the pitfall of post-mortem tissue shrinkage and warping.

My expectation would be that I should be able to quantitatively measure whether lateral connections increase in size in ferrets, and remain constant in cats. If I observed different results, this would suggest that a central prediction of the "zig-zag" reorganizational model is incorrect and revisions would need to be made to the model. This finding is also important beyond just computational models. Careful, quantitative measurements on the growth of lateral connections are largely absent in the literature and it is unknown how well lateral connections scale with the growing visual cortex.

5.1.3 FUTURE EXPERIMENT – Implicate GABA in Column Spacing Changes

Another set of experiments would be to validate the "GABA" connection. So far I have only presented circumstantial evidence that GABA levels and column spacing are correlated. The definitive experiment would be to infuse diazepam, a GABA agonist, and DMCM, an inverse GABA agonist, into the visual cortex of a critical period ferret or cat. Previous experiments in kitten visual cortex showed that diazepam treatment locally expanded ocular dominance columns, while DMCM locally shrunk ocular dominance columns (Hensch and Stryker, 2004). However, as I describe above, there is the

possibility that the visual cortex is instead locally expanding, and functional reorganization is not taking place. Thus, I propose combining chronic infusion of diazepam/DMCM with longitudinal imaging of orientation columns. If my hypothesis is correct, I should observe that the local brain expands/shrinks near the infusion site when I respectively infuse diazepam/DMCM. Thus, a central prediction of my hypothesis is that while the local column spacing might change, the functional organization of the orientation map at the infusion site should remain stable. If functional reorganization does NOT occur as I hypothesize, this would suggest that modulation of GABA signaling can alter the gross structure of the visual cortex. If true, this might provide exciting evidence that the level of cortical inhibition is intimately tied to gross brain size. Alternatively if I observe functional reorganization to occur, this would disprove my GABA hypothesis. Instead this would directly validate the original hypothesis first proposed by Takao Hensch and Michael Stryker (Hensch and Stryker, 2004). In this hypothesis, they state that the functional organization of columns is controlled by intracortical inhibitory circuits, and visual experience through modulation of inhibitory circuits might modify the functional organization of cortical maps.

5.1.4 Finding 3 and 4: Ocular dominance plasticity in the ferret visual cortex is not just confined to the first month after eye opening, and chronic treatment with fluoxetine cannot reinstate adult ocular dominance plasticity

Traditionally ocular dominance plasticity has been considered a developmental process restricted to younger animals during a special developmental window dubbed the “critical

period" of ocular dominance plasticity. However, recent reports have indicated that ocular dominance plasticity lasts well into adulthood in rodents (Sawtell et al., 2003; Pham et al., 2004; Tagawa et al., 2005; Hofer et al., 2006; Lehmann and Lowel, 2008; Sato and Stryker, 2008). In Chapter 3, we sought to investigate whether "post-critical period" plasticity was a peculiar feature of rodents or could be directly observed in another animal model, such as ferrets. Indeed, we found that ocular dominance plasticity is still present in young adult ferrets, but to a much less pronounced degree. But by the time ferrets reach one year old, ocular dominance plasticity is absent.

A holy grail of visual neuroscience over the last fifty years has been to seek effective ways to reinstate neural plasticity in adult animals. The therapeutic benefit of such feats would be tremendous, as enhanced plasticity would likely promote recovery of function in amblyopic patients or individuals that have suffered stroke. And recent studies over the last decade have demonstrated the tantalizing prospect that reinstating adult ocular dominance plasticity is a real possibility. Groups have shown that monocular deprivation can still induce ocular dominance plasticity if done in conjunction with external manipulations, such as altering an animal's environment or visual experience (He et al., 2006; Sale et al., 2007), reducing intracortical inhibition (Sale et al., 2007; Maya Vetencourt et al., 2008; Harauzov et al., 2010), transplanting immature inhibitory interneurons into the visual cortex (Southwell et al., 2010), degrading perineuronal nets with chondroitinase ABC (Pizzorusso et al., 2002; Vorobyov et al., 2013), and disrupting the OTX2 homeoprotein that reduces the in vivo expression of paravalbumin cells and perineuronal nets (Sugiyama et al., 2008; Spatazza et al., 2013). Each of these

manipulations points to a common theme that the regulation of inhibitory interneurons is a key feature in enhancing ocular dominance plasticity in adult animals.

Interestingly, adult plasticity in the visual system has also been demonstrated through the modulation of major neurotransmitter systems, such as nicotinic acetycholine signaling through a Lynx1 knockout (Morishita et al., 2010), serotonin signaling through fluoxetine treatment or direction infusion of serotonin (Bastos et al., 1999; Maya Vetencourt et al., 2008; Maya Vetencourt et al., 2011; Bachatene et al., 2013), and noradrenalinergic signaling through L-threo-3,4-dihydroxyphenylserine treatment (Mataga et al., 1992). My advisor and I were particularly interested in chronic fluoxetine treatment, as fluoxetine is a potentially non-invasive therapeutic treatment for humans suffering amblyopia. However, as we show in Chapter 3, chronic treatment of fluoxetine in ferrets does not reinstate adult ocular dominance plasticity, unlike it does rats (Maya Vetencourt et al., 2008; Maya Vetencourt et al., 2011). Although disappointing, the negative result does suggest the role of neuromodulators promoting plasticity is likely to be complicated and should be carefully evaluated on a species-by-species basis.

5.1.5 FUTURE EXPERIMENT – Test whether Chronic Tianeptine Treatment Reinstates Adult Ocular Dominance Plasticity

Although we were unable to reintroduce ocular dominance plasticity in adult ferrets, we observed a “reverse” ocular dominance shift in young ferrets. A “reverse” ocular dominance shift occurs whenever the spared eye’s responses are weakened, rather than the deprived eye’s responses. This result is noteworthy, since reverse ocular dominance

shifts have also been reported in cat visual cortex when muscimol, a GABA agonist, or neurotrophins were infused into the cat visual cortex (Reiter and Stryker, 1988; Gu et al., 1994; Galuske et al., 2000). Reiter and Stryker proposed that a reverse ocular dominance shift occurs when increased tonic inhibition promoting a weakening of the spared eye inputs (Reiter and Stryker, 1988). Thus, chronic fluoxetine treatment in ferrets might mediate the enhancement of GABAergic inhibition, whereas it's been shown to weaken GABAergic inhibition in rat visual cortex (Maya Vetencourt et al., 2008). This effect would be interesting as the vast majority of adult plasticity studies suggest lowering GABAergic inhibition is important in reinstating adult ocular dominance plasticity.

If true, this would suggest serotonin and fluoxetine in the ferret visual system might impact ocular dominance plasticity. To investigate the viability of this hypothesis, I propose repeating the longitudinal imaging study in Chapter 3. However, instead of combining monocular deprivation with chronic fluoxetine treatment, I propose replacing fluoxetine with tianeptine (Mennini et al., 1987). The actions of tianeptine, a selective-serotonin reuptake enhancer, are the opposite of fluoxetine, which is a selective-serotonin reuptake inhibitor; thus, tianepetine reduces the efficacy of serotonin modulation, while fluoxetine enhances it. This approach may have merit, as there are recent reports showing that tianeptine promotes neural plasticity (Spedding and Gressens, 2008; Zhang et al., 2013). If chronic treatment with tianeptine reintroduced ocular dominance plasticity in ferrets, this would be an exciting result, since it would indicate that modulation of serotonin is a viable strategy to promote neural plasticity. And in that case, fluoxetine or tianeptine might then pose as viable drugs to promote neural plasticity in the visual

system. On the other hand, a negative result would imply that modulation of serotonin levels is much more complicated and simple treatment strategies of SSRIs or SSREs might not be viable as a therapeutic strategy in humans.

5.1.6 FINDING 5: Pairing-induced plasticity depends on the local functional architecture of the orientation preference

This last finding demonstrates that neurons nearer to pinwheel centers are "less plastic" to pairing than neurons located in iso-orientation domains of ferret visual cortex. Schuett et al. reported similar findings in cat visual cortex (Schuett et al., 2001). Similar observations have been made been made by other groups recently that suggest pinwheel centers might also be less sensitive to extraclassical surround modulation (Hashemi-Nezhad and Lyon, 2011; Okamoto et al., 2011). Thus, homogeneity in the functional properties of cell populations might lead cells in iso-orientation domains to be more sensitive to modulation by top-down influences or from visual output outside a cell's receptive field. In contrast, cells at pinwheel centers might more faithfully relay geniculo-cortical input into the visual cortex.

However, we also note that not only are pinwheels less susceptible to pairing-induced plasticity, but also that cortical stimulation progressively nearer to pinwheel centers weakens the overall pairing-induced changes for all neurons located within 0.5-1.0mm of the stimulation site. And interestingly, for two-site stimulation experiments, the stimulation site nearest to a pinwheel center also seemed to better predict the pairing-induced changes in the functional maps. This second finding suggests an interaction

between the two stimulation sites that may not merely be a simple summation of activation by the two sites. Rather it seems pairing-induced activation near pinwheel centers has a destabilizing effect on pairing-induced plasticity in the local functional map.

5.1.7 FUTURE EXPERIMENT – Pairing Induced Plasticity in Mice

Current studies thus far have only evaluated pairing-induced plasticity in the context of carnivores. However, rodents do not exhibit columnar organization and lack patchy horizontal connectivity (Ohki et al., 2005; Van Hooser et al., 2005). Thus, it's natural to wonder if the salt-and-pepper functional organization in rodents (ie a neuron's physically adjacent partner may have a completely different orientation preference) is permissive to pairing-induced plasticity. Studies suggest neurons in rodent visual cortex receive broadly tuned synaptic input, which is similar to pinwheel centers in carnivores (Van Hooser et al., 2005; Ko et al., 2011). Thus, one might suspect that pairing-induced plasticity in rodents is absent.

I would investigate pair-induced plasticity in a rodent animal model, such as mice. As rodents lack meaningful functional maps, we would only use two-photon calcium imaging to evaluate orientation tuning of cells before and after pairing. I would conduct the study in the same manner that we described in Chapter 4 concerning the two-photon calcium imaging experiments. Briefly we would measure the orientation tuning of cells before and after pairing a visual stimulus with electrical stimulation of the cortex. If we find an absence of pairing-induced plasticity, or even repulsive shifts away from the paired-orientation, this would indicate that the functional architecture of rodents more closely resembles pinwheel centers. In contrast, if we find significant pairing-induced

plasticity, this would call into question our hypothesis that homogeneity in activated cell populations makes them more permissive to pairing-induced plasticity. Both results would be very interesting, as they would provide us a better understanding of the relevancy of columnar organization in carnivores and primates. If rodent's lacked pairing-induced plasticity, one possible role for cortical columns is that neurons in iso-orientation domains might be more sensitive to contextual modulation by the presence of other stimuli in the visual field.

5.1.8 FUTURE EXPERIMENT – Pairing Induced Plasticity at Multiple Sites and Earlier in Development

In the two-site stimulation experiments with ChR2, we found evidence for non-linear interactions between closely adjoined stimulation sites. I would propose that more complicated experiments would be insightful. For example, could activation of nearby iso-orientation domains of similar orientation selectivity drive exhibit stronger shifts towards the paired orientation? In a similar vein, would activation of two nearby iso-orientation domains of orthogonal orientation preferences display weaker shifts? The ultimate goal would be to characterize whether similarity (with respect to orientation tuning) of simultaneously activated stimulation sites induces stronger or weaker pairing-induced shifts. To conduct this research, we would carry out optical imaging experiments as we previously described in Chapter 4. However, we would also need to perform optical imaging of intrinsic signal to visualize the orientation preference map as we make viral injections of ChR2 into layer 2/3 cells. This would allow us to select the sites of stimulation.

Another arguably even more valuable area for research would be to optically stimulate multiple map locations transfected with CHR2 before eye-opening in the ferret (between PD20-30). One of the major mysteries is how seemingly neurons in carnivores and primates appear to be already segregated in orientation domains before visual experience. In this paradigm, we would perform short longitudinal imaging experiments through a chronic imaging window where we optically stimulate multiple transfected sites in the visual cortex every day for 2-3 hours before eye-opening. The goal would be to examine if enforcing correlated spiking activity in neurons before eye-opening influences the layout of functional maps. In support of this hypothesis, recent research indicates that local neighborhood biases influence the development of direction preference maps in ferret visual cortex (Li et al., 2008b; Van Hooser et al., 2012). We would evaluate the success of the experiment by correlating the sites of transfections with the pattern of orientation columns after eye-opening.

5.2FINAL CONCLUSIONS

In conclusion, I have shown in this dissertation work that functional maps of the visual cortex rapidly mature after eye-opening and that the functional organization of these maps remains stable through the lifespan of the ferret. Even in cases where we applied plasticity-inducing paradigms, we still found that functional maps maintained their existing spatial relationships (relative location and shape of cortical columns, as well the location of pinwheel centers). Thus, the functional architecture of neural connections that develops in the visual cortex places constraints on the extent of cortical plasticity And

stability in the representation of stimulus feature properties in functional maps of the visual cortex makes a great deal of sense from an evolutionary perspective, since vision in mammals needs to remain a stable and robust sensory system.

6 REFERENCES

Adams DL, Sincich LC, Horton JC (2007) Complete pattern of ocular dominance columns in human primary visual cortex. J Neurosci 27:10391-10403.

Alexander DM, Bourke PD, Sheridan P, Konstandatos O, Wright JJ (2004) Intrinsic connections in tree shrew V1 imply a global to local mapping. Vision Res 44:857-876.

Antonini A, Stryker MP (1993) Rapid remodeling of axonal arbors in the visual cortex. Science 260:1819-1821.

Antonini A, Stryker MP (1996) Plasticity of geniculocortical afferents following brief or prolonged monocular occlusion in the cat. J Comp Neurol 369:64-82.

Apfelbach R, Kruska D (1979) On the postnatal development of the brain of the ferret Mustela putorius f. furo (Mustelidae; Mammalia). Z Säugetierkunde 44:127–131.

Arenkiel BR, Peca J, Davison IG, Feliciano C, Deisseroth K, Augustine GJ, Ehlers MD, Feng G (2007) In vivo light-induced activation of neural circuitry in transgenic mice expressing channelrhodopsin-2. Neuron 54:205-218.

Bachatene L, Bharmauria V, Cattan S, Molotchnikoff S (2013) Fluoxetine and serotonin facilitate attractive-adaptation-induced orientation plasticity in adult cat visual cortex. Eur J Neurosci 38:2065-2077.

Baker TI, Issa NP (2005) Cortical maps of separable tuning properties predict population responses to complex visual stimuli. J Neurophysiol 94:775-787.

Barnette AR, Neil JJ, Kroenke CD, Griffith JL, Epstein AA, Bayly PV, Knutsen AK, Inder TE (2009) Characterization of brain development in the ferret via MRI. Pediatr Res 66:80-84.

Bartfeld E, Grinvald A (1992) Relationships between orientation-preference pinwheels, cytochrome oxidase blobs, and ocular-dominance columns in primate striate cortex. Proc Natl Acad Sci U S A 89:11905-11909.

Basole A, White LE, Fitzpatrick D (2003) Mapping multiple features in the population response of visual cortex. Nature 423:986-990.

Bastos EF, Marcelino JL, Amaral AR, Serfaty CA (1999) Fluoxetine-induced plasticity in the rodent visual system. Brain Res 824:28-35.

Bear MF, Singer W (1986) Modulation of visual cortical plasticity by acetylcholine and noradrenaline. Nature 320:172-176.

Berkes P, Orban G, Lengyel M, Fiser J (2011) Spontaneous cortical activity reveals hallmarks of an optimal internal model of the environment. Science 331:83-87.

Bhardwaj RD, Curtis MA, Spalding KL, Buchholz BA, Fink D, Bjork-Eriksson T, Nordborg C, Gage FH, Druid H, Eriksson PS, Frisen J (2006) Neocortical neurogenesis in humans is restricted to development. Proc Natl Acad Sci U S A 103:12564-12568.

Blakemore C, Cooper GF (1970) Development of the brain depends on the visual environment. Nature 228:477-478.

Blasdel G, Obermayer K, Kiorpes L (1995) Organization of ocular dominance and orientation columns in the striate cortex of neonatal macaque monkeys. Vis Neurosci 12:589-603.
Blasdel GG, Salama G (1986) Voltage-sensitive dyes reveal a modular organization in monkey striate cortex. Nature 321:579-585.
Bonhoeffer T, Grinvald A (1991) Iso-orientation domains in cat visual cortex are arranged in pinwheel-like patterns. Nature 353:429-431.
Bosking WH, Crowley JC, Fitzpatrick D (2002) Spatial coding of position and orientation in primary visual cortex. Nat Neurosci 5:874-882.
Bosking WH, Zhang Y, Schofield B, Fitzpatrick D (1997) Orientation selectivity and the arrangement of horizontal connections in tree shrew striate cortex. J Neurosci 17:2112-2127.
Boyden ES, Zhang F, Bamberg E, Nagel G, Deisseroth K (2005) Millisecond-timescale, genetically targeted optical control of neural activity. Nat Neurosci 8:1263-1268.
Callaway EM, Katz LC (1990) Emergence and refinement of clustered horizontal connections in cat striate cortex. J Neurosci 10:1134-1153.
Chapman B, Stryker MP (1993) Development of orientation selectivity in ferret visual cortex and effects of deprivation. J Neurosci 13:5251-5262.
Chapman B, Zahs KR, Stryker MP (1991) Relation of cortical cell orientation selectivity to alignment of receptive fields of the geniculocortical afferents that arborize within a single orientation column in ferret visual cortex. J Neurosci 11:1347-1358.
Chapman B, Stryker MP, Bonhoeffer T (1996) Development of orientation preference maps in ferret primary visual cortex. J Neurosci 16:6443-6453.
Chung S, Ferster D (1998) Strength and orientation tuning of the thalamic input to simple cells revealed by electrically evoked cortical suppression. Neuron 20:1177-1189.
Coppola DM, White LE (2004) Visual experience promotes the isotropic representation of orientation preference. Vis Neurosci 21:39-51.
Courchesne E, Chisum HJ, Townsend J, Cowles A, Covington J, Egaas B, Harwood M, Hinds S, Press GA (2000) Normal brain development and aging: quantitative analysis at in vivo MR imaging in healthy volunteers. Radiology 216:672-682.
Crair MC, Gillespie DC, Stryker MP (1998) The role of visual experience in the development of columns in cat visual cortex. Science 279:566-570.
Crair MC, Ruthazer ES, Gillespie DC, Stryker MP (1997a) Relationship between the ocular dominance and orientation maps in visual cortex of monocularly deprived cats. Neuron 19:307-318.
Crair MC, Ruthazer ES, Gillespie DC, Stryker MP (1997b) Ocular dominance peaks at pinwheel center singularities of the orientation map in cat visual cortex. J Neurophysiol 77:3381-3385.
Crowley JC, Katz LC (1999) Development of ocular dominance columns in the absence of retinal input. Nat Neurosci 2:1125-1130.
Crowley JC, Katz LC (2000) Early development of ocular dominance columns. Science 290:1321-1324.
Darian-Smith C, Gilbert CD (1994) Axonal sprouting accompanies functional reorganization in adult cat striate cortex. Nature 368:737-740.

Das A, Gilbert CD (1995) Long-range horizontal connections and their role in cortical reorganization revealed by optical recording of cat primary visual cortex. Nature 375:780-784.
Das A, Gilbert CD (1999) Topography of contextual modulations mediated by short-range interactions in primary visual cortex. Nature 399:655-661.
Daw NW, Fox K, Sato H, Czepita D (1992) Critical period for monocular deprivation in the cat visual cortex. J Neurophysiol 67:197-202.
DeAngelis GC, Ohzawa I, Freeman RD (1993) Spatiotemporal organization of simple-cell receptive fields in the cat's striate cortex. I. General characteristics and postnatal development. J Neurophysiol 69:1091-1117.
Dragoi V, Sharma J, Sur M (2000) Adaptation-induced plasticity of orientation tuning in adult visual cortex. Neuron 28:287-298.
Dragoi V, Rivadulla C, Sur M (2001) Foci of orientation plasticity in visual cortex. Nature 411:80-86.
Drenhaus U, Rager G, Eggli P, Kretz R (2006) On the postnatal development of the striate cortex (V1) in the tree shrew (Tupaia belangeri). Eur J Neurosci 24:479-490.
Duffy KR, Murphy KM, Jones DG (1998) Analysis of the postnatal growth of visual cortex. Vis Neurosci 15:831-839.
Dufour A, Seibt J, Passante L, Depaepe V, Ciossek T, Frisen J, Kullander K, Flanagan JG, Polleux F, Vanderhaeghen P (2003) Area specificity and topography of thalamocortical projections are controlled by ephrin/Eph genes. Neuron 39:453-465.
Durack JC, Katz LC (1996) Development of horizontal projections in layer 2/3 of ferret visual cortex. Cereb Cortex 6:178-183.
Durbin R, Mitchison G (1990) A dimension reduction framework for understanding cortical maps. Nature 343:644-647.
Edagawa Y, Saito H, Abe K (2000) The serotonin 5-HT2 receptor-phospholipase C system inhibits the induction of long-term potentiation in the rat visual cortex. Eur J Neurosci 12:1391-1396.
Edagawa Y, Saito H, Abe K (2001) Endogenous serotonin contributes to a developmental decrease in long-term potentiation in the rat visual cortex. J Neurosci 21:1532-1537.
Fagiolini M, Hensch TK (2000) Inhibitory threshold for critical-period activation in primary visual cortex. Nature 404:183-186.
Ferster D, Chung S, Wheat H (1996) Orientation selectivity of thalamic input to simple cells of cat visual cortex. Nature 380:249-252.
Field DJ, Hayes A, Hess RF (1993) Contour integration by the human visual system: evidence for a local "association field". Vision Res 33:173-193.
Foote SL, Morrison JH (1984) Postnatal development of laminar innervation patterns by monoaminergic fibers in monkey (Macaca fascicularis) primary visual cortex. J Neurosci 4:2667-2680.
Fox JG (1998) Biology & Diseases of the Ferret, 2nd Edition: Lippincott William & Wilkins.
Fregnac Y, Shulz D, Thorpe S, Bienenstock E (1988) A cellular analogue of visual cortical plasticity. Nature 333:367-370.

Frenkel MY, Bear MF (2004) How monocular deprivation shifts ocular dominance in visual cortex of young mice. Neuron 44:917-923.
Fritschy JM, Garey LJ (1986) Quantitative changes in morphological parameters in the developing visual cortex of the marmoset monkey. Brain Res 394:173-188.
Galuske RA, Kim DS, Castren E, Singer W (2000) Differential effects of neurotrophins on ocular dominance plasticity in developing and adult cat visual cortex. Eur J Neurosci 12:3315-3330.
Galuske RA, Kim DS, Castren E, Thoenen H, Singer W (1996) Brain-derived neurotrophic factor reversed experience-dependent synaptic modifications in kitten visual cortex. Eur J Neurosci 8:1554-1559.
Gao WJ, Newman DE, Wormington AB, Pallas SL (1999) Development of inhibitory circuitry in visual and auditory cortex of postnatal ferrets: immunocytochemical localization of GABAergic neurons. J Comp Neurol 409:261-273.
Giedd J (1999) Brain development, IX: human brain growth. Am J Psychiatry 156:4.
Gilbert CD, Wiesel TN (1983) Clustered intrinsic connections in cat visual cortex. J Neurosci 3:1116-1133.
Godde B, Leonhardt R, Cords SM, Dinse HR (2002) Plasticity of orientation preference maps in the visual cortex of adult cats. Proc Natl Acad Sci U S A 99:6352-6357.
Godecke I, Kim DS, Bonhoeffer T, Singer W (1997) Development of orientation preference maps in area 18 of kitten visual cortex. Eur J Neurosci 9:1754-1762.
Goodhill GJ, Cimponeriu A (2000) Analysis of the elastic net model applied to the formation of ocular dominance and orientation columns. Network 11:153-168.
Gordon JA, Stryker MP (1996) Experience-dependent plasticity of binocular responses in the primary visual cortex of the mouse. J Neurosci 16:3274-3286.
Gu Q, Singer W (1995) Involvement of serotonin in developmental plasticity of kitten visual cortex. Eur J Neurosci 7:1146-1153.
Gu Q, Patel B, Singer W (1990) The laminar distribution and postnatal development of serotonin-immunoreactive axons in the cat primary visual cortex. Exp Brain Res 81:257-266.
Gu Q, Liu Y, Cynader MS (1994) Nerve growth factor-induced ocular dominance plasticity in adult cat visual cortex. Proc Natl Acad Sci U S A 91:8408-8412.
Guizar-Sicairos M, Thurman ST, Fienup JR (2008) Efficient subpixel image registration algorithms. Opt Lett 33:156-158.
Harauzov A, Spolidoro M, DiCristo G, De Pasquale R, Cancedda L, Pizzorusso T, Viegi A, Berardi N, Maffei L (2010) Reducing intracortical inhibition in the adult visual cortex promotes ocular dominance plasticity. J Neurosci 30:361-371.
Hashemi-Nezhad M, Lyon DC (2011) Orientation tuning of the suppressive extraclassical surround depends on intrinsic organization of V1. Cereb Cortex 22:308-326.
Hata Y, Ohshima M, Ichisaka S, Wakita M, Fukuda M, Tsumoto T (2000) Brain-derived neurotrophic factor expands ocular dominance columns in visual cortex in monocularly deprived and nondeprived kittens but does not in adult cats. J Neurosci 20:RC57.
He HY, Hodos W, Quinlan EM (2006) Visual deprivation reactivates rapid ocular dominance plasticity in adult visual cortex. J Neurosci 26:2951-2955.
Hensch TK (2005) Critical period plasticity in local cortical circuits. Nat Rev Neurosci 6:877-888.

Hensch TK, Stryker MP (2004) Columnar architecture sculpted by GABA circuits in developing cat visual cortex. Science 303:1678-1681.
Hofer SB, Mrsic-Flogel TD, Bonhoeffer T, Hubener M (2006) Prior experience enhances plasticity in adult visual cortex. Nat Neurosci 9:127-132.
Horikawa K, Armstrong WE (1988) A versatile means of intracellular labeling: injection of biocytin and its detection with avidin conjugates. J Neurosci Methods 25:1-11.
Hornung JP, Fritschy JM, Tork I (1990) Distribution of two morphologically distinct subsets of serotoninergic axons in the cerebral cortex of the marmoset. J Comp Neurol 297:165-181.
Horton JC, Hedley-Whyte ET (1984) Mapping of cytochrome oxidase patches and ocular dominance columns in human visual cortex. Philos Trans R Soc Lond B Biol Sci 304:255-272.
Horton JC, Adams DL (2005) The cortical column: a structure without a function. Philos Trans R Soc Lond B Biol Sci 360:837-862.
Hoyert D, Xu J (2012) Deaths: Preliminary Data for 2011. National Vital Statistics Reports 61.
Huang S, Gu Y, Quinlan EM, Kirkwood A (2010) A refractory period for rejuvenating GABAergic synaptic transmission and ocular dominance plasticity with dark exposure. J Neurosci 30:16636-16642.
Huang ZJ, Kirkwood A, Pizzorusso T, Porciatti V, Morales B, Bear MF, Maffei L, Tonegawa S (1999) BDNF regulates the maturation of inhibition and the critical period of plasticity in mouse visual cortex. Cell 98:739-755.
Hubel DH, Wiesel TN (1962) Receptive fields, binocular interaction and functional architecture in the cat's visual cortex. J Physiol 160:106-154.
Hubel DH, Wiesel TN (1963) Receptive Fields of Cells in Striate Cortex of Very Young, Visually Inexperienced Kittens. J Neurophysiol 26:994-1002.
Hubel DH, Wiesel TN (1965) Comparison of the effects of unilateral and bilateral eye closure on cortical unit responses in kittens. J Neurophysiol 28:1029-1040.
Hubel DH, Wiesel TN (1970) The period of susceptibility to the physiological effects of unilateral eye closure in kittens. J Physiol 206:419-436.
Hubener M, Shoham D, Grinvald A, Bonhoeffer T (1997) Spatial relationships among three columnar systems in cat area 17. J Neurosci 17:9270-9284.
Huberman AD, Wang GY, Liets LC, Collins OA, Chapman B, Chalupa LM (2003) Eye-specific retinogeniculate segregation independent of normal neuronal activity. Science 300:994-998.
Humphrey AL, Saul AB (1998) Strobe rearing reduces direction selectivity in area 17 by altering spatiotemporal receptive-field structure. J Neurophysiol 80:2991-3004.
Issa NP, Trepel C, Stryker MP (2000) Spatial frequency maps in cat visual cortex. J Neurosci 20:8504-8514.
Issa NP, Rosenberg A, Husson TR (2008) Models and measurements of functional maps in V1. J Neurophysiol 99:2745-2754.
Issa NP, Trachtenberg JT, Chapman B, Zahs KR, Stryker MP (1999) The critical period for ocular dominance plasticity in the Ferret's visual cortex. J Neurosci 19:6965-6978.
Jackson CA, Hickey TL (1985) Use of ferrets in studies of the visual system. Lab Anim Sci 35:211-215.

Jackson CA, Peduzzi JD, Hickey TL (1989) Visual cortex development in the ferret. I. Genesis and migration of visual cortical neurons. J Neurosci 9:1242-1253.
Jakab RL, Goldman-Rakic PS (2000) Segregation of serotonin 5-HT2A and 5-HT3 receptors in inhibitory circuits of the primate cerebral cortex. J Comp Neurol 417:337-348.
Kaas JH, Krubitzer LA, Chino YM, Langston AL, Polley EH, Blair N (1990) Reorganization of retinotopic cortical maps in adult mammals after lesions of the retina. Science 248:229-231.
Kalatsky VA, Stryker MP (2003) New paradigm for optical imaging: temporally encoded maps of intrinsic signal. Neuron 38:529-545.
Kapadia MK, Ito M, Gilbert CD, Westheimer G (1995) Improvement in visual sensitivity by changes in local context: parallel studies in human observers and in V1 of alert monkeys. Neuron 15:843-856.
Kaschube M, Wolf F, Geisel T, Lowel S (2002) Genetic influence on quantitative features of neocortical architecture. J Neurosci 22:7206-7217.
Kaschube M, Schnabel M, Wolf F, Lowel S (2009) Interareal coordination of columnar architectures during visual cortical development. Proc Natl Acad Sci U S A 106:17205-17210.
Kaschube M, Schnabel M, Lowel S, Coppola DM, White LE, Wolf F (2010) Universality in the evolution of orientation columns in the visual cortex. Science 330:1113-1116.
Kaschube M, Wolf F, Puhlmann M, Rathjen S, Schmidt KF, Geisel T, Lowel S (2003) The pattern of ocular dominance columns in cat primary visual cortex: intra- and interindividual variability of column spacing and its dependence on genetic background. Eur J Neurosci 18:3251-3266.
Katz LC, Crowley JC (2002) Development of cortical circuits: lessons from ocular dominance columns. Nat Rev Neurosci 3:34-42.
Keck T, Mrsic-Flogel TD, Vaz Afonso M, Eysel UT, Bonhoeffer T, Hubener M (2008) Massive restructuring of neuronal circuits during functional reorganization of adult visual cortex. Nat Neurosci 11:1162-1167.
Keil W, Wolf F (2011) Coverage, continuity, and visual cortical architecture. Neural Syst Circuits 1:17.
Keil W, Schmidt KF, Lowel S, Kaschube M (2010) Reorganization of columnar architecture in the growing visual cortex. Proc Natl Acad Sci U S A 107:12293-12298.
Keil W, Kaschube M, Schnabel M, Kisvarday Z, Lowel S, Coppola DM, White LE, Wolf F (2012) Response to Comment on “Universality in the Evolution of Orientation Columns in the Visual Cortex“. Science 336:413.
Kim DS, Matsuda Y, Ohki K, Ajima A, Tanaka S (1999) Geometrical and topological relationships between multiple functional maps in cat primary visual cortex. Neuroreport 10:2515-2522.
Kisvarday ZF, Toth E, Rausch M, Eysel UT (1997) Orientation-specific relationship between populations of excitatory and inhibitory lateral connections in the visual cortex of the cat. Cereb Cortex 7:605-618.

Ko H, Hofer SB, Pichler B, Buchanan KA, Sjostrom PJ, Mrsic-Flogel TD (2011) Functional specificity of local synaptic connections in neocortical networks. Nature 473:87-91.
Koulakov AA, Chklovskii DB (2001) Orientation preference patterns in mammalian visual cortex: a wire length minimization approach. Neuron 29:519-527.
Krahe TE, Medina AE (2010) Activation of NMDA receptors is necessary for the recovery of cortical binocularity. J Neurophysiol 103:2700-2706.
Krahe TE, Medina AE, de Bittencourt-Navarrete RE, Colello RJ, Ramoa AS (2005) Protein synthesis-independent plasticity mediates rapid and precise recovery of deprived eye responses. Neuron 48:329-343.
Kruska D (1993) Evidence of decrease in brain size in ranch mink, Mustela vison f. dom., during subadult postnatal ontogenesis. Brain Behav Evol 41:303-315.
Lee HY, Yahyanejad M, Kardar M (2003) Symmetry considerations and development of pinwheels in visual maps. Proc Natl Acad Sci U S A 100:16036-16040.
Lehmann K, Lowel S (2008) Age-dependent ocular dominance plasticity in adult mice. PLoS One 3:e3120.
LeVay S, Stryker MP, Shatz CJ (1978) Ocular dominance columns and their development in layer IV of the cat's visual cortex: a quantitative study. J Comp Neurol 179:223-244.
Levitt JB, Lund JS (1997) Contrast dependence of contextual effects in primate visual cortex. Nature 387:73-76.
Li W, Gilbert CD (2002) Global contour saliency and local colinear interactions. J Neurophysiol 88:2846-2856.
Li W, Piech V, Gilbert CD (2008a) Learning to link visual contours. Neuron 57:442-451.
Li Y, Fitzpatrick D, White LE (2006) The development of direction selectivity in ferret visual cortex requires early visual experience. Nat Neurosci 9:676-681.
Li Y, Van Hooser SD, Mazurek M, White LE, Fitzpatrick D (2008b) Experience with moving visual stimuli drives the early development of cortical direction selectivity. Nature 456:952-956.
Liao DS, Mower AF, Neve RL, Sato-Bigbee C, Ramoa AS (2002) Different mechanisms for loss and recovery of binocularity in the visual cortex. J Neurosci 22:9015-9023.
Liao DS, Krahe TE, Prusky GT, Medina AE, Ramoa AS (2004) Recovery of cortical binocularity and orientation selectivity after the critical period for ocular dominance plasticity. J Neurophysiol 92:2113-2121.
Lidov HG, Grzanna R, Molliver ME (1980) The serotonin innervation of the cerebral cortex in the rat--an immunohistochemical analysis. Neuroscience 5:207-227.
Luskin MB, Shatz CJ (1985) Neurogenesis of the cat's primary visual cortex. J Comp Neurol 242:611-631.
Maffei A, Turrigiano G (2008) The age of plasticity: developmental regulation of synaptic plasticity in neocortical microcircuits. Prog Brain Res 169:211-223.
Maldonado PE, Godecke I, Gray CM, Bonhoeffer T (1997) Orientation selectivity in pinwheel centers in cat striate cortex. Science 276:1551-1555.
Malkova L, Heuer E, Saunders RC (2006) Longitudinal magnetic resonance imaging study of rhesus monkey brain development. Eur J Neurosci 24:3204-3212.

Mante V, Carandini M (2005) Mapping of stimulus energy in primary visual cortex. J Neurophysiol 94:788-798.
Mardia KV, P. J (2000) Directional Statistics, 2nd Edition Edition: John Wiley and Sons Ltd., .
Marino J, Schummers J, Lyon DC, Schwabe L, Beck O, Wiesing P, Obermayer K, Sur M (2005) Invariant computations in local cortical networks with balanced excitation and inhibition. Nat Neurosci 8:194-201.
Maya Vetencourt JF, Tiraboschi E, Spolidoro M, Castren E, Maffei L (2011) Serotonin triggers a transient epigenetic mechanism that reinstates adult visual cortex plasticity in rats. Eur J Neurosci 33:49-57.
Maya Vetencourt JF, Sale A, Viegi A, Baroncelli L, De Pasquale R, O'Leary OF, Castren E, Maffei L (2008) The antidepressant fluoxetine restores plasticity in the adult visual cortex. Science 320:385-388.
Medina AE, Ramoa AS (2005) Early alcohol exposure impairs ocular dominance plasticity throughout the critical period. Brain Res Dev Brain Res 157:107-111.
Medina AE, Krahe TE, Coppola DM, Ramoa AS (2003) Neonatal alcohol exposure induces long-lasting impairment of visual cortical plasticity in ferrets. J Neurosci 23:10002-10012.
Mennini T, Mocaer E, Garattini S (1987) Tianeptine, a selective enhancer of serotonin uptake in rat brain. Naunyn Schmiedebergs Arch Pharmacol 336:478-482.
Moon CH, Fukuda M, Park SH, Kim SG (2007) Neural interpretation of blood oxygenation level-dependent fMRI maps at submillimeter columnar resolution. J Neurosci 27:6892-6902.
Morales B, Choi SY, Kirkwood A (2002) Dark rearing alters the development of GABAergic transmission in visual cortex. J Neurosci 22:8084-8090.
Morishita H, Hensch TK (2008) Critical period revisited: impact on vision. Curr Opin Neurobiol 18:101-107.
Morishita H, Miwa JM, Heintz N, Hensch TK (2010) Lynx1, a cholinergic brake, limits plasticity in adult visual cortex. Science 330:1238-1240.
Morrison JH, Foote SL, Molliver ME, Bloom FE, Lidov HG (1982) Noradrenergic and serotonergic fibers innervate complementary layers in monkey primary visual cortex: an immunohistochemical study. Proc Natl Acad Sci U S A 79:2401-2405.
Morrone MC, Burr DC, Maffei L (1982) Functional implications of cross-orientation inhibition of cortical visual cells. I. Neurophysiological evidence. Proc R Soc Lond B Biol Sci 216:335-354.
Mower AF, Kwok S, Yu H, Majewska AK, Okamoto K, Hayashi Y, Sur M (2011) Experience-dependent regulation of CaMKII activity within single visual cortex synapses in vivo. Proc Natl Acad Sci U S A 108:21241-21246.
Mrsic-Flogel TD, Hofer SB, Ohki K, Reid RC, Bonhoeffer T, Hubener M (2007) Homeostatic regulation of eye-specific responses in visual cortex during ocular dominance plasticity. Neuron 54:961-972.
Mrsic-Flogel TD, Hofer SB, Creutzfeldt C, Cloez-Tayarani I, Changeux JP, Bonhoeffer T, Hubener M (2005) Altered map of visual space in the superior colliculus of mice lacking early retinal waves. J Neurosci 25:6921-6928.

Muller T, Stetter M, Hubener M, Sengpiel F, Bonhoeffer T, Godecke I, Chapman B, Lowel S, Obermayer K (2000) An analysis of orientation and ocular dominance patterns in the visual cortex of cats and ferrets. Neural Comput 12:2573-2595.
Nagel G, Szellas T, Huhn W, Kateriya S, Adeishvili N, Berthold P, Ollig D, Hegemann P, Bamberg E (2003) Channelrhodopsin-2, a directly light-gated cation-selective membrane channel. Proc Natl Acad Sci U S A 100:13940-13945.
Nakagama H, Tani T, Tanaka S (2006) Theoretical and experimental studies of relationship between pinwheel centers and ocular dominance columns in the visual cortex. Neurosci Res 55:370-382.
Nauhaus I, Benucci A, Carandini M, Ringach DL (2008) Neuronal selectivity and local map structure in visual cortex. Neuron 57:673-679.
Nauhaus I, Busse L, Carandini M, Ringach DL (2009) Stimulus contrast modulates functional connectivity in visual cortex. Nat Neurosci 12:70-76.
Obermayer K, Blasdel GG (1993) Geometry of orientation and ocular dominance columns in monkey striate cortex. J Neurosci 13:4114-4129.
Obermayer K, Ritter H, Schulten K (1990) A principle for the formation of the spatial structure of cortical feature maps. Proc Natl Acad Sci U S A 87:8345-8349.
Ohki K, Chung S, Ch'ng YH, Kara P, Reid RC (2005) Functional imaging with cellular resolution reveals precise micro-architecture in visual cortex. Nature 433:597-603.
Ohki K, Chung S, Kara P, Hubener M, Bonhoeffer T, Reid RC (2006) Highly ordered arrangement of single neurons in orientation pinwheels. Nature 442:925-928.
Okamoto T, Ikezoe K, Tamura H, Watanabe M, Aihara K, Fujita I (2011) Predicted contextual modulation varies with distance from pinwheel centers in the orientation preference map. Sci Rep 1:114.
Oster AM, Bressloff PC (2006) A developmental model of ocular dominance column formation on a growing cortex. Bull Math Biol 68:73-98.
Paul AP, Medina AE (2012) Overexpression of serum response factor in astrocytes improves neuronal plasticity in a model of early alcohol exposure. Neuroscience 221:193-202.
Paul AP, Pohl-Guimaraes F, Krahe TE, Filgueiras CC, Lantz CL, Colello RJ, Wang W, Medina AE (2010) Overexpression of serum response factor restores ocular dominance plasticity in a model of fetal alcohol spectrum disorders. J Neurosci 30:2513-2520.
Pham TA, Graham SJ, Suzuki S, Barco A, Kandel ER, Gordon B, Lickey ME (2004) A semi-persistent adult ocular dominance plasticity in visual cortex is stabilized by activated CREB. Learn Mem 11:738-747.
Pinto JG, Hornby KR, Jones DG, Murphy KM (2010) Developmental changes in GABAergic mechanisms in human visual cortex across the lifespan. Front Cell Neurosci 4:16.
Pizzorusso T, Medini P, Berardi N, Chierzi S, Fawcett JW, Maffei L (2002) Reactivation of ocular dominance plasticity in the adult visual cortex. Science 298:1248-1251.
Pizzorusso T, Medini P, Landi S, Baldini S, Berardi N, Maffei L (2006) Structural and functional recovery from early monocular deprivation in adult rats. Proc Natl Acad Sci U S A 103:8517-8522.

Polat U, Mizobe K, Pettet MW, Kasamatsu T, Norcia AM (1998) Collinear stimuli regulate visual responses depending on cell's contrast threshold. Nature 391:580-584.
Priebe NJ, Ferster D (2008) Inhibition, spike threshold, and stimulus selectivity in primary visual cortex. Neuron 57:482-497.
Priebe NJ, Mechler F, Carandini M, Ferster D (2004) The contribution of spike threshold to the dichotomy of cortical simple and complex cells. Nat Neurosci 7:1113-1122.
Purushothaman G, Khaytin I, Casagrande VA (2009) Quantification of optical images of cortical responses for inferring functional maps. J Neurophysiol 101:2708-2724.
Purves D, LaMantia A (1993) Development of blobs in the visual cortex of macaques. J Comp Neurol 334:169-175.
Rakic P (1974) Neurons in rhesus monkey visual cortex: systematic relation between time of origin and eventual disposition. Science 183:425-427.
Rao SC, Toth LJ, Sur M (1997) Optically imaged maps of orientation preference in primary visual cortex of cats and ferrets. J Comp Neurol 387:358-370.
Rathjen S, Schmidt KE, Lowel S (2002) Two-dimensional analysis of the spacing of ocular dominance columns in normally raised and strabismic kittens. Exp Brain Res 145:158-165.
Rathjen S, Schmidt KE, Lowel S (2003) Postnatal growth and column spacing in cat primary visual cortex. Exp Brain Res 149:151-158.
Reader TA (1978) The effects of dopamine, noradrenaline and serotonin in the visual cortex of the cat. Experientia 34:1586-1588.
Redies C, Diksic M, Riml H (1990) Functional organization in the ferret visual cortex: a double-label 2-deoxyglucose study. J Neurosci 10:2791-2803.
Reichl L, Heide D, Lowel S, Crowley JC, Kaschube M, Wolf F (2012a) Coordinated optimization of visual cortical maps (I) symmetry-based analysis. PLoS Comput Biol 8:e1002466.
Reichl L, Heide D, Lowel S, Crowley JC, Kaschube M, Wolf F (2012b) Coordinated optimization of visual cortical maps (II) numerical studies. PLoS Comput Biol 8:e1002756.
Reiter HO, Stryker MP (1988) Neural plasticity without postsynaptic action potentials: less-active inputs become dominant when kitten visual cortical cells are pharmacologically inhibited. Proc Natl Acad Sci U S A 85:3623-3627.
Reiter HO, Waitzman DM, Stryker MP (1986) Cortical activity blockade prevents ocular dominance plasticity in the kitten visual cortex. Exp Brain Res 65:182-188.
Ringach DL, Hawken MJ, Shapley R (1997) Dynamics of orientation tuning in macaque primary visual cortex. Nature 387:281-284.
Roerig B, Katz LC (1997) Modulation of intrinsic circuits by serotonin 5-HT3 receptors in developing ferret visual cortex. J Neurosci 17:8324-8338.
Ruthazer ES, Baker GE, Stryker MP (1999) Development and organization of ocular dominance bands in primary visual cortex of the sable ferret. J Comp Neurol 407:151-165.
Sale A, Maya Vetencourt JF, Medini P, Cenni MC, Baroncelli L, De Pasquale R, Maffei L (2007) Environmental enrichment in adulthood promotes amblyopia recovery through a reduction of intracortical inhibition. Nat Neurosci 10:679-681.

Santini S (1996) The self-organizing field [Kohonen maps]. IEEE Trans Neural Netw 7:1415-1423.
Sato H, Katsuyama N, Tamura H, Hata Y, Tsumoto T (1995) Mechanisms underlying direction selectivity of neurons in the primary visual cortex of the macaque. J Neurophysiol 74:1382-1394.
Sato H, Katsuyama N, Tamura H, Hata Y, Tsumoto T (1996) Mechanisms underlying orientation selectivity of neurons in the primary visual cortex of the macaque. J Physiol 494 (Pt 3):757-771.
Sato M, Stryker MP (2008) Distinctive features of adult ocular dominance plasticity. J Neurosci 28:10278-10286.
Sawtell NB, Frenkel MY, Philpot BD, Nakazawa K, Tonegawa S, Bear MF (2003) NMDA receptor-dependent ocular dominance plasticity in adult visual cortex. Neuron 38:977-985.
Schmidt KE, Stephan M, Singer W, Lowel S (2002) Spatial analysis of ocular dominance patterns in monocularly deprived cats. Cereb Cortex 12:783-796.
Schnabel M, Kaschube M, Wolf F (2008) Pinwheel stability, pattern selection and the geometry of visual space. New J Phys 10.
Schuett S, Bonhoeffer T, Hubener M (2001) Pairing-induced changes of orientation maps in cat visual cortex. Neuron 32:325-337.
Schummers J, Marino J, Sur M (2002) Synaptic integration by V1 neurons depends on location within the orientation map. Neuron 36:969-978.
Schummers J, Yu H, Sur M (2008) Tuned responses of astrocytes and their influence on hemodynamic signals in the visual cortex. Science 320:1638-1643.
Schummers J, Cronin B, Wimmer K, Stimberg M, Martin R, Obermayer K, Koerding K, Sur M (2007) Dynamics of orientation tuning in cat v1 neurons depend on location within layers and orientation maps. Front Neurosci 1:145-159.
Sengpiel F, Stawinski P, Bonhoeffer T (1999) Influence of experience on orientation maps in cat visual cortex. Nat Neurosci 2:727-732.
Sengpiel F, Godecke I, Stawinski P, Hubener M, Lowel S, Bonhoeffer T (1998) Intrinsic and environmental factors in the development of functional maps in cat visual cortex. Neuropharmacology 37:607-621.
Shapley R, Hawken M, Ringach DL (2003) Dynamics of orientation selectivity in the primary visual cortex and the importance of cortical inhibition. Neuron 38:689-699.
Sherwood CC, Gordon AD, Allen JS, Phillips KA, Erwin JM, Hof PR, Hopkins WD (2011) Aging of the cerebral cortex differs between humans and chimpanzees. Proc Natl Acad Sci U S A 108:13029-13034.
Shmuel A, Grinvald A (1996) Functional organization for direction of motion and its relationship to orientation maps in cat area 18. J Neurosci 16:6945-6964.
Shouval HZ, Goldberg DH, Jones JP, Beckerman M, Cooper LN (2000) Structured long-range connections can provide a scaffold for orientation maps. J Neurosci 20:1119-1128.
Shtoyerman E, Arieli A, Slovin H, Vanzetta I, Grinvald A (2000) Long-term optical imaging and spectroscopy reveal mechanisms underlying the intrinsic signal and stability of cortical maps in V1 of behaving monkeys. J Neurosci 20:8111-8121.

Sillito AM (1975) The contribution of inhibitory mechanisms to the receptive field properties of neurones in the striate cortex of the cat. J Physiol 250:305-329.
Singer W (1983) Mechanisms of experience dependent self-organization of neuronal assemblies in the mammalian visual system. Arch Biol Med Exp (Santiago) 16:317-327.
Smith SL, Trachtenberg JT (2007) Experience-dependent binocular competition in the visual cortex begins at eye opening. Nat Neurosci 10:370-375.
Sohya K, Kameyama K, Yanagawa Y, Obata K, Tsumoto T (2007) GABAergic neurons are less selective to stimulus orientation than excitatory neurons in layer II/III of visual cortex, as revealed by in vivo functional Ca2+ imaging in transgenic mice. J Neurosci 27:2145-2149.
Somers DC, Todorov EV, Siapas AG, Toth LJ, Kim DS, Sur M (1998) A local circuit approach to understanding integration of long-range inputs in primary visual cortex. Cereb Cortex 8:204-217.
Southwell DG, Froemke RC, Alvarez-Buylla A, Stryker MP, Gandhi SP (2010) Cortical plasticity induced by inhibitory neuron transplantation. Science 327:1145-1148.
Sowell ER, Peterson BS, Thompson PM, Welcome SE, Henkenius AL, Toga AW (2003) Mapping cortical change across the human life span. Nat Neurosci 6:309-315.
Spatazza J, Lee HH, Di Nardo AA, Tibaldi L, Joliot A, Hensch TK, Prochiantz A (2013) Choroid-plexus-derived otx2 homeoprotein constrains adult cortical plasticity. Cell Rep 3:1815-1823.
Spedding M, Gressens P (2008) Neurotrophins and cytokines in neuronal plasticity. Novartis Found Symp 289:222-233; discussion 233-240.
Stettler DD, Das A, Bennett J, Gilbert CD (2002) Lateral connectivity and contextual interactions in macaque primary visual cortex. Neuron 36:739-750.
Sugiyama S, Di Nardo AA, Aizawa S, Matsuo I, Volovitch M, Prochiantz A, Hensch TK (2008) Experience-dependent transfer of Otx2 homeoprotein into the visual cortex activates postnatal plasticity. Cell 134:508-520.
Swindale NV (1996) The development of topography in the visual cortex: a review of models. Network 7:161-247.
Swindale NV, Shoham D, Grinvald A, Bonhoeffer T, Hubener M (2000) Visual cortex maps are optimized for uniform coverage. Nat Neurosci 3:822-826.
Tagawa Y, Kanold PO, Majdan M, Shatz CJ (2005) Multiple periods of functional ocular dominance plasticity in mouse visual cortex. Nat Neurosci 8:380-388.
Tanaka S, Miyashita M, Ribot J (2004) Roles of visual experience and intrinsic mechanism in the activity-dependent self-organization of orientation maps: theory and experiment. Neural Netw 17:1363-1375.
Tolhurst DJ, Smyth D, Thompson ID (2009) The sparseness of neuronal responses in ferret primary visual cortex. J Neurosci 29:2355-2370.
Torborg CL, Hansen KA, Feller MB (2005) High frequency, synchronized bursting drives eye-specific segregation of retinogeniculate projections. Nat Neurosci 8:72-78.
Toth LJ, Rao SC, Kim DS, Somers D, Sur M (1996) Subthreshold facilitation and suppression in primary visual cortex revealed by intrinsic signal imaging. Proc Natl Acad Sci U S A 93:9869-9874.

Trachtenberg JT, Stryker MP (2001) Rapid anatomical plasticity of horizontal connections in the developing visual cortex. J Neurosci 21:3476-3482.
Van Hooser SD, Heimel JA, Chung S, Nelson SB, Toth LJ (2005) Orientation selectivity without orientation maps in visual cortex of a highly visual mammal. J Neurosci 25:19-28.
Van Hooser SD, Li Y, Christensson M, Smith GB, White LE, Fitzpatrick D (2012) Initial neighborhood biases and the quality of motion stimulation jointly influence the rapid emergence of direction preference in visual cortex. J Neurosci 32:7258-7266.
Voigt T, de Lima AD (1991) Serotoninergic innervation of the ferret cerebral cortex. I. Adult pattern. J Comp Neurol 314:403-414.
von der Malsburg C (1973) Self-organization of orientation sensitive cells in the striate cortex. Kybernetik 14:85-100.
Vorobyov V, Kwok JC, Fawcett JW, Sengpiel F (2013) Effects of digesting chondroitin sulfate proteoglycans on plasticity in cat primary visual cortex. J Neurosci 33:234-243.
Wang BS, Sarnaik R, Cang J (2010) Critical period plasticity matches binocular orientation preference in the visual cortex. Neuron 65:246-256.
Weliky M, Bosking WH, Fitzpatrick D (1996) A systematic map of direction preference in primary visual cortex. Nature 379:725-728.
White LE, Fitzpatrick D (2007) Vision and cortical map development. Neuron 56:327-338.
White LE, Bosking WH, Fitzpatrick D (2001a) Consistent mapping of orientation preference across irregular functional domains in ferret visual cortex. Vis Neurosci 18:65-76.
White LE, Coppola DM, Fitzpatrick D (2001b) The contribution of sensory experience to the maturation of orientation selectivity in ferret visual cortex. Nature 411:1049-1052.
White LE, Bosking WH, Williams SM, Fitzpatrick D (1999) Maps of central visual space in ferret V1 and V2 lack matching inputs from the two eyes. J Neurosci 19:7089-7099.
Wiesel TN, Hubel DH (1963) Single-Cell Responses in Striate Cortex of Kittens Deprived of Vision in One Eye. J Neurophysiol 26:1003-1017.
Wiesel TN, Hubel DH, Lam DM (1974) Autoradiographic demonstration of ocular-dominance columns in the monkey striate cortex by means of transneuronal transport. Brain Res 79:273-279.
Wolf F (2005) Symmetry, Multistability, and Long-Range Interactions in Brain Development. PRL 95.
Wolf F, Geisel T (1998) Spontaneous pinwheel annihilation during visual development. Nature 395:73-78.
Wright JJ, Bourke PD (2008) An outline of functional self-organization in V1: synchrony, STLR and Hebb rules. Cogn Neurodyn 2:147-157.
Wright JJ, Alexander DM, Bourke PD (2006) Contribution of lateral interactions in V1 to organization of response properties. Vision Res 46:2703-2720.
Xiang Z, Prince DA (2003) Heterogeneous actions of serotonin on interneurons in rat visual cortex. J Neurophysiol 89:1278-1287.

Xu X, Anderson TJ, Casagrande VA (2007) How do functional maps in primary visual cortex vary with eccentricity? J Comp Neurol 501:741-755.
Yacoub E, Harel N, Ugurbil K (2008) High-field fMRI unveils orientation columns in humans. Proc Natl Acad Sci U S A 105:10607-10612.
Yacoub E, Shmuel A, Logothetis N, Ugurbil K (2007) Robust detection of ocular dominance columns in humans using Hahn Spin Echo BOLD functional MRI at 7 Tesla. Neuroimage 37:1161-1177.
Yamada MK, Nakanishi K, Ohba S, Nakamura T, Ikegaya Y, Nishiyama N, Matsuki N (2002) Brain-derived neurotrophic factor promotes the maturation of GABAergic mechanisms in cultured hippocampal neurons. J Neurosci 22:7580-7585.
Yousef T, Toth E, Rausch M, Eysel UT, Kisvarday ZF (2001) Topography of orientation centre connections in the primary visual cortex of the cat. Neuroreport 12:1693-1699.
Yu H, Majewska AK, Sur M (2011) Rapid experience-dependent plasticity of synapse function and structure in ferret visual cortex in vivo. Proc Natl Acad Sci U S A 108:21235-21240.
Yu H, Farley BJ, Jin DZ, Sur M (2005) The coordinated mapping of visual space and response features in visual cortex. Neuron 47:267-280.
Zhang H, Etherington LA, Hafner AS, Belelli D, Coussen F, Delagrange P, Chaouloff F, Spedding M, Lambert JJ, Choquet D, Groc L (2013) Regulation of AMPA receptor surface trafficking and synaptic plasticity by a cognitive enhancer and antidepressant molecule. Mol Psychiatry 18:471-484.
Zhang LI, Tao HW, Holt CE, Harris WA, Poo M (1998) A critical window for cooperation and competition among developing retinotectal synapses. Nature 395:37-44.
Zilles KJ (1978) Ontogenesis of the visual system. Adv Anat Embryol Cell Biol 54:3-138.